FLOW AND ACOUSTIC PROPERTIES OF LOW REYNOLDS NUMBER UNDEREXPANDED SUPERSONIC JETS

By

TIEH-FENG HU

Diploma
Taipei Institute of Technology
Taipei, Taiwan
1973

Master of Science
Oklahoma State University
Stillwater, Oklahoma
1977

Submitted to the Faculty of the
Graduate College of the
Oklahoma State University
in partial fulfillment of
the requirements for
the Degree of
DOCTOR OF PHILOSOPHY
December, 1981

FLOW AND ACOUSTIC PROPERTIES OF LOW REYNOLDS NUMBER UNDEREXPANDED SUPERSONIC JETS

Thesis Approved:

Dennis K. McLaughlin
Thesis Adviser

David G. Lilley

B. J. Lowery

Donald D. Fisher

P. W. Mocek

Norman N. Durham
Dean of the Graduate College

ACKNOWLEDGMENTS

The author wishes to express his appreciation to his principal adviser, Dr. Dennis K. McLaughlin, and to the members of his thesis committee, Dr. D. G. Lilley, Dr. D. D. Fisher, Dr. R. L. Lowery, and Dr. P. M. Moretti, for their invaluable advice and guidance.

Appreciation is also extended to Mr. S. A. Gallagher, and Mr. M. D. Politte for their assistance with the experiments. A note of thanks is extended to Mr. M. Yu, and Ms. S. W. Tai for their help with typing and preparing the figures.

The author would like to express gratitude to his parents, Mr. and Mrs. Tsu-Chung Hu, for their all-aspect support for the past 29 years.

Finally, the author would like to recognize the National Aeronautics and Space Administration of the United States of America whose financial support (Grants No. NAG 1-10 and NAG 1-159) made this study possible.

TABLE OF CONTENTS

LIST OF TABLES

LIST OF FIGURES

NOMENCLATURE

a_o	ambient acoustic velocity
A_m	sensitivity coefficient for mass velocity fluctuation
A_t	sensitivity coefficient for stagnation temperature fluctuation
c	axial phase velocity
d	nozzle exit diameter
D	effective diameter, $D = d\sqrt{A/A^*}$
e	electrical voltage
f	frequency
k	complex wave number
k_i	imaginary part of the complex wave number
k_r	real part of the complex wave number, $k_r=2\pi/\lambda$
L	average shock cell length
M	Mach number
n	azimuthal mode number
p	pressure
P_a	ambient air pressure
P_{atm}	standard atmoshperic pressure
P_{ch}	test chamber pressure
P_n	nozzle exit static pressure
P_o	stagnation pressure upstream of nozzle
r	radial distance from jet centerline, cylindrical coordinate system

R	radial distance from the center of nozzle exit, spherical coordinate system
Re	Reynolds number, UD/ν
St	Strouhal number, fD/U
t	time
T	temperature
T_o	stagnation temperature of the jet
T_a	ambient air temperature
T_w	temperature of hot-wire
u	local axial velocity
U	fully expanded axial velocity evaluated at the centerline
x	downstream distance from nozzle exit
y	vertical distance from the centerline
z	horizontal distance from the centerline
β	angular coordinate in spherical coordinate system, measured from x axis
θ	azimuthal angle, cylindrical coordinate system
λ	axial wavelength
ν	kinematic viscosity
ρ	density
ρu	mass velocity
τ	time shift
ω	angular frequency (radians/sec)
$(\ )_e$	quantity evaluated at the fully expanded jet Mach number
$(\ )_o$	quantity evaluated at the jet exit

$( )_{rms}$ root mean square of quantity

$( )_t$ quantity evaluated at stagnation conditions

$\bar{( )}$ quantity being time averaged

$\langle \rangle$ quantity being phase averaged

$( )'$ overall fluctuations within a given frequency band width, $( )' = \tilde{( )} + ( )''$

$( )''$ random portion of fluctuations

$\tilde{( )}$ periodic portion of fluctuations

CHAPTER I

INTRODUCTION

A. The Problem of Jet Noise

Ever since the introduction of turbojet powerplants for aircraft propulsion, jet noise has been a real annoyance to the general public. The objections from the public have led to more and more stringent civil aviation laws which stipulate the legal limit of noise radiation of civil transport aircraft. Consequently, the noise consideration has become an integral part of modern civilian aircraft design, and the problem of jet noise has received increased attention from scientists and engineers.

Over the past 30 years, the research activities associated with the jet noise problem have been increasing. The results from these research activities, either theoretical or experimental, are diverging and complicated which sometimes blur the physics. However, one should bear in mind that the ultimate goal of jet noise research is noise suppression. In pursuing this goal, jet engine designers have been using empirical rules and trial and error methods. Many scientists, on the other hand, are taking a more integrated view of approaching this problem. They believe that the jet noise is a byproduct of

turbulence, and before an effective means can be developed for noise suppression, there is an essential need to improve the understanding of the basic turbulent fluid mechanics and the noise production mechanism in high speed jets. Theoreticians and experimentalists thus have been working together toward the development of a comprehensive theory in aerodynamic noise with the objectives that the noise production of a given jet may finally be predicted and then controlled.

B. Background

B.1 High Speed Jet noise

Lighthill (1, 2) was the first to develop a theory in aerodynamic noise by rewriting the governing equations of fluid motion and using dimensional analysis to predict the eighth power dependence on velocity for subsonic jet noise. Positive experimental confirmation of this classical eighth power law led to extensions of his approach to high speed jets by Ffowcs Williams (3) who postulated that eddies convecting supersonically with respect to the ambient air would radiate noise in the form of Mach waves. Improvements and extensions of Lighthill's basic subsonic theory were also made by a number of authors (4-7). The assumption made by these early theoreticians was that the turbulent fluctuations in the jet flow are completely random in nature, and there is little hope of predicting them successfully. Consequently, their general approach was to

assume a distribution of acoustic sources (quadrupoles) or turbulent properties and proceed with an acoustic computation.

During the last decade, however, experimental evidence has established that in almost all turbulent flows there is some degree of large-scale organized fluctuations (8-15). These organized flow fluctuations, often referred to as coherent structures, play an important role in developing turbulent shear flows, namely mixing layers, boundary layers, and the initial regions of jets and wakes.

At the present time, it is not clear what the coherent structures are, but some of them are beginning to be recognized and described. The earliest and most decisive attempts to define the form of such structures were made by Townsend and his students (8, 9) in the late fifties. However, Brown and Roshko (10) were the first ones who established clear and irrefutable optical evidence of the existence of coherent structures in two-dimensional turbulent mixing layers. Using shadowgraph techniques, Brown and Roshko identified coherent structures as large-scale, organized, two-dimensional, spanwise vorticies in low speed two-dimensional turbulent mixing layers. These coherent structures are a distinct feature of the mixing layers at all Reynolds numbers corresponding to what is known as fully turbulent flow, they control the mixing layer development, and they are little affected by small-scale turbulence appearing at higher values of Reynolds number.

Although the physical picture in other flows has not emerged as clearly as in the mixing layers, optical evidence for the existence of coherent structures in other turbulent shear flows has been accumulating, preceding in some cases the discoveries in mixing layers. The best known example is probably the classical experiment showing vortex shedding from cylinders. This occurs up to very high Reynolds numbers where the organized, periodic motion is superimposed on a background of random turbulence or, perhaps more accurately, vice versa. Another example is the organized large-scale wave-like oscillation near the end of the potential core in a turbulent jet (16-20).

The potential for noise production by coherent structures was initially suggested by Mollo-Christensen (21) with later contributions by Sedel'nikov (22), Michalke (23); and Bishop, Ffowcs Williams and Smith (24). Much experimental evidence supporting this idea has been accumulating (25-28). Of all the experimentalists, McLaughlin et al. (29) were the ones who first established convincing experimental evidence substantiating the fact that coherent flow fluctuations are dominant noise producers in high speed jets. Later Troutt and McLaughlin (30) performed microphone measurements with a moderate Reynolds number (Re=68,000) perfectly expanded jet of Mach number 2.1, artificially excited at frequencies of dominant acoustic production. By comparing the coherent portion of the acoustic signal to the overall signal picked up by a

microphone at locations of dominant noise radiation, they concluded that a significant fraction of the radiated acoustic energy can be directly caused by coherent flow fluctuations.

A number of theoreticians (31-37) have recognized the fact that such coherent fluctuations in a turbulent shear flow develop in a fashion resembling hydrodynamic instability waves, and dominate the shear flow development. In the case of high speed flows, they postulate that the large-scale organized fluctuations produce a major portion of the radiated acoustic energy. They have used hydrodynamic instability theory to model the development of coherent flow fluctuations and therefrom calculate the acoustic radiation. The basic idea introduced in this type of theory is that the turbulent fluctuations may be modeled by a superposition of traveling waves of broad spectrum with random phase and orientation. As these waves travel downstream, their amplitude evolution is governed by certain natural frequency selection mechanism which is poorly understood at the present time. The most advanced of these theories were performed by Morris and Tam (36) and Tester et al. (37). Recent comparison of their predictions with experimental observations showed encouraging agreement (30, 38). Further development of this type of theoretical model appears to hold strong promise.

B.2 Shock Associated Noise

It has been recognized for many years that the noise radiation from an underexpanded jet displays different features when compared to shock-free jets (39-44). In addition to the noise due to turbulent mixing, a significant amount of the noise produced involves mechanisms of shock-turbulence interaction, since an imperfectly expanded supersonic jet contains shock cells as well as turbulent structures. The shock associated noise is defined in Figure 1 (p. 78) where the acoustic spectrum from a conventional underexpanded jet is compared with the corresponding spectrum from a perfectly expanded jet at identical operation conditions. When a nozzle is operated at the design pressure ratio, the acoustic spectrum is fairly broad and smooth and consists of pure mixing noise. On the other hand, when a convergent nozzle is operated at super-critical pressure ratios, or when a convergent-divergent nozzle is operated at off-design Mach numbers (underexpanded or overexpanded), the resulting acoustic spectrum contains an extra noise contribution due to the presence of shock structures in the jet.

The shock associated noise is normally considered to have two distinct components. The first component is harmonically related discrete tones often referred to as screech tones. The second component is broadband in nature with a well defined peak frequency and is called the broadband shock noise. It has been found that supersonic

perfectly expanded jets produce turbulent mixing noise which is broadband and whose lower frequencies radiate predominantly downstream at angles less than 45 degrees to the jet axis. In the case of imperfectly expanded supersonic jets, normally higher frequencies and upstream radiation characterize the shock noise. The strength of shock noise depends on the jet Mach number and nozzle design Mach number, and is capable of dominating the mixing noise, especially in the upstream direction of the jet where the mixing noise is lowest.

Shock associated noise was first investigated by Powell (39) who studied the screech phenomenon, and empirically modeled the screech with an acoustic feedback mechanism where flow fluctuations interacting with shock cells produce intense acoustic radiation. This noise propagates upstream in the ambient fluid, excites new flow fluctuations near the nozzle exit, and thus completes the feedback loop. The screech phenomenon was subsequently investigated by a number of researchers (19, 20, 40).

The broadband shock noise was first theorized by Lighthill (41) and Ribner (42), and extensively investigated in recent years by Harper-Bourne and Fisher (43), Tanna (44), and Seiner and Norum (45-47). Lighthill introduced a theory based on a generalization of his theory of aerodynamic sound that models the process as scattering of turbulence energy into sound waves when incident upon a weak shock wave. Ribner offered a physically appealing

theoretical model structured on the idealized situation of the interaction of a column vortex with a plane shock wave. Harper-Bourne and Fisher extended Powell's (39) original theory and proposed an empirical model which regards each shock cell end as a broadband noise emitter with relative phasing set by the time lag for eddy convection between them. This leads to a prediction for the peak frequency of broadband shock noise as a function of both jet Mach number and angle of observation, and this prediction is confirmed by experimental results. Recently, Howe and Ffowcs Williams (48) extended Lighthill's analysis (41) and theorized that the interaction of random turbulence with weak shock waves is representative of the process of broadband shock noise production.

Once again, theoreticians assumed that there was little likelihood of being able to calculate from first principles, the essential ingredients in the aeroacoustic sources, namely the turbulence. The general approach was to assume a distribution of acoustic sources or turbulent properties and proceed with an acoustic computation. Little attention has been given to the role played by large-scale coherent flow fluctuations. This is despite the fact that their existance and their interaction with shock waves were initially recognized in the Schlieren photographs of Powell's early papers (39, 49) and a number of later publications (19, 20, 50).

The experimental data published by Tanna (44) and

Seiner and Norum (46) demostrated that the range of frequencies of the broadband shock noise and the screech tones fall within the domain of the so called large-scale noise (i.e., noise produced by large-scale instabilities). Hence, it is reasonable to assume that large-scale coherent flow fluctuations may play an important role in shock noise production. Considering the fact that instability analyses have achieved encouraging success in predicting major flow and acoustic properties of perfectly expanded jets, it is hoped that a similar analysis incorporating modifications of shock-turbulence interaction should also prove useful with shock-containing jets.

The progress of theoretical analyses can be greatly aided by experimental studies on the coherent structures in shock-containing jets. Consequently, the present study was devoted to establish an experimental data base upon which development of instablity analyses, refinements of current theories, and improvements of practical shock noise reduction techniques may be accomplished with underexpanded jets.

C. Objectives

The goal of the present study was to provide a better understanding of the large-scale flow fluctuations and associated acoustic radiation of underexpanded supersonic jets by performing detailed experimental measurements on low Reynolds number (Re=8000) underexpanded Mach 1.4 and 2.1

jets. The Mach number of the underexpanded jets refers to the Mach number that would be achieved with a perfectly expanded jet operating at a given pressure ratio. The specific objectives of this study are listed as follows:

1. to characterize the naturally occuring flowfield processes in supersonic underexpanded jets by performing Schlieren photography, Pitot and static pressure measuremnets, and hot-wire measurements.
2. to characterize the naturally occuring acoustic radiation properties of supersonic underexpanded jets by performing microphone surveys.
3. to determine the effect of artificial excitation on the flow and acoustic properties of the jets.
4. to determine the turbulent flow instability properties (such as the frequency selection, wave length, wave speed, wave amplitude, and azimuthal behavior) of the supersonic underexpanded jets by using artificial excitation and cross correlation techniques.
5. to determine the characteristic properties of the acoustic radiation (such as the directivity, wave orientation, and noise source locations) produced by large-scale flow fluctuations by using artificial excitation and cross correlation techniques.
6. to determine the principal noise production mechanism(s) in supersonic underexpanded jets by

relating flow fluctuation information to measured acoustic properties.

D. Experimental Conditions

Most measurements reported in this study were obtained at a Reynolds number of approximately 8000 and at Mach numbers of 1.4 and 2.1. A limited amount of acoustic measurements were also preformed on a moderate Reynolds number (Re=68,000) Mach 1.6 underexpanded jet. All jets were unheated and exhausted from convergent nozzles. The operating Mach and Reynolds numbers were selected to match some of the test conditions of low Reynolds number supersonic perfectly expanded jets (51-53), so direct comparisons can be made. A summary of the test conditions is presented in Table I (p. 129). The effective diameter of the jet in Table I is defined as

$$D = d \sqrt{A/A^*}$$

where A/A* is the isentropic area ratio determined for the fully expanded jet Mach number corresponding to the operational pressure ratio of the jet, and d is the nozzle exit diameter. This definition of effective jet diameter D is appropriate for comparison of flow and acoustic measurements with perfectly expanded jets.

In contrast to conventional jet noise research which typically involves Reynolds numbers of 10^6 to 10^7, the selected Reynolds numbers are several orders of magnitude

lower. This is because there are important advantages in undertaking research at lower Reynolds numbers as pointed out by previous researchers (51-53). First, standard hot-wire anemometry can be used, whereas in conventional high Reynolds number jets the large dynamic forces destroy the wires. Second, the random turbulent fluctuations in lower Reynolds number jets are suppressed but coherent large-scale flow fluctuations are retained. This makes the identification and characterization of coherent flow fluctuations much easier. Consequently, the mechanism of noise production can be measured rather than hypothesized as is the case in conventional jet noise research.

Previous observations of the flow properties of low Reynolds number perfectly expanded high speed jets demonstrated that the mean flow properties of the low Reynolds number jets are similar to reported high Reynolds number measurements in profile shape (52). Another perhaps more important finding was that low Reynolds number jets radiate noise equivalent in strength to the noise produced by high Reynolds number jets (29, 53). An additional advantage can be realized in undretaking experiments under low pressure, low Reynolds number environments that is artificial excitation of the turbulent shear layer with a glow discharge device (p. 16) can be achieved. The above discussion explains the selection of experimental conditions.

CHAPTER II

EXPERIMENTAL APPARATUS

A. General Facility

A.1 Wind Tunnel

The present study was carried out at the Oklahoma State University aeroacoustic facility (Figures 2-3, pp. 79-80) which is basically a high speed wind tunnel especially designed for jet noise research at low and moderate Reynolds number regimes. The way of achieving low Reynolds number in high speed jets is to exhaust a jet of relatively low pressure and density into a controlled vacuum environment. The heart of the facility is a 114 cm x 76 cm x 71 cm vacuum test chamber which is lined with five centimeters of Scott Pyrel acoustic foam. This produces an anechoic environment for frequencies above 1 kHz. The reverberant pressure field has been estimated to be less than 3 dB for the range of frequencies (1 kHz to 50 kHz) encountered during measurements.

The static pressure within the chamber is controlled by evacuating the air through a variable throat area diffuser with a vacuum system. The vacuum system which runs continuously during experiments consists of an Ingersoll-

Rand vacuum pump connected in series with a 0.1 cms Kinney vacuum pump (the latter can be operated independently). Vacuum pressure fluctuations are effectively dampened by isolating the pumps from the test chamber with a 30 cubic meter vacuum tank. The mechanical vibrations of the vacuum pumps are also isolated from the test chamber with a section of flexible pipe.

The upstream end of the facility starts with a high pressure Worthington air compressor (rated at 5000 psi), an automatic air dryer (designed to filter and dry the air up to instrument standard), and an 1.8 cubic meter spherical high pressure storage tank. The tank pressure is usually kept around 400 psi before the facility starts, and the tank volume is sufficient to allow continuous facility operation with the compressor and its associated pressure fluctuations shut down for several hours. The actual continuous operation time depends on the experimental pressure conditions and varies from 36 hours to less than an hour corresponding to Reynolds numbers of approximately 3,000 to 150,000 respectively. Downstream of the tank are a pressure regulator, coarse and fine throttling valves, a muffler, a stilling section, a contoured contraction section (area ratio 325 : 1), and a contoured nozzle which expands the air into the anechoic chamber up to the Mach number of interest.

The pressure regulator regulates compressed air to around 60 psi. The muffler consists of a cylindrical casing 55 cm long and 15.2 cm in internal diameter with half-moon

baffle plates forming 11 resonance chambers (four are foam filled) tuned to the center frequency of 2 kHz. The muffler effectively attenuates the throttle valve noise to below 80 dB for all the experimental conditions experienced. The cylindrical stilling section is 55 cm long and 14.3 cm in internal diameter. It consists of 5 cm of foam, three perforated plates, a 7.6 cm honeycomb section and six fine mesh screens.

The facility test chamber is equipped with an electrically driven, remotely controlled precision probe drive system capable of translation in three orthogonal directions (Figure 4, p. 81, x, y, and z), and rotation (yaw) about the y axis. Various probe adapters can be attached to the basic probe drive platform to facilitate the use of hot-wire probes, Pitot or static pressure probes, or microphone probes. In addition to the traversing probe drive system, a second stationary probe mount is attached to the top of the test chamber. Prior to an experiment, this stationary probe mount can be adjusted in the axial direction on the vertical plane (z=0) of the jet centerline.

Precision ten-turn potentiometers provide the probe drive system with DC voltages linearly proportional to the probe locations in the y, z and yaw directions; a precision mechanical counter registers the probe position in the axial (x) direction. This system enables accurate and repeatable probe positioning (within 0.1 mm) when care is taken to eliminate mechanical backlash.

A.2 Artificial Excitation

The facility is equipped with two artificial flow fluctuation excitation devices (Figure 5, p. 82) similar to the one developed by Kendall (54) and reported earlier by McLaughlin et al. (28). The exciters are mounted 180 degrees apart near the nozzle exit plane. Each exciter consists of an 1/32 inch diameter tungsten electrode insulated with ceramic tubing, and is very similar to an automotive spark plug in construction. In low density environments, when the electrode is subjected to a negative-biased AC voltage of approximately 400 volts peak-to-peak, an electron discharge ionizes the air and forms a small oscillating glow which turns on and off at the frequency of the high voltage AC current supplied to the electrode. This oscillating glow locally heats up the air, acts like a localized selective flow fluctuation amplifier which enhances those naturally occuring flow fluctuations whose frequency and phase angle agree with the glow oscillation, and causes them to become the dominant instability wave upon exiting from the nozzle.

Since the phase angle of enhanced flow fluctuations locks onto the glow oscillation in time, the wave properties of enhanced fluctuations can be quite precisely determined by employing cross-correlation and phase averaging techniques. The amplitude of the glow excitation can be controlled over a limited range by adjusting the electical power through the circuit, and is usually kept low (less

than 0.15% of the jet's exit kinetic energy flux typically) so as not to change the flow and acoustic properties of the jet appreciably. When the jet is excited at its natural instability frequencies, the jet's flow and acoustic properties are most responsive to the excitation.

A.3 Nozzles

Two contoured convergent nozzles of exit diameters 7.92 mm and 6.99 mm were used for this study. The contour coordinates were obtained from Smith and Wang (55) who designed a family of nozzle contours to provide uniform parallel flow at the nozzle exit. Measurements associated with perfectly expanded jets were obtained using convergent-divergent nozzles of design Mach numbers 1.4 and 2.1, whose contours are obtained by the method of characteristics following Johnson and Boney (56).

B. Instrumentation

B.1 Pressure Instruments

The Oklahoma State University aeroacoustic facility is equipped with mercury and silicon oil (specific gravity 0.93) vacuum manometers which are referenced to an absolute pressure of less than 50 micrometers of mercury. Pressure taps are provided at locations just upstream of the contraction section, near the nozzle exit, and on top of the test chamber. A Statham PL96Tcd-3-350 strain gauge differential pressure transducer was used for Pitot and

static pressure measurements in the flow. The Pitot probe consisted of a 0.51 mm (outside diameter) square-ended tube attached to a thin brass wedge (57). The static pressure probe made of 0.88 mm outside diameter tube fitted with a slender nose cone was of a similar construction (57). A Vishay V/E-20A digital strain indicator was used to supply power to the transducer and provide digital readout linearly proportional to the sensed pressure.

B.2 Hot-Wire Anemometer

The normal hot-wire probe used in this study was a DISA 55A53 subminiature probe mounted on a thin brass wedge (58). The associated constant temperature hot-wire anemometer electronics consisted of a DISA 55M01 main frame with a 55M10 standard bridge. The frequency response of the hot-wire and associated electronics were assumed to be flat within $\pm$ 3 dB for frequencies up to 60 kHz based on square wave tests.

B.3 Microphone

Bruel & Kjaer 3.175 mm diameter Type 4138 condenser microphones were used for acoustic measurements. Based on manufacturer's specifications, the microphones were assumed to have omni-directional response within $\pm$ 3 dB for angles $\pm$ 90 degrees to the microphone axis and for frequencies up to 60 kHz. Calibration of the microphones was performed on a periodic basis with a Bruel & Kjaer Type 4220 piston

phone. Associated microphone electronics included a Bruel & Kjaer Type 2618 preamplifier and Type 2804 power supply.

B.4 Additional Instruments

Frequency spectra of the microphone and hot-wire signals were obtained using a Tektronix 7L5 spectrum analyzer. A Honeywell Saicor Model SAI 43A correlation and probability analyzer was used for correlation and phase averaging measurements. A Spencer-Kennedy Laboratories Model 311 variable electronic band-pass filter, and two Multimetrics Series AF-100 variable active filters were used for band-pass filtering the signals. A Ballatine Laboratories Model 710A liner AC to DC converter and three Hewlett-Packard Model 2401B integrating digital voltmeters were used for general purpose quantitative measurements.

CHAPTER III

EXPERIMENTAL PROCEDURES

A. General

The desired nozzle exit Mach number and Reynolds number were set by independent control of the upstream stagnation pressure (P_o) and the test chamber pressure (P_{ch}). The upstream stagnation pressure was controlled by reducing the reservoir pressure with a regulator valve and then throttling this reduced pressure with coarse and fine throttle valves. The anechoic test chamber pressure was controlled with a variable throat area diffuser located at the test chamber exit (Figure 3, p. 80). Both pressures were constantly monitored with vacuum manometers, and the nozzle operating Mach number was monitored with the aid of a Texas Instruments TI-59 programmable calculator. The jet's stagnation temperature was assumed to be room temperature and remains approximately constant throughout the flow field based on previous findings (51). All measurements were performed with P_o held within $\pm 2\%$ and nozzle operating Mach number within $\pm 1\%$ of the target values. Most of the measurement and data reduction procedures were semi-computerized by using time-averaging digital electronics,

the programmable calculator, and the OSU IBM 370/169 computer. A diagram of the coordinate systems is shown in Figure 4 (p. 81).

B. Mean Velocity Measurements

The characterization of the mean flowfield of supersonic underexpanded jets requires both Pitot and static pressure measurements. The measurement procedure employed a Statham PL96Tcd-3-350 strain gauge pressure transducer coupled with a Vishay V/E-20A digital strain indicator. Calibration of this equipment was performed with known pressure values. The local mean Mach number was determined from the measured Pitot and static pressures using standard compressible flow relations.

C. Hot-Wire Data Analysis

The instantaneous voltage fluctuations measured from a hot-wire probe in supersonic flow can be represented mathematically by the following expression (59):

$$\frac{e'}{\bar{e}} = A_m \frac{(\rho u)'}{\overline{\rho u}} + A_t \frac{T_o'}{\bar{T}_o}$$

Since the stagnation temperature of the jet is approximately equal to the ambient temperature in the test chamber, it is assumed that stagnation temperature fluctuations are negligible (51). The voltage fluctuations are thus proportional to mass velocity fluctuations only. This

proportionality factor, A_m, was determined by direct calibration of each hot-wire probe where

$$A_m = \frac{\overline{\rho u}\, d(\bar{e})}{\bar{e}\, d(\overline{\rho u})}$$

The calibration was performed by locating the hot-wire probe on the centerline of the jet near the nozzle exit and varying local $\overline{\rho u}$ by adjusting the upstream stagnation pressure. Measurements of $\bar{e}$ were then made with T_w held constant. Values of A_m were found to be negligibly affected by changes in overheat and to be primarily a function of mean ρu. This result is similar to findings observed by Rose in a supersonic boundary layer study (60).

D. Acoustic Measurements

Since acoustic measurements were performed in a low density environment, the reference pressure used to calculate the standard sound pressure level (SPL) in dB was scaled by the ratio of the chamber pressure to standard atmospheric pressure. The equation used to calculate SPL is given by

$$SPL = 20 \log_{10} \frac{(p')rms}{2 \times 10^{-5} (P_{ch}/P_{atm})}$$

E. Cross-Correlation and Phase Averaging

The fluctuation signal from a sensor probe can always

be approximated by the Fourier series expansion:

$$f(t) = \frac{A_o}{2} + \sum_{n=1}^{\infty} a_n \cos(n\omega t) + b_n \sin(n\omega t)$$

$$= \sum_{n=-\infty}^{\infty} C_n e^{in\omega t}$$

where a_n and b_n, or C_n represents the amplitude of a harmonic component, t is time, ω is the fundamental frequency, $n\omega$ is the frequency of a harmonic, and the product of $n\omega t$ can be interpreted as the phase angle of a harmonic. $A_o/2$ is actually the mean, and the terms within the summation are fluctuations.

As pointed out clearly by the Fourier series, we require amplitude, frequency and time to describe a signal precisely. The conventional measurement electronics which typically measure the mean, or the root-mean-square amplitude of the fluctuation portion of a signal, yield quantities with no time or phase identity. In order to describe a signal completely, the time information must be established. This can be achieved by cross-correlation which is mathematically expressed as

$$R_{12}(\tau) = \int_{-\infty}^{\infty} f(t)\, f(t - \tau)\, dt$$

When two pure tone signals of identical frequency are cross-correlated, the τ value which yields maximum R_{12} gives relative time, hence phase information. Experimentally, this can be realized by using digital electronics to perform short time averaged cross-correlations on two predominantly

pure tone signals. The two signals can be obtained by placing two sensor probes at different locations and band-pass filtering the sensor signals around the frequency of interest. An alternative method is using artificial excitation of the flow fluctuations and cross-correlating the band-pass filtered sensor signal with the exciter signal to obtain relative phase information.

The amplitude of a fluctuation quantity can be decomposed into

$$f(t) = \overline{f} + \widetilde{f}(t) + f''(t)$$

where $\overline{f}$ is the mean (time averaged), $\widetilde{f}(t)$ is the organized wave (coherent) portion, and $f''(t)$ is the random contribution. Conventional measurement electronics can not separate the coherent portion of the signal, $\widetilde{f}$, from overall fluctuations sensed by a sensor probe. However, by introducing a special form of cross-correlation (called phase averaging), an experimentalist can determine $\widetilde{f}$ quite precisely. The phase averaging is expressed as

$$\langle f(\tau) \rangle = \lim_{N \to \infty} \frac{1}{N+1} \sum_{n=0}^{N} \int_{-\infty}^{\infty} f(t)\, \delta\,(t-nb-\tau)\,dt$$

where $f(t)$ is the signal being phase averaged. N and n are integers, δ is the Dirac Delta function, t is time, b is the period of a coherent fluctuation component, and τ is the amount of time shift. Since the random fluctuations average

to zero, phase averaging yields

$$\langle f(\tau) \rangle = \overline{f} + \widetilde{f}(\tau)$$

If the mean is subtracted from this equation, only the organized (coherent) portion remains. In this manner the coherent fluctuations can be extracted from the full signal.

CHAPTER IV

RESULTS OF FLOW FIELD MEASUREMENTS

A. Mean Flow Field

The centerline Mach number distributions for both low Reynolds number underexpanded M=1.4 and 2.1 jets were determined by Pitot and static pressure measurements and are shown in Figures 6 and 7 (pp. 83-84). These data show that the central region of both jets accelerates to considerably above the fully expanded jet Mach number within a very short distance from the nozzle exit, then the jets experience a series of deceleration and accerlation due to the presence of shock cells. The modulation of the centerline Mach number of the low Reynolds number Mach 1.4 underexpanded jet appears to be relatively mild, of short-duration, and supersonic throughout. The Mach 2.1 jet on the other hand encounters severe modulation due to the presence of shock cells and a strong Mach disc which leaves a subsonic core extending to five jet diameters from the nozzle exit.

An artistic impression of the shock cell structures was established by considering the axial static pressure distributions, hot-wire mean voltage data, and the optical evidence obtained by Schlieren photography. Schematic diagrams of these structures are depicted in Figure 8 and

Figure 9 (pp. 85-86) for the underexpanded Mach 1.4 and 2.1 jets respectively.

The shock structure of underexpanded jets has been known in general terms for many years. As the air exhausts from a choked convergent nozzle, it goes through a Prandtl-Meyer expansion fan, expanding to the ambient pressure at the jet boundary. The internal reflections of these expansion waves from the free boundary of the jet cause many compression waves to be sent back into the flow. Some of these reflected compression waves coalesce to form a shock wave. Due to the intersection of expansion and compression waves, regions of wave reinforcement and cancellation are formed resulting in regions of expansion (e), neutral (n), and compression (c) which returns the flow to an underexpanded state quite similar to that at the nozzle exit.

For slightly underexpanded jets, such as the M=1.4 jet shown in Figure 8, intercepting shocks meet at the centerline of the jet forming the familar diamond-shaped cell structure. As the pressure ratio across the nozzle is increased, such as the case in the M=2.1 underexpanded jet, the intercepting shocks no longer meet at the centerline but are connected with a normal shock, or Riemann wave, as pictured in Figure 9. In both cases, expansion waves reflect as compression waves, and vice versa, to preserve the constant pressure along the jet boundary, and the whole process is repeated. The repetition is continued until

viscous effects cause shock structure to lose its identity.

The shock cell pattern of these low Reynolds number jets is basically the same as that found previously for high Reynolds number choked jets. (See, for example, Reference 19.) Also, the shock cell spacings in these low Reynolds number underexpanded jets agree with those spacings obtained by other researchers, such as Seiner and Norum (45), in high Reynolds number underexpanded jets. (Proper accounting must be taken of the difference between jet exit diameter d and the effective diameter D used in this study.)

Pitot and static pressure surveys were also performed at various axial and radial locations in both jets in order to determine the Mach number distributions and map the flow fields. A few of the Mach number profiles of both jets are presented in Figure 10 and Figure 11 (pp. 87-88). When these profiles are compared to the meam Mach number profiles of perfectly expanded jets (51), significant differences are evident. The underexpanded jets have a lower velocity core and higher velocity annulus downstream from the end of the first shock cell and extending several diameters downstream. As the jet progresses downstream, the Mach number difference between the core and annulus diminishes, and simultaneously the Mach number profile changes into a Gaussian shape near where the shock structure disappears.

B. Reynolds Number Dependence of Fluctuations

Although McLaughlin, Morrison and Troutt (29, 52, 53) reported that low Reynolds number perfectly expanded supersonic jets display flow and acoustic properties similar to reported high Reynolds number measurements, there is a need to demonstrate that the low Reynolds number approach is still adequate in the underexpanded regime to model conventional high Reynolds number counterparts. The flow and acoustic properties undergo significant modifications in underexpanded jets due to the presence of shock structures, so that the equivalence of low and high Reynolds number supersonic jets determined previously (29) needs to be investigated again in the shock containing jet condition. Presented in the earlier section was convincing evidence substantiating the fact that in the underexpanded jet case a change in Reynolds number does not introduce noticeable change into the mean flow field. Discussed hereafter is the Reynolds number dependence of flow fluctuation and acoustic properties of shock-containing jets.

As part of this investigation, measurements of flow fluctuation spectra and acoustic spectra were obtained with hot-wire and microphone probes using a convergent nozzle to exhaust jets from Mach 0.9 to 2.1 at low Reynolds numbers ($Re < 15{,}000$). Typical spectra are quite similar to the ones presented in Figure 13 (this will be discussed in more detail later) which posses large peaks that are

characteristic of both shock screech tones and of natural instabilities in low Reynolds number jets. In all cases above a jet Mach number of 1.0, the peaks in the flow fluctuation and acoustic spectra occur at identical frequencies.

Figure 12 (p. 89) plots the frequency of dominant fluctuations as a function of Mach number. Also included in the figure are the dominant instability frequencies of perfectly expanded low Reynolds number jets (51), and shock screech tones of conventional high Reynolds number jets (46). The most striking correlation as shown in the figure is that at Mach numbers above 1.2, the Mach number dependence of the dominant fluctuation frequency in the present study is almost identical to that corresponding to the natural instability frequency of low Reynolds number prefectly expanded jets and the shock screech tones of conventional high Reynolds number jets. These data suggest that the large-scale structure of the low Reynolds number underexpanded jets is similar to that of conventional high Reynolds number jets that are undergoing screech.

C. Fluctuation Flow Field

C.1 Spectral Content

Figure 13 (p. 90) shows several flow fluctuation spectra obtained by a hot-wire probe in the shear layer of the low Reynolds number Mach 1.4 underexpanded jet. These spectra indicate that two large amplitude discrete peaks

centered at a Strouhal number St=0.21 and 0.37 dominate the initial fluctuations. As the flow progresses downstream, the St=0.21 component and several other peaks are found to appear and disappear from the spectra. The St=0.37 component grows much faster than other components and dominates the flow fluctuations from the nozzle exit until approximately x/D=5 to 6. As shown in Figure 6 (p. 83), this is also the location where the shock structures disappear from the mean flow data indicating that the evolution of the St=0.37 fluctuations is related to the strength of shock cells. Around x/D=6, the St=0.21 component has grown to its maximum amplitude and dominates the fluctuations for several diameters downstream. At approximately x/D=10, the fluctuation spectrum becomes fully developed. Flow fluctuation distributions discussed in the following section provides a quantitative description of these spectral evolutions. The production of discrete frequencies and the rapid broadening of spectra downstream of x/D=3 indicate stages of non-linear spectral interaction processes as previously observed by several investigators.

The flow fluctuation spectra of the low Reynolds number Mach 2.1 underexpanded jet, shown in Figure 14 (p. 91), display a similar behavior as described above, except there is an increase in the number of large amplitude discrete peaks which persist over a longer distance, and the dominant instability is now the St=0.17 component throughout.

C.2 Evolution of Flow Fluctuations

Flow fluctuation measurements were performed with a traversing hot-wire probe in the shear layer along a constant radial location of r/D=0.5. Shown in Figure 15 (p. 92) is the evolution of the overall fluctuations (frequency band width St=0.04 to 1.2), and Figure 16 (p. 93) are the evolutions of the two dominant spectral components (1/3 octave band-pass filtered St=0.21 and 0.37) of the M=1.4 jet. The overall fluctuations are initially dominated by the St=0.37 component and grow approximately exponentially for the first 2.5 jet diameters, saturate between x/D=3 to 4, and then decay steadily.

Accompanying the saturation and decay is an expansion of the shear layer thickness and the production of broadband fluctuations (turbulence). A few diameters downstream from the satuation, the mean Mach number profile changes into a Gaussian shape. Note also that the initial fluctuations of this jet are concentrated at St=0.37 which represents over 70% of the total fluctuation energy and grows at almost the same rate as the overall fluctuations. However, the St=0.37 component decays much faster after satuation leaving the St=0.21 component to dominate the flow fluctuations between x/D=6 and 7. When Figure 16 is studied together with the mean flow data (Figures 6 and 8), it is apparent that the St=0.37 component rises and falls with the shock cell structures much more than the St=0.21 component does. This indicates that the St=0.37 instability preferentially

interacts with the shock cells. Azimuthal measurements discussed in a latter section suggest that this natural selection mechanism prefers instabilities of helical ($n=\pm1$) modes.

The sharp growth and decay of the flow fluctuations characterize the evolution of large-scale instabilities in the jet flow field, and the spectral broadening and shear layer thickening are typical of non-linear interaction which has been established for many years. The modulation of the flow fluctuation amplitude is evident especially in the initial growth region of the evolution. This modulation is coincident with the shock cell spacing and qualitatively characterizes the interaction between the shocks and the large-scale structure. In general, this evolution is similar to the instability evolution previously established in a low Reynolds number Mach 1.4 perfectly expanded jet except that the underexpanded jet data has an apparent upstream shift of the axial position where the fluctuations saturate.

The instability evolution of the Mach 2.1 underexpanded jet (Figure 17, p. 94) displays a similar behavior as aforementioned with a slightly stretched length scale associated with the higher mean flow velocity and more pronounced modulation of the fluctuation amplitude in the initial growth part of the evolution due to the presence of shock cells. The saturation of flow fluctuations in this M=2.1 jet occurs near x/D=5 to 7, the Gaussian mean flow

profile appears near x/D=9 to 10, and fully turbulent spectrum developes around x/D=15. The growth of the shear layer thickness and the production of broad band turbulence are evident down stream of x/D=7 where the flow fluctuations saturate and start to decay. Two band-passed components are shown in Figure 18 (p. 95). The dominant instability component (St=0.17) follows almost the same evolution as the overall fluctuations and dominates the entire fluctuation field before x/D=15. This St=0.17 component is also found to be primarily composed of helical ($n=\pm 1$) modes as presented in a latter section. The St=0.45 component, although of much smaller amplitude, grows and decays following the basic trend as the other component, and is included for latter comparison.

To understand the influence of the shock structure on the low Reynolds number jets, direct comparisons were made of the flow fluctuations of underexpanded and perfectly expanded jets. Figure 19 (p. 96) presents the axial evolution of overall mass velocity fluctuations of the two M=1.4 jets under identical operating conditions. These data were obtained at the radial location where the overall fluctuations maximized which is approximately the center of the shear layer. The fluctuations in the two M=1.4 jets have almost the identical growth rate and similar evolution. However, the significant difference is that the underexpanded jet has much stronger initial fluctuations which saturate and begin to decay considerably upstream of

the corresponding data in the perfectly expanded jet. The stronger initial fluctuations also cause a premature saturation with a peak amplitude slightly lower than the peak in the perfectly expanded jet case.

A similar comparison were made for the M=2.1 underexpanded and perfectly expanded jets, and are shown in Figure 20 (p. 97). The fluctuations in the underexpanded M=2.1 jet have a slightly higher initial growth rate and an upstream shifted saturation when compared with the data in the perfectly expanded case. These apperent changes demonstrate the influence of shock cells on the development of flow fluctuations.

C.3 Growth Rates of Fluctuations

The growth rates of flow fluctuations were determined for both jets following Morrison and McLaughlin (52) as shown in Table II (p. 130) which will be discussed further in latter sections. The growth rates of perfectly expanded jets are known to have a Mach number dependence which is a trend of decreasing growth rate with increasing Mach number. The growth rates of these underexpanded jets shown in the tabel display a similar trend. The fluctuation growth rates of perfectly expanded jets are also known to have a Strouhal number dependence which is a trend of increasing growth rate with increasing Strouhal number. The growth rates of the Mach 1.4 underexpanded jet seem to follow this basic trend quite well, but the growth rates of the Mach number 2.1

underexpanded jet depart from this trend completely.

D. Coherent Instability Measurements

In order to investigate the nature of coherent fluctuations, it is essential to establish a time and hence phase standard in the measurements. (This is explained in Chapter III, E.) One of the well-proven techniques to establish a precision time standard is to artificially excite the jet using a pure tone signal driving a glow discharge exciter (Chapter II, A.2). Other than establishing a time reference, an added advantage of using excitation is that the frequency that the jet's natural selection mechanism prefers can be easily determined. However, this excitation technique should be used prudently, since the short-coming of excitation is that the jet's natural flow and acoustic properties may be changed if excessively excited. Hence before coherent experimental data can be considered representative of what the natural properties are, the excited flow and acoustic fields must be demonstrated to have minimal departure from the natural processes.

In all of the excited low Reynolds number experiments reported in this study, the exciter power output was controlled at a constant level and was less than 0.15% of the jet's exit kinetic energy flux. The effect of excitation on the acoustic field is presented in Chapter V, and the effect of excitation on the flow fluctuations is

reported in the following section.

D.1 Effects of Excitation on Flow Fluctuations

Figure 21 (p. 98) presents hot-wire frequency spectra obtained at a constant radial location of r/D=0.5 and at successive downstream stations in the M=1.4 jet with the jet excited at St=0.37. The effect of excitation as seen from these spectra is an enhancement of the fundamental forcing frequency and its second harmonic, and suppression of other spectral components. Over the initial region of the jet, the fundamental develops in a fashion resembling its natural counterpart reaching saturation near x/D=3 and decays steadily afterwards. The evolution of the second harmonic is largely limited to the first 4 to 5 jet diameters, similar to the natural jet case. At approximately x/D=9, the frequency spectrum is fully turbulent. These spectra are typical of excited spectra for both the M=1.4 and 2.1 jets excited at several instability frequencies, the only difference being that at lower excitation frequencies more harmonics appear.

The axial distribution of streamwise mass velocity fluctuations of two excited fluctuation components in the M=1.4 jet are shown in Figure 22 (p. 99). The corresponding data for the M=2.1 jet are shown in Figure 23 (p. 100). These data were taken with a 1/3 octave band-pass filter centered at the frequency of excitation, and the hot-wire

probe was positioned approximately at the center of the shear layer where the band-passed signal maximized. As a consequence of excitation the initial region of exponential growth for a given fluctuation component is bypassed. Overall, the excited components display similar evolutions to their natural counterparts except for an enhanced initial fluctuation amplitude followed by a faster rate of decay. Further, these axial and spectral evolutions are closely analogous to reported measurements in perfectly expanded jets, such as those established by Troutt and McLaughlin (30), and Morrison (51).

By exciting the underexpanded jets, an important discovery was that the jets unstable frequencies were sharply tuned (within $\pm$ 0.5%) at the frequency of natural instabilities. Excitation with a frequency other than the natural unstable frequencies yielded extremely poor coherence. When the frequency of excitation was properly adjusted, both the flow and acoustic fluctuations responded well to excitation, but a stable phase-lock relation between the exciter signal and the sensor fluctuation signal was sometimes impossible to establish, particularly in the jets' acoustic field.

This suggests that low Reynolds number underexpanded jets have a sharp but nonstationary natural selection mechanism which introduces random frequency modulation into each instability component thus making artificial excitation with a pure tone signal difficult to phase-lock the flow and

acoustic fluctuations. Due to this difficulty, some of the correlation measurements reported in this study were accomplished by using two-probe cross-correlation with the jet unexcited.

To summarize, aritficial excitation does not significantly alter the flow fluctuation properties. However, the excitation does provide a phase reference which enables the relative phase of the dominant spectral components of flow fluctuations to be determined. Such phase data are invaluable in establishing the physical features of the noise generation process.

D.2 Axial Phase Measurements

The characterization of coherent instabilities requires the determination of their axial wave length and phase velocity other than growth and evolution properties. Hence axial phase measurements were performed for several instability components by exciting the jets and then measuring the relative phase difference between the excitation signal and the band-passed hot-wire signal. Results of such measurements with the low Reynolds number underexpanded Mach 1.4 jet excited at St=0.21 and 0.37, and with the Mach 2.1 underexpanded jet excited at St=0.17 and 0.45 are shown in Figure 24 (p. 101) where the relative phase difference is plotted as a function of axial distance. Over the first few diameters, the phase angle of excited coherent fluctuations changes approximately linearly with

downstream distance. The wavelength of the excited coherent fluctuations was determined by the slope of the fitted straight line, and the phase velocity was then calculated from the frequency and wave length by the relation $c=\lambda f$. The resulting wave properties of major spectral components of both jets, tabulated in Table II (p. 130), indicate that large-scale instabilities are traveling at around 0.6 of the fully expanded jet exit velocity. This is virtually identical to the findings previously established in perfectly expanded jets (51).

It is worthwhile to note that Tam in one of his early theories (32) used the weak shock structure as the natural selection mechamism of flow instabilities and predicted a linear relation between the axial wave number (k_r) and Strouhal number (St). This linear relation appears also true for underexpanded jets, since Morrison (51) and the present study demonstrate that large scale fluctuations of different frequencies are traveling at approximately the same speed in low Reynolds number jets. Following Tam's suggestion, an empirical correlation was established by considering the data obtained by the present study and Morrison (51). This leads to

$$k_r D = -0.00865 + 10.8\ St$$

To further demonstrate that the excitation technique gives a realistic estimate of the wave properties of natural coherent structures, the phase velocity of the St=0.37

component in the M=1.4 jet was determined by the above method and then by hot-wire/microphone cross-correlation with the jet unexcited. The latter method used a stationary microphone positioned at 40 diameters from the nozzle exit and at the radial location of maximum noise emission to provide the timing reference. The resulting phase velocity (c=0.62U) differs only slightly from the phase velocity (c=0.55U) obtained by the method of artificial excitation, and demonstrates that the excitation does not introduce significant change into the jet's flow field. Furthermore, this phase velocity of 0.62 U is in exact agreement with the phase velocity obtained optically by Harper-Bourne and Fisher (43) in a conventional high Reynolds number Mach 1.41 underexpanded jet. This provides additional evidence that the low Reynolds number jets are behaving somewhat similarly to high Reynolds number jets.

D.3 Coherent Wave Evolution

Depicted in Figure 25 (p. 102) is the axial evolution of coherent mass-velocity fluctuations of the St=0.37 instability component in the shear layer of the M=1.4 jet, and Figure 26 (p. 103) are the corresponding data of the St=0.45 component in the M=2.1 jet. These data were measured by band-pass filtering the hot-wire signal around the frequency of excitation and then phase averaging the signal, and the measurement station in the shear layer was chosen at the position of maximum band-passed signal. The

amplitude of the coherent fluctuations oscillates through shock cells and saturates at approximately the same axial location as the natural band-passed fluctuations. However, the coherent fluctuations decay much faster after saturation than in the natural jet case. Similar decay behavior was also observed in perfectly expanded jets (30, 51), and postulated by Liu (34) as an important noise generation mechanism.

D.4 Azimuthal Behavior of Instabilities

It is important to understand the azimuthal behavior of coherent fluctuations especially to instability analyses. Tam (32) in his 1972 analysis assumed that the dominant fluctuations in supersonic jets were helical ($n=\pm 1$) modes which were single thread left and right hand helices. Optical evidence established by Schlieren photography and Shadowgraph supporting this idea emerged from perfectly expanded jets as well as underexpanded jets (32, 50). However, the few published quantitative experimental data describing the azimuthal behavior of coherent fluctuations were devoted to perfectly expanded jets only, and were rather primitively interpreted by a trial and error method (30, 51). So the author undertook the development of a reliable data analysis scheme in addition to experiments providing azimuthal data for underexpanded jets.

As part of this study, an efficient and reliable analysis was developed and proved valuable to interpret the

azimuthal behavior of coherent fluctuations. This analysis was based upon the elementary instability solution model, and is reported in detail in Appendix A. The experimental part of this study was conducted by cross-correlating a time reference signal with the signal from a traversing microphone located at various azimuthal angles (θ). The time reference signal was usually obtained from a stationary microphone positioned at the same axial station as the traversing one. Signals from both microphones were 1/3 octave band-pass filtered around the frequency of interest, and the jet was unexcited. This was due to the fact that the artificial excitation of low Reynolds number underexpanded jets often failed to establish stable phase-lock relation between the exciter signal and microphone signal, and introduced considerable uncertainty into the measurement. The traversing microphone was located at the axial station where the acoustic signal maximized, and was driven along a cylindrical circle of constant radius (r) just outside the flow field.

In this manner, the azimuthal distribution of the relative phase and coherent (phase averaged) amplitude were measured and then Fourier analyzed following the method described in Appendix A to establish the azimuthal modal composition of coherent fluctuations. A few samples of such experimental data and results of the analysis are shown in Figures 27-30 (pp. 104-107) for dominant fluctuations in the M=1.4 jet. The measured coherent amplitude data are

normalized by the maximum coherent amplitude on the circle, and the resulting azimuthal modal "spectrum" are normalized by the complex value of the n=0 mode (axisymmetric varicose). When the n=0 mode is absent from the spectrum, the mode of the largest amplitude is selected as the normalization reference.

The St=0.37 fluctuations which interact strongly with the shocks in the M=1.4 jet are primarily composed of helical ($n=\pm1$) modes of instabilities as shown in Figures 27 and 28 (pp. 104-105). On the other hand, the St=0.21 fluctuations which develop much slower in the M=1.4 jet than the St=0.37 component are predominantly axisymmetric varicose (n=0) as shown in Figures 29 and 30 (pp. 106-107). The St=0.17 component of instability which dominates the flow fluctuations in the M=2.1 jet is also concentrated at $n=\pm1$ modes when investigated by the same procedure. Additional azimuthal measurements (reported in Chapter V, E.4) established with a moderate Reynolds number M=1.6 underexpanded jet demonstrate that $n=\pm1$ are the dominant instability modes. These findings provide quantitative evidence to describe the large structure behavior previously visualized by a number of researchers, and suggest that the natural selection mechanism in supersonic underexpanded jets prefers helical ($n=\pm1$) modes of instabilities.

CHAPTER V

RESULTS OF ACOUSTIC MEASUREMENTS

A. Acoustic Spectral Content

Presented in Figure 31 (p. 108) are the spectral analysis of the microphone signal in the near acoustic field of the M=1.4 jet at successive downstream locations along a constant radial coordinate. The acoustic field of this jet is dominated by large amplitude discrete peaks centered at St=0.21 and 0.37, and the spectra show a shift toward lower frequency content as downstream distance is increased. This is in general agreement with the corresponding hot-wire spectra reported earlier.

Similar spectral measurements were also performed for the M=2.1 jet and are shown in Figure 32 (p. 109) which display a similar trend as mentioned above. When these acoustic spectra are studied together with the flow fluctuation data discussed in Chapter IV, it is apparent that the acoustic field of low Reynolds number supersonic underexpanded jets is dominated by shock screech tones which are produced by large-scale instabilities in the jets. However, due to the fact that low Reynolds number suppresses broadband fluctuations in the flow field, the presence of the broadband shock noise cannot be clearly identified from

these spectra. This suggests that in the case of underexpanded jets the results of the low Reynolds number experiments are characteristic of shock screech phenomenon only.

B. Sound Pressure Level Distributions

Sound pressure level (SPL) contours of the overall noise and the St=0.37 component which dominates the near acoustic field of the M=1.4 jet are shown in Figures 33 and 34 (pp. 110-111), while the sound pressure level contours of the overall noise and the St=0.45 acoustic component of the M=2.1 jet are depicted in Figures 35 and 36 (pp. 112-113). In terms of shape and amplitude, these contours bear a strong resemblance to the sound pressure level contours previously established with perfectly expanded jets at similar Mach and Reynolds numbers (51). The only noticeable difference (particular at M=2.1) is an upstream shift of the contour lobes in the underexpanded data which is no doubt a consequence of the increased initial fluctuations and resulting saturation of the instability closer to the nozzle exit.

To understand the influence of the shock cells on the low Reynolds number jets, direct comparisons were made of the radiated noise of underexpanded and perfectly expanded jets. Figure 37 (p. 114) shows the sound pressure level directivity of the two M=1.4 jets while Figure 38 (p. 115) shows the data for the M=2.1 jets. These directivity

measurements were made with a microphone traversed along an arc (R) 30 effective diameters from the nozzle exit.

These directivity data show a slight increase in the sideline (90 deg.) radiated noise associated with underexpanded jets. The increase, however, is nothing like that experienced in the shock associated noise of conventional high Reynolds number jets (44, 46). The apparent excess noise in the downstream direction of the M=2.1 perfectly expanded jet in comparison with its underexpanded counterpart is a result of the center of the dominant noise generation region being further downstream in the jet. This is shown to be the case in acoustic phase front measurements presented in the next section.

The mean flow measurements presented in the previous chapter showed significant differences between the low Reynolds number underexpanded and perfectly expanded jets (particularly at M=2.1). However, the radiated sound fields are not significantly different. More detailed acoustic measurements helped to sort out this apparent anomaly.

C. Acoustic Phase Front Measurements

Previous observations suggested that the acoustic phase front measurement could reveal valuable information to establish the link between flow fluctuations and acoustic radiation, and discover the nature of the noise production mechanism. This experimental investigation involves cross-correlating a time reference signal with the signal (band

pass filtered around the frequency of interest) from a traversing microphone at various locations in the acoustic field to establish contours of constant relative phase. By tracing lines normal to the acoustic phase fronts, one can determine the direction of acoustic propagation and possibly discover the acoustic source locations.

Figure 39 (p. 116) are the resulting data from one such measurement which show the acoustic phase front distributions of the St=0.37 component in the near acoustic field of the M=1.4 jet. These data were obtained by two-microphone cross-correlation with the jet unexcited, while the time reference signal was established by band-pass filtering the St=0.37 signal from a stationary microphone positioned at the maximum noise emission angle. This figure together with the sound pressure level contours (Figure 34, p. 111) demonstrate that the dominant acoustic production region is located between x/D=3 to 4. As presented earlier, this is also the axial location where the large-scale St=0.37 flow fluctuations saturate and start to decay. The acoustic phase front distributions of the St=0.45 component of the M=2.1 jet were determined using artificial excitation to establish the time reference (Figure 40, p. 117). The dominant noise production region of this component also coincides with the axial location where the St=0.45 flow fluctuations saturate and begin to decay. When these data are compared with the corresponding data previously established in perfectly expanded jets (51), the dominant

noise location in these underexpanded jets shows a shift upstream which is a consequence of stronger initial fluctuations and the resulting satuation of flow fluctuations closer to the nozzle exit as mentioned earlier.

The experimental evidence established here demonstrates that the satuation and decay of large-scale fluctuations play an important role in the acoustic production similar to screech of conventional high Reynolds number underexpanded jets. Further, this is the same mechanism identified by Morrison and McLaughlin (53) as dominating the low Reynolds number perfectly expanded noise generation process.

D. Excited Acoustic Measurements

To provide further understanding of the role played by large-scale instabilities in the shock noise production process, the jets were excited and the resulting acoustic properties measured. The effect of excitation on acoustic spectral content was very similar to that previously described on flow fluctuation spectra. A slight enhancement concentrated at the fundamental forcing frequency and its harmonics was evident, but other frequency components were suppressed, so the excited acoustic field was little changed in the overall (St=0.04 to 1.2) noise production as shown in Figure 41 (p. 118) which will be discussed in more detail later.

All of the excited experimental data discussed so far were obtained with the traditional single electrode

excitation device, however, near the latter part of this research, Politte (61) demonstrated that excitation of low to moderate Reynolds number supersonic jets with two-electrodes, which were positioned 180 degrees apart near the nozzle exit, provided a very good method of separating the axisymmetric varicose (n=0) and the helical ($n=\pm1$) modes of jet instability. Excitation with two electrodes driven in phase with each other produced primarily an n=0 disturbance, and with the electrodes driven out of phase with each other, an $n=\pm1$ disturbance dominated the flow fluctuations. This newly proven excitation technique was then implemented on a few acoustic directivity experiments with the M=1.4 underexpanded jet excited at St=0.37.

By performing phase averaging measurements at various observer angle (β) along an arc (R) of 30 effective diameters, the coherent sound pressure level distributions were determined with either method of excitation and are illustrated in Figure 42 (p. 119). These data undoubtedly demonstrate the powerful noise production capability of the $n=\pm1$ modes of flow fluctuations, and the sharp rejection of the natural selection mechanism to the n=0 mode of flow fluctuations. (Recall from Chapter IV, D.4, azimuthal behavior of instabilities, that the mean flow field naturally prefers $n=\pm1$ modes of fluctuations.)

Another perhaps rather surprising result from these dual-electrode experiments was that the excited overall acoustic directivity distributions were independent of the

method of excitation (i.e. either with single electrode, two electrodes in phase, or two electrodes out of phase). This is demonstrated in Figure 41 (p. 118). If the interaction of shocks with coherent flow fluctuations were representative of the broadband shock noise production, then when the $n=\pm 1$ modes of coherent fluctuations were enhanced by the electrodes, there should have been an increase in the overall noise production. On the other hand, when the n=0 mode was enhanced, the overall noise should have been suppressed, since the shock-containing mean flow field is less unstable to this mode of fluctuations. The data presented in Figure 41 fail to support these conjectures and suggest that the production of broadband shock noise is not related to large-scale coherent flow fluctuations.

E. Additional Measurements At Moderate Reynolds Number

E.1 Experimental Philosophy

The fact that the acoustic properties of the low Reynolds number underexpanded jets and perfectly expanded jets are so similar indicates that these measurements do not provide direct information on the process normally refered to as the broadband shock associated noise which reportedly has more practical significance than the screech. Hence it is appropriate to perform a number of acoustic measurements at a significantly higher Reynolds number, so the broadband shock noise can be better characterized.

The experimental objectives were directed towards: 1) the characterization of the general features of shock associated noise, and 2) the determination of the relevance between large-scale coherent flow fluctuations and shock associated noise, particularly the broadband shock noise. The experimental techniques involved including spectral analysis, acoustic directivity measurements, azimuthal modal analysis, and dual-electrode excitation.

The experimental conditions were chosen as M=1.6 underexpanded jet exhausted from a convergent nozzle and at Re=68,000 which were largely dictated by experimental apparatus limitations. (The Mach number refers to the Mach number that would be achieved with a perfectly expanded jet operating at the same pressure ratio.) At these jet conditions, the excitation device required 20 times more power than that experienced previously, since the power requirement was primarily a function of the air density which was increased substantially. However, due to the increased mass flow rate at Re=68,000, the exciter power output only corresponded to approximately 0.4% of the jet's exit kinetic energy flux, and will be shown later that the excitation introduced insignificant change to the acoustic field.

E.2 Acoustic Spectral Evolutions

Figure 43 (p.120) shows several acoustic spectra measured along an arc radius (R) of 30 effective diameters

at increasing observer's angle (β) in the acoustic field of this M=1.6 underexpanded jet. When these spectra are compared to the corresponding low Reynolds number measurements, it is apparent that only the shock screech tone (centered at St=0.3) and its harmonics are present along with increased broadband noise; all other smaller spectral peaks appearing at low Reynolds numbers are eliminated. Also included in the figure is the empirical prediction of Harper-Bourne and Fisher (43) for the peak frequency of broadband shock noise. This frequency reportedly increases (44) as the observer angle (β) decreases which is a trend contrary to the spectral evolution of perfectly expanded jets. At observer angles greater than 50 degrees, the broadband noise produced by this underexpanded M=1.6 jet displays a spectral peak whose frequency is in general agreement with the prediction and with reported high Reynolds number measurements (44). Such broadband spectral evolution was hard to detect from low Reynolds number experiments. This indicates that the M=1.6 Re=68,000 underexpanded jet provides a more realistic model than low Reynolds number jets for broadband shock noise experiments.

E.3 Acoustic Directivities, Natural Jets

A direct comparison of the sound pressure level directivities is made between the underexpanded jet and a perfectly expanded jet of identical Mach and Reynolds

numbers along the same arc radius (R) of 30 effective diameters as shown in Figure 44 (p. 121). This figure clearly demonstrates that the underexpanded jet radiates much louder noise than the perfectly expanded jet near the 90-degree sideline indicating increased noise radiation toward the upstream direction which is characterstic of the shock associated noise as reported by other investigators.

E.4 Azimuthal Behavior of St=0.3 Fluctuations

It is essential to establish the natural azimuthal behavior of large-scale coherent flow fluctuations before using dual-electrode excitation. The azimuthal measurements presented here was obtained following closely the experimental technique described in the previous chapter where two-microphone cross-correlation was used with the jet unexcited. Shown in Figure 45 (p. 122) are the experimentally measured azimuthal phase and coherent amplitude distributions, and shown in Figure 46 (p. 123) is the output of the azimuthal modal analysis which establishes that the natural St=0.3 component of instability is primarily composed of helical ($n=\pm 1$) modes. These data support the previous assumption that the helical modes are more unstable in the shock containing mean flow field.

E.5 Effect of Excitation on the Acoustic Field

Figure 47 (p. 124) presents a direct comparison between the natural acoustic spectrum and its excited counterpart at a fixed station in the near acoustic field of the M=1.6 jet. The jet was excited with two electrodes driven out of phase with each other at the frequency of shock screech tone (St=0.3). The major effect of excitation on the spectral distributions is a change of amplitude of the St=0.3 component and its harmonics, and an insignificant suppression of the broadband components. These spectra are representative of the spectra measured at various stations with either method of excitation, and seem to suggest that the coherent fluctuations are not responsible for the broadband shock noise production.

Recall from previous low Reynolds number experiments that the excitation was often ineffective in establishing stable phase-lock relation between the acoustic signal and excitation signal indicating the excitation failed to eliminate the natural phase randomness of large-scale fluctuations. Surprisingly, this difficulty of phase randomness does not exist at this moderate Reynolds number. The jet's most unstable frequency was found to be St=0.3 $\pm$3% by using artificial excitation and measuring the resulting acoustic production. When compared with the corresponding low Reynolds number properties, this information suggests that the sharply tuned natural selection mechanism is

somewhat nullified by an increase in Reynolds number.

E.6 Excited Acoustic Directivities

The moderate Reynolds number M=1.6 jet was artificially excited with dual electrodes driven in and out of phase. At an arc radius (R) of 30 effective diameters, the excited overall sound pressure level was measured, and the resulting data are presented in Figure 48 (p. 125). Also included in this figure are the natural sound pressure level distributions for comparison. These data demonstrate that the excited acoustic directivity distributions are independent of the excitation method, and are not significantly different from the natural data. Near the 90-degree sideline, the excited sound pressure level shows an insignificant increase which is primarily due to enhanced higher homonics. The broadband noise is little changed.

By exciting the jet and phase averaging the microphone signal, the coherent portion of the acoustic radiation directly caused by the excited flow fluctuations was determined. Figure 49 (p. 126) shows the St=0.3 coherent sound pressure level directivities at the same probe stations as aforementioned. Unexpectedly, with either n=0 or $n=\pm 1$ modes of excitation, almost the same coherent sound pressure level was recorded. (Recall from E.4 that the $n=\pm 1$ modes dominate the natural instabilities.) The only difference between the two sets of data obtained by different modes of excitation is a change in the amplitude

distributions.

Over most of the acoustic field, the coherent St=0.3 component represents over 87% of the narrow bandpass filtered acoustic energy centered at this frequency, and near the 30-degree station, the coherent component represents over 80% of the overall acoustic energy. Hence the powerful noise production capability of large-scale coherent flow fluctuations is again demonstrated.

Previous acoustic measurements performed with dual-electrode excitation on low Reynolds number underexpanded jets established that in these jets the natural instability process has a very selective mechanism in the frequency and azimuthal mode of preference. The experimental data presented here indicate that the natural selection mechanism is less discriminatory in the moderate Reynolds number jet.

Based on the findings derived from the above experiments, it is apparent that the large-scale coherent fluctuations are directly responsible for the shock screech production, but of little importance in the broadband shock noise. This concludes the acoustic measurements.

CHAPTER VI

CONCLUSIONS

The present study was devoted to the fundamental jet noise experimental research on underexpanded supersonic jets with the special emphasis on determining the role played by large-scale organized flow fluctuations in the flow and acoustic processes. The experimental conditions of the present study were chosen as low Reynolds number (Re=8,000) Mach 1.4 and 2.1, and moderate Reynolds number (Re=68,000) Mach 1.6 underexpanded supersonic jets. All jets were unheated and exhausted from axisymmetric convergent nozzles. At these chosen conditions, detailed experimental measurements were conducted to improve the understanding of the flow and acoustic properties of underexpanded supersonic jets.

Mean flow properties of the low Reynolds number jets were measured with Pitot and static pressure probes, flow fluctuation measurements were performed with the hot-wire anemometry, and acoustic measurements were made with a condenser microphone. Artificial excitation of the jets' flow field and cross-correlation measurements were also performed to characterize the instability properties of underexpanded supersonic jets. The findings and conclusions

are discussed in the following text.

Mean Mach number measurements demonstrate that the low Reynolds number underexpanded supersonic jets develop similarly to their conventional high Reynolds number counterparts with almost identical shock cell structures. These shock cells cause the central region of the jets to decelerate and accelerate rapidly as it evolves downstream. When compared with corresponding perfectly expanded measurements, the mean Mach number profiles in these shock-containing jets are significantly different particularly at the higher jet Mach number (M=2.1) where a strong Mach disk is formed leaving a subsonic core extending a few diameters downstream.

Hot-wire and microphone spectral analyses indicate that large amplitude discrete peaks that are characteristic of both shock screech tones and of natural instabilities dominate the flow fluctuations and the resulting acoustic radiation of low Reynolds number underexpanded jets. At Mach numbers above 1.2, the Mach number dependence of the dominant flow fluctuation or acoustic frequency in the present study is almost identical to that corresponding to the natural instability frequency of low Reynolds number perfectly expanded jets and shock screech tones of conventional high Reynolds number underexpanded jets. These findings suggest that the large-scale structure of the low Reynolds number underexpanded jets is similar to that of conventional high Reynolds number jets that are undergoing

screech.

The instability properties of low Reynolds number underexpanded jets are quite similar to those of corresponding perfectly expanded jets. However, the significant difference is that the large-scale instabilities in underexpanded jets have considerably stronger initial fluctuations, hence saturate and begin to decay considerably upstream of corresponding data in perfectly expanded jets. Experimental findings with artificial excitation suggest that in these low Reynolds number jets the natural instability process has a very selective mechanism in the frequency and azimuthal mode of preference. However, as Reynolds number increased to a much higher value (Re=68,000), this natural selection mechanism becomes less discriminatory.

Despite these significant differences in the mean flow field, the shock cell strength, and the large-scale instability evolution, the resulting acoustic radiation of the underexpanded and perfectly expanded low Reynolds number supersonic jets are almost the same. This suggests that the broad band shock associated noise of conventional high Reynolds number jets is not directly related to the large-scale jet instability.

Further acoustic measurements demonstrate the powerful noise production capability of the large-scale structure of helical ($n=\pm 1$) modes, and indicate that the saturation and disintegration of the large-scale structure, the same

mechanism for noise production of perfectly expanded jets (53), are responsible for shock screech production.

Additional acoustic measurements performed on a moderate Reynolds number (Re=68,000) M=1.6 jet have demonstrated that the broadband shock noise phenomenon is measureable under these test conditions.

Moderate Reynolds number jets are known to have more realistic turbulence production than low Reynolds number jets, and preliminary acoustic measurements, performed with a microphone probe traversed just outside the jet boundary of the M=1.6, Re=68,000 jet, suggest that the large-scale St=0.3 component saturates near x/D=1.5 which represents a significant upstream shift when compared with the fact that the disintegration of large-scale instabilities in both the low Reynolds number M=1.4 and 2.1 jets occur much further downstream near the location where the shock structure vanishes. Since the shock structure has been demonstrated to be independent of the Reynolds number, this suggests that at a higher Reynolds number more shock cells are exposed to increased turbulence and the resulting shock-turbulence interaction may be important for the broadband shock noise production (41, 43, 48). Consequently, the author believes that performing detailed flow and acoustic measurements, such as those conducted in this study, on the moderate Reynolds number M=1.6 jet will be fruitful in developing an

improved understanding of the broadband shock noise phenomenon, and thus recommends such activities in future aeroacoustic research.

BIBLIOGRAPHY

(1) Lighthill, M. J., "On Sound Generated Aerodynamically, I General Theory," Proc. Roy. Soc., A221 (1952), pp. 546-587.

(2) Lighthill, M. J., "On Sound Generated Aerodynamically, II Turbulence as a Source of Sound," Proc. Roy. Soc., A222 (1954), pp. 1-32.

(3) Ffowcs Williams, J. E., "The Noise from Turbulence Convected at High Speed," Phil. Trans. Roy. Soc., A255 (1963), p. 459.

(4) Ribner, H. S., "The Generation of Sound by Turbulent Jets," Advances in Applied Mechanics, Vol. 8, (1964), pp. 103-182.

(5) Pao, S. P., and Lowson, M. V., "Some Applications of Jet Noise Theory," AIAA Paper No. 70-233 (1970), American Institute of Aeronautics and Astronautics, New York.

(6) Lilley, G. M., Morris, P., and Tester, B. J., "On the Theory of Jet Noise and its Applications," AIAA Paper No. 73-987 (1973), American Institute of Aeronautics and Astronautics, New York.

(7) Doak, P. E., "Analysis of Internally Generated Sound in Continuous Materials: 2. A Critical Review of the Conceptual Adequacy and Physical Scope of Existing Theories of Aerodynamic Noise, with Special Reference to Jet Noise," Journal of Sound and Vibration, Vol. 25 (1972), pp. 263-355.

(8) Townsend, A. A., "The Structure of Turbulent Shear Flow," Cambridge University Press, 1956.

(9) Grant, H. L., "The Large Eddies of Turbulent Motion," J. of Fluid Mech., Vol. 4 (1958), pp. 149-190.

(10) Brown, G., and Roshko, A., "The Effect of Density Difference on the Turbulent Mixing Layer," AGARD Conference on Turbulent Shear Flows, Conference Proc. 93 (1971), pp. 23(1-12).

(11) Crow, S., C., and Champagne, F. H., "Orderly Structure

in Jet Turbulence," J. of Fluid Mechanics, Vol. 48 (1971), pp. 547-591.

(12) Winant, C. D., and Browand, F. K., "Vortex Pairing, the Mechanism of Turbulent Mixing Layer Growth at Moderate Reynolds Number," J. of Fluid Mech., Vol. 63 (1974), pp. 237-256.

(13) Lau, J. C., and Fisher, M. J., "The Vortex-Street Structure of 'Turbulent' Jets, Part 1," J. of Fluid Mech., Vol. 67 (1975), pp. 299-337.

(14) Chan, Y. Y., "Noise Generated Wavelike Eddies in a Turbulent Jet," Internatioanl Council of the Aerospace Sciences, 10th Congress, ICAS Paper No. 76-42 (1976), National Research Council of Canada, Ottawa, Canada.

(15) Brunn, H. H., "A Time Domain Analysis of the Large Scale Flow Structure in a Circular Jet, Part 1. Moderate Reynolds Number," J. of Fluid Mech. Vol. 83, Part 4 (1977), pp. 641-671.

(16) Salant, R. F., "Investigation of Jet Noise using Optical Holography," U.S. Department of Transportation Report No. DOT-TSC-146-1, Springfield, Virginia: National Technical Information Service, 1972.

(17) Higuchi, H., "An Experimental Investigation on Axisymmetric Turbulent Wakes with Zero Momentum Defect," (Ph.D. dissertation, Cal. Tech., Pasadena, California, 1976.)

(18) Krothapalli, A., Baganoff, D., Hsia, Y., and Karamcheti, K., "Some Features of Tones Generated by an Underexpanded Rectangular Jet," AIAA Paper No. 81-0060 (1981), American Institute of Aeronautics and Astronautics, New York.

(19) Sherman, P. M., Glass, D. R., and Duleep, K., G., "Jet Flow Field During Screech," Appl. Sci. Res., 32 (Aug. 1976), pp. 283-303.

(20) Hammitt, A. G., "The Oscillation and Noise of an Overpressure Sonic Jet," J. of the Aerospace Sciences, Vol. 28, No. 9 (1961), pp. 673-680.

(21) Mollo-Christensen, E., "Jet Noise and Shear Flow Instability Seen from an Experimenter's Viewpoint," J. Appl. Mech., Vol. 34 (1976), pp. 1-7.

(22) Sedel'nikov, T. K., "The Frequency Spectrum of the

Noise of a Supersonic Jet," Phy. Aero. Noise, Nauka. (Trans. 1969 NASA TTF-538, pp. 71-75.)

(23) Michalke, A., "Sound Generation by Amplified Disturbance in Free Shear Layers," Deutsche Luft- und Raumfahrt Rep. No. 69-90.

(24) Bishop, K. A., Ffowcs Williams, J. E., and Smith, W., "On the Noise Sources of the Unsuppressed High-Speed Jet," J. of Fluid Mech., Vol. 50 (1971), pp. 12-31.

(25) Moore, C. J., "The Role of Shear-Layer Instability Waves in Jet Exhaust Noise," J. of Fluid Mech., Vol. 80, Part 2 (1977), pp. 321-357.

(26) Laufer, J., Kaplan, R. E., and Chu, W. T., "On the Generation of Jet Noise," AGARD Conference Proc. 131 on Noise Mechanisms, (1973).

(27) Dutt, B., "Role of Large Scale Structures in the Noise Generation of a Turbulent Supersonic Jet," (Ph.D. dissertation, University of Southern California, University Park, California, 1977.)

(28) McLaughlin, D. K., Morrison, G. L., and Troutt, T. R., "Experiments on the Instability Waves in a Supersonic Jet and Their Acoustic Radiation," J. of Fluid Mech., Vol. 69 (1975), pp. 73-95.

(29) McLaughlin, D. K., Morrison, G. L., and Troutt, T. R., "Reynolds Number Dependence in Supersonic Jet Noise," AIAA Journal Vol. 15 (1977), pp. 526-532.

(30) Troutt, T. R., and McLaughlin, D. K., "Experiments on the Flow and Acoustic Properties of a Moderate Reynolds Number Supersonic Jet," submitted for publication, J. of Fluid Mechanics.

(31) Tam, C. K. W., "Supersonic Jet Noise Generated by Large-Scale Disturbances," J. of Sound and Vibration, Vol. 38 (1975), pp. 51-79.

(32) Tam, C. K. W., "On the Noise of a Nearly Ideally Expanded Supersonic Jet," J. of Fluid Mech., Vol. 51 (1972), pp. 69-95.

(33) Chan Y. Y., "Discrete Acoustic Radiation from a High-Speed Jet as a Singular Perturbation Problem," Canadian Aeronautics and Space Journal, Vol. 21, No. 6 (1975), pp. 221-234.

(34) Liu, J. T. C., "Developing Large-Scale Wavelike Eddies and the Near Jet Noise Field," J. of Fluid Mech.,

Vol. 62 (1974), pp. 437-464.

(35) Morris, P. J., "Flow Characteristics of the Large-Scale Wave-Like Structure of a Supersonic Round Jet," J. of Sound and Vibration, Vol. 53 (1977), pp. 223-244.

(36) Morris P. J., and Tam, C. K. W., "Near and Far Field Noise from Large-Scale Instabilities of Axisymmetric Jets," AIAA Paper No. 77-1351, (1977), American Institute of Aeronautics and Astronautics, New York.

(37) Tester, B. J., Morris, P. J., Lau, J. C., and Tanna, H. K., "The Generation, Radiation and Prediction of Supersonic Jet Noise Volume 1," Technical Report AFAPL-TR-78-85, Marrietta, Georgia: Lockheed-Georgia Company, 1978.

(38) McLaughlin, D. K., Seiner, J. M., and Liu, C. H., "On the Noise Generated by Large Scale Instabilities in Supersonic Jets," AIAA Paper No. 80-0964 (1980), American Institute of Aeronautics and Astronautics, New York.

(39) Powell, A., "On the Mechanism of Choked Jet Noise," Proc., Phy. Soc., B, Vol. 66 (1953), pp. 1039-1056.

(40) Westley, R., and Wooley, J. H., "The Near Field Sound Pressure of a Choked Jet when Oscillating in the Spining Mode," AIAA Paper No. 75-479 (1975), American Institute of Aeronautics and Astronautics, New York.

(41) Lighthill, M. J., "On the Energy Scattered from the Interaction of Turbulence with Sound or Shock Waves," Proc. Camb. Phil. Soc., 49, (1953), pp. 531-551.

(42) Ribner, H. S., "Convection of a Pattern of Vorticity Through a Shock Wave," NACA TN 2864 (1953), & NACA Rep. 1164 (1954).

(43) Harper-Bourne, M., and Fisher M. J., "The Noise from Shock Waves in Supersonic Jets," AGARD Conference Proc. 131 (1973), p. 11.

(44) Tanna, H., K., "An Experimental Study of Jet Noise, Part II: Shock Associated Noise," J. of Sound and Vibration, 50(3) (1977), pp. 429-444.

(45) Seiner, J., M., and Norum T. D., "Aerodynamic Aspects of Shock Containing Jet Plumes," AIAA Paper No.

80-0965 (1980), American Institute of Aeronautics and Astronautics, New York.

(46) Seiner, J. M., and Norum, T. D., "Experiments of Shock Associated Noise on Supersonic Jets," AIAA Paper No. 79-1526 (1979), American Institute of Aeronautics and Astronautics, New York.

(47) Norum, T. D., and Seiner, J. M., "Location and Propagation of Shock Associated Noise from Supersonic Jets," AIAA Paper No. 80-0983 (1980), American Institute of Aeronautics and Astronautics, New York.

(48) Howe, M. S., and Ffowcs Williams, J. E., "On the Noise Generated by an Imperfectly Expanded Supersonic Jet," Phil. Trans. Roy. Soc., London, Vol. 289 A1358 (1978), pp. 271-314.

(49) Powell, A., "On the Noise Emanating from a Two-Dimensional Jet Above the Critical Pressure," The Aeronautical Quarterly, Vol. IV (Feb. 1953), pp. 103-122.

(50) Martlew, D. L., "Noise Associated with Shock Waves in Supersonic Jets," AGARD Conference Proc. 42 (1969), p. 7(1-10).

(51) Morrison G. L., "Flow Instability and Acoustic Radiation Measurements of Low Reynolds Number Supersonic Jets," (Ph.D. dissertation, Oklahoma State University, Stillwater, Oklahoma, 1977.)

(52) Morrison, G. L. and McLaughlin, D. K., "Instability Process in Low Reynolds Number Supersonic Jets," AIAA Journal, Vol. 18, No. 7 (July 1980), pp. 793-800.

(53) Morrison, G. L., and McLaughlin D., K., "Noise Generation by Instabilities in Low Reynolds Number Supersonic Jets," J. of Sound and Vibration, Vol. 65 (1979), pp. 177-191.

(54) Kendall, J. M., "Supersonic Boundary Layer Stability Experiments," Proc. Boundary Layer Trans. Study Group, Meeting, II, Aerospace Rep. TR-0158 (S3816-63)-1, 1967.

(55) Smith R. H., and Wang, C. T., "Contracting Cones Giving Uniform Throat Speeds," J. of the Aeronautical Sciences (Oct. 1944), pp. 356-360.

(56) Johnson, C. B., and Boney, L. R., "A Method for Calculating a Real-Gas Two-Dimensional Nozzle

Contour Including the Effect of Gamma," NASA TMX-3243, Hampton, Virginia: NASA Langley Research Center, 1975.

(57) Stromberg, J. L., "Flowfield and Acoustic Measurements of Low Reynolds Number Jets in the Transonic Range," (M.S. thesis, Oklahoma State University, Stillwater, Oklahoma, 1978.)

(58) Troutt, T. R., "Measurements on the Flow and Acoustic Properties of a Moderate Reynolds Number Supersonic Jet," (Ph.D. dissertation, Oklahoma State University, Stillwater, Oklahoma, 1978.)

(59) Kovasznay, L. S. G., "The Hot-Wire Anemometer in Supersonic Flow," J. Aero. Sci., Vol. 17, No. 9 (1950), pp. 565-572.

(60) Rose, W. C., "The Behavior of a Compressible Turbulent Boundary Layer in a Shock-Wave-Induced Adverse Pressure Gradient," NASA TND-7092, 1973.

(61) Politte, M. D., private communication, Stillwater, Oklahoma, Oct. 1981.

(62) McLaughlin, D. K., "Experimental Investigation of the Mean Flow and Stability of the Laminar Supersonic Cone Wake," AFOSR 70-0072TR, (Massachusetts Institute of Technology, Aerophysics Laboratory Technical Report 164, p. 122, Cambridge, Massachusetts, 1970.)

APPENDIX A

AZIMUTHAL MODAL ANALYSIS

A. Theoretical Background

A method based on the elementary instability model has been derived by the author for azimuthal modal analysis. This method which yields a unique analytical solution in terms of a Discrete Fourier Transform has been proved valuable to the experimental data analysis. The derivation of the method is quite similar to the derivation of the Discrete Fourier Transform which can be found in many literatures discussing Fourier Analysis.

Instability analyses model the fluctuation quantities as four-dimensional traveling waves of broad spectrum with random phase and orientation, typically

$$Q'(x,r,\theta,t) = q(r)\, e^{i(k_r x-\omega t+n\theta)-k_i x} \tag{A.1}$$

where Q' is a complex fluctuation quantity; x, r, and θ are the cylindrical coordinate frames, t is time, q(r) is the complex amplitude eigenfunction, k is the complex wave number (subscripts r and i stand for real and imaginary parts), ω is the angular frequency of the wave, and n is the azimuthal mode number. These waves are cylindrical helices with the number of threads given by n and with the orientation of the helix (left- or right-hand) given by the sign of n. The instability wave fronts of various azimuthal modes can be found in Reference 62.

If one assumes q(r) has azimuthal modal dependence, then the above can be modified as

$$Q'(x,r,\theta,t) = \sum_{n=-\infty}^{\infty} q(r,n)\, e^{i(k_r x-\omega t+n\theta)-k_i x} \qquad (A.2)$$

Hence, the phase angle of a traveling wave at a given frequency has x, t, θ, and n dependence. Experimentally, the axial phase and amplitude evolutions of an instability wave can be determined by performing cross-correlation and phase averaging measurements along the axial direction of the jet while holding r and θ constant. However, the azimuthal phase component ($e^{in\theta}$) is a function of both n and θ which requires special effort to analyze. If one performs phase and coherent amplitude measurements around the azimuth of a jet at known locations of x and r, at a known instance of time (relative to a timing reference), and for a given frequency component, then A.2 reduces to

$$\tilde{Q}\,(\theta) = C \sum_{n=-\infty}^{\infty} q(n)\, e^{in\theta} \qquad (A.3)$$

where $C = e^{i(k_r x-wt)-k_i x}$ is now a known quantity, and $\tilde{Q}(\theta)$ is now the measured quantity. Let the azimuthal angle θ be $I(2\pi/N)$ where N is the number of data points measured around the azimuthal angle from 0 to 2π, and I=0, 1, 2, 3 ..... (N-1), then (A.3) becomes

$$\tilde{Q}\,(I) = C \sum_{n=-\infty}^{\infty} q(n)\, e^{inI(\frac{2\pi}{N})} \qquad (A.4)$$

The right hand side of A.4 can be identified as the Fourier series representation of $\tilde{Q}(I)$. By multiplying both sides of A.4 by $e^{-iI(2\pi/N)m}$ (m is an integer), and summing over I, A.4 becomes

$$\sum_{I=0}^{N-1} \tilde{Q}(I)\, e^{-iI(\frac{2\pi}{N})m} = C \sum_{I=0}^{N-1} \sum_{n=-\infty}^{\infty} q(n)\, e^{iI(\frac{2\pi}{N})(n-m)} \qquad (A.5)$$

By reversing the order of summation, (A.5) becomes

$$\sum_{I=0}^{N-1} \tilde{Q}(I)\, e^{-iI(\frac{2\pi}{N})m} = C \sum_{n=-\infty}^{\infty} q(n) \sum_{I=0}^{N-1} e^{iI(\frac{2\pi}{N})(n-m)} \qquad (A.6)$$

Since higher order modes don't contribute significantly to $\tilde{Q}(I)$. When N (the number of data points measured) is fairly large, it is reasonable to approximate A.6 by setting n=0, ±1, ±2, ±3, ... $\pm(N-1)$, hence

$$\sum_{I=0}^{N-1} \tilde{Q}(I)\, e^{-iI(\frac{2\pi}{N})m} = C \sum_{n=-(N-1)}^{N-1} q(n) \sum_{I=0}^{N-1} e^{iI(\frac{2\pi}{N})(n-m)} \qquad (A.7)$$

Now, note the fact that

$$\sum_{n=0}^{N-1} e^{i(\frac{2\pi}{N})nm} = \begin{cases} N, & \text{if } m=JN, \text{ where J is an integer.} \\ 0, & \text{otherwise.} \end{cases} \qquad (A.8)$$

Introducing this orthorgonal identity into the right-hand side of A.7, and changing the dummy variable m to n, one gets

$$\sum_{I=0}^{N-1} \tilde{Q}(I)\, e^{-iI(\frac{2\pi}{N})n} = \begin{cases} CNq(n), & n=0 \\ CN(q(n)+q(n-N)), & n=1,2,..(N-1) \end{cases} \qquad (A.9)$$

where q(n) is the complex representation of right-hand helices, and q(n-N) is the complex representation of left-hand helices, since n-N is always negative. The left hand side of A.9 is readily identified as the Discrete Fourier Transform, and the right hand side can now be call the raw "modal spectrum" which is periodic in n with the period of N. A.9 can be computed easily using the Fast Fourier Transform (FFT) computer algorithm, however each spectral component from FFT represents the sum of q(n) and q(n-N) except when n=0. Mathematically, it is very difficult to separate q(n) from q(n-N), but based on experimental observations higher order azimuthal modes can be assumed negligible in amplitude. When N is fairly large, A.9 reduces into

(A.10)

$$\sum_{I=0}^{N-1} \tilde{Q}(I)\, e^{-iI(\frac{2\pi}{N})n} = \begin{cases} CNq(n), & n=0,1,2,3,\ldots\frac{N}{2} \\ CNq(n-N), & n=(\frac{N}{2}+1),(\frac{N}{2}+2),(\frac{N}{2}+3), \\ & \ldots\ldots\ldots(N-1) \end{cases}$$

where (N/2) is assumed to be the "cut-off" point of the spectrum. Beyond this point the amplitude of the higher order modes are assumed to be zero. A graphical presentation of equation A.9 is shown in Figure 50 (p. 127) where hypothesized distributions of q(+n) and q(-n) overlap in the spectrum. The amount of overlapping increases towards N/2 where equation A.10 leads to considerable error. However, with increasing data points (N), equation A.10 becomes increasingly accurate near the spectral locations of n=0 and n=(N-1).

B. Application of the Analysis

This method provides a computerized scheme to reduce experimental data into a precise description of the azimuthal modal composition of the fluctuations in terms of amplitude and relative phase angle as functions of azimuthal modal number. The method is superior than the previous one (30) in that the solution procedure is fully autonomous (i.e. no guess work is required). The accuracy and resolution of the analysis relies on an input of fairly large number of data points (N) which must cover a full period of azimuth (θ=0 to 2π). Intuitively, a large number of data points can be obtained by either performing a measurement with a great many probe stations or only a few stations and then interpolating to yield more data points. However, problems with probe resolution limit the number of data points obtainable, and experimental uncertainties

introduce scattering of the data thus making interpolation rather difficult. In this study, a combined interpolation (using cubic spline algorithm) and ensemble average technique was sometimes used to improve the accuracy and resolution of the modal spectrum. Some of the azimuthal measurements were repeated one or two times. Data obtained were then analyzed separately, and the resulting spectra were ensemble averaged. The number of data points (N) measured was either 18 or 36 which was found satisfactory to separate left hand helices q(n-N) from right hand helices q(n), since the q(n) spectrum is always concentrated at very small |n| values.

The complex vector in the azimuthal plane describing instability fluctuations, $\tilde{Q}(I)$, was constructed as follows:

$$\mathrm{Re}[\,\tilde{Q}(I)\,] = \tilde{P}(I)\cos(\phi) \qquad I=1,\ 2,\ 3\ \ldots\ldots\ (N-1)$$
$$\mathrm{Im}[\,\tilde{Q}(I)\,] = \tilde{P}(I)\sin(\phi)$$

where $\tilde{P}(I)$ was the coherent portion of the fluctuations measured with x and r held constant and at the azimuthal angle equal to $(2\pi I)/N$, and ϕ was the relative phase difference between $\tilde{P}(I)$ and the timing reference signal. The complex vector representing each azimuthal mode, q(n), was reduced into amplitude and relative phase angle using standard complex analysis where the amplitude of each mode was obtained by

$$|q(n)| = \sqrt{\mathrm{Re}[\,q(n)\,]^2 + \mathrm{Im}[\,q(n)\,]^2}$$

and the relative phase angle was obtained by

$$\Phi = \tan^{-1}\left(\frac{\mathrm{Im}[\ q(n)\ ]}{\mathrm{Re}[\ q(n)\ ]}\right)$$

APPENDIX B

FIGURES

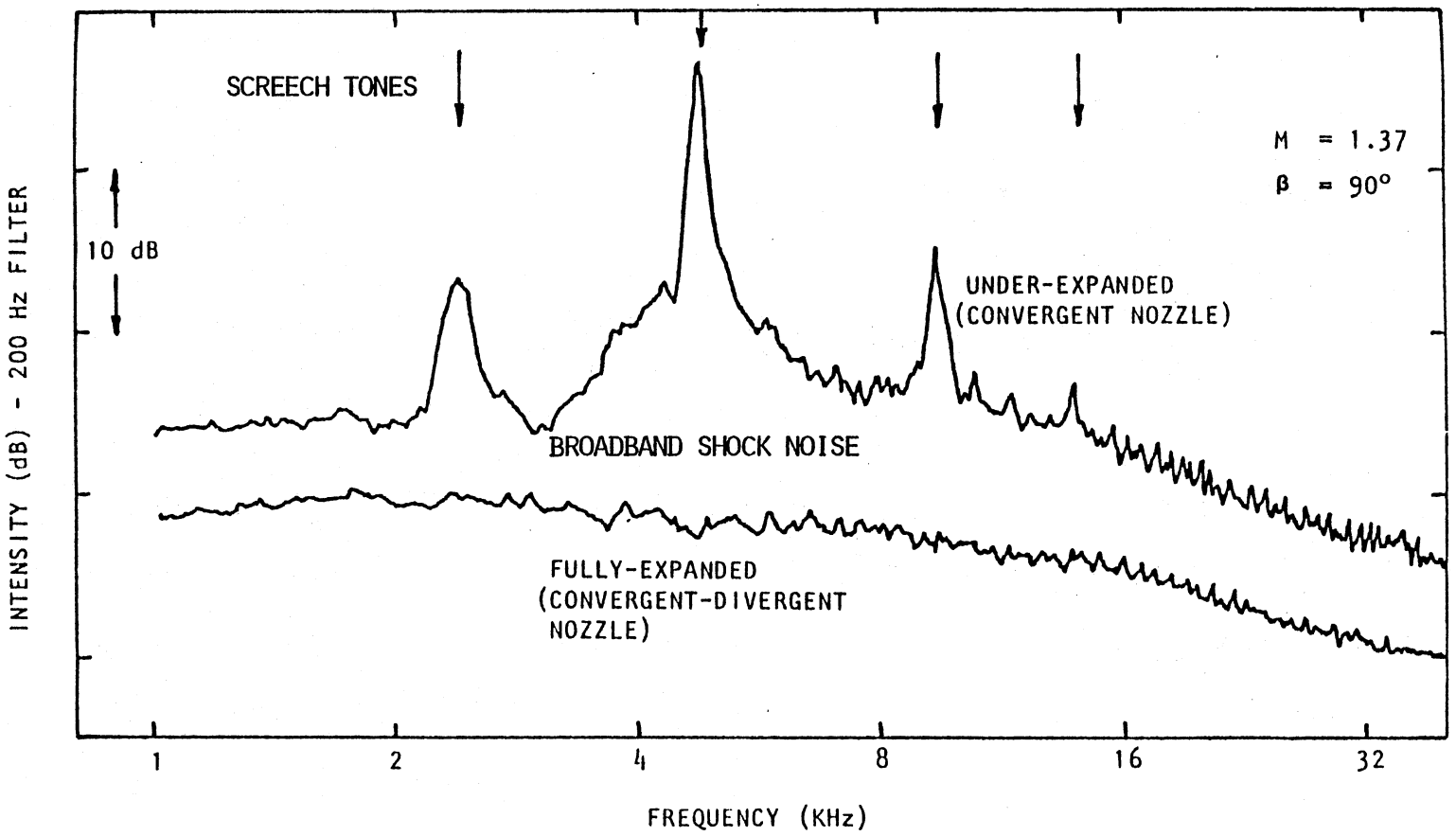

Figure 1. Comparison of Acoustic Spectra from Fully Expanded and Underexpanded Jets (44)

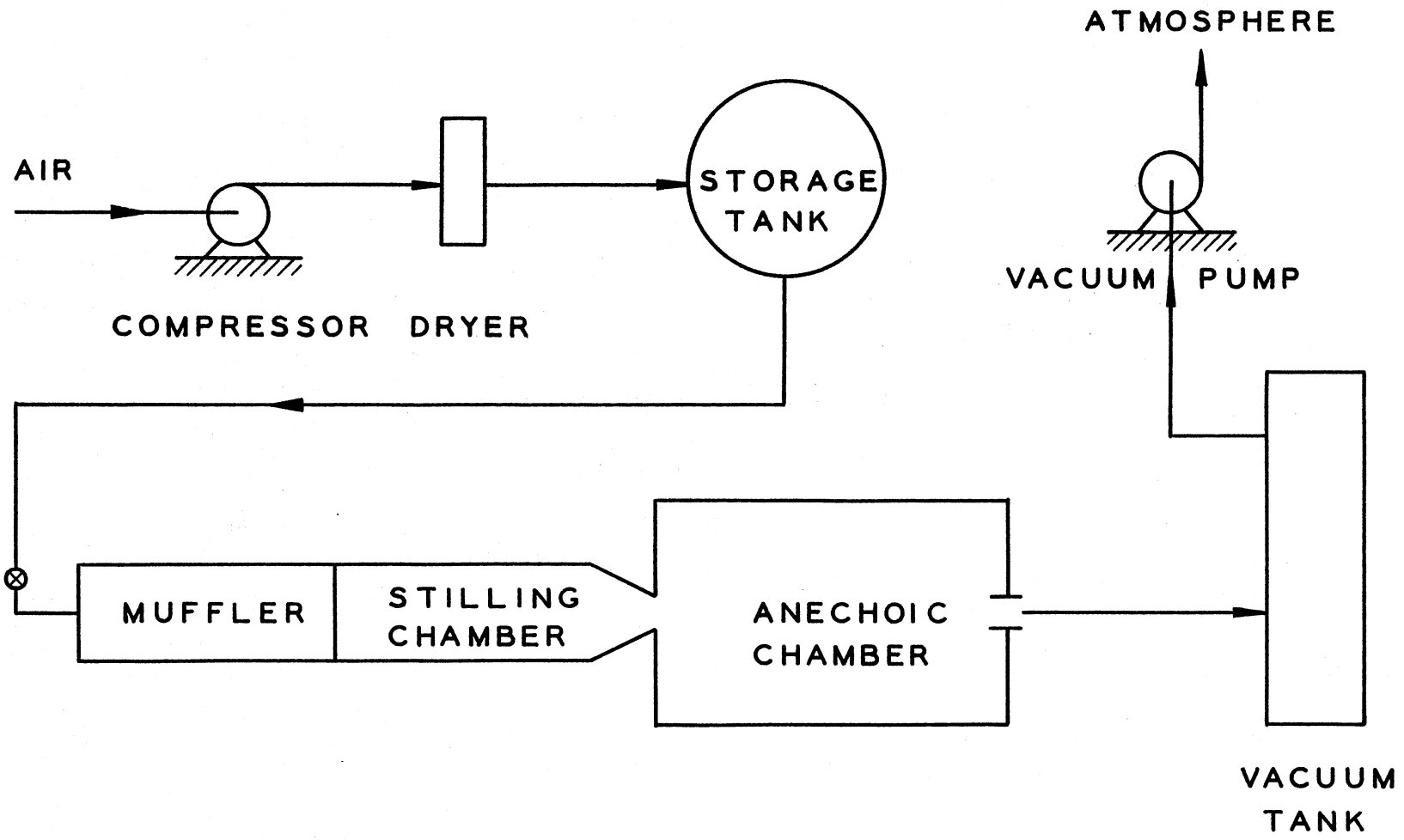

Figure 2. Schematic of Test Facility

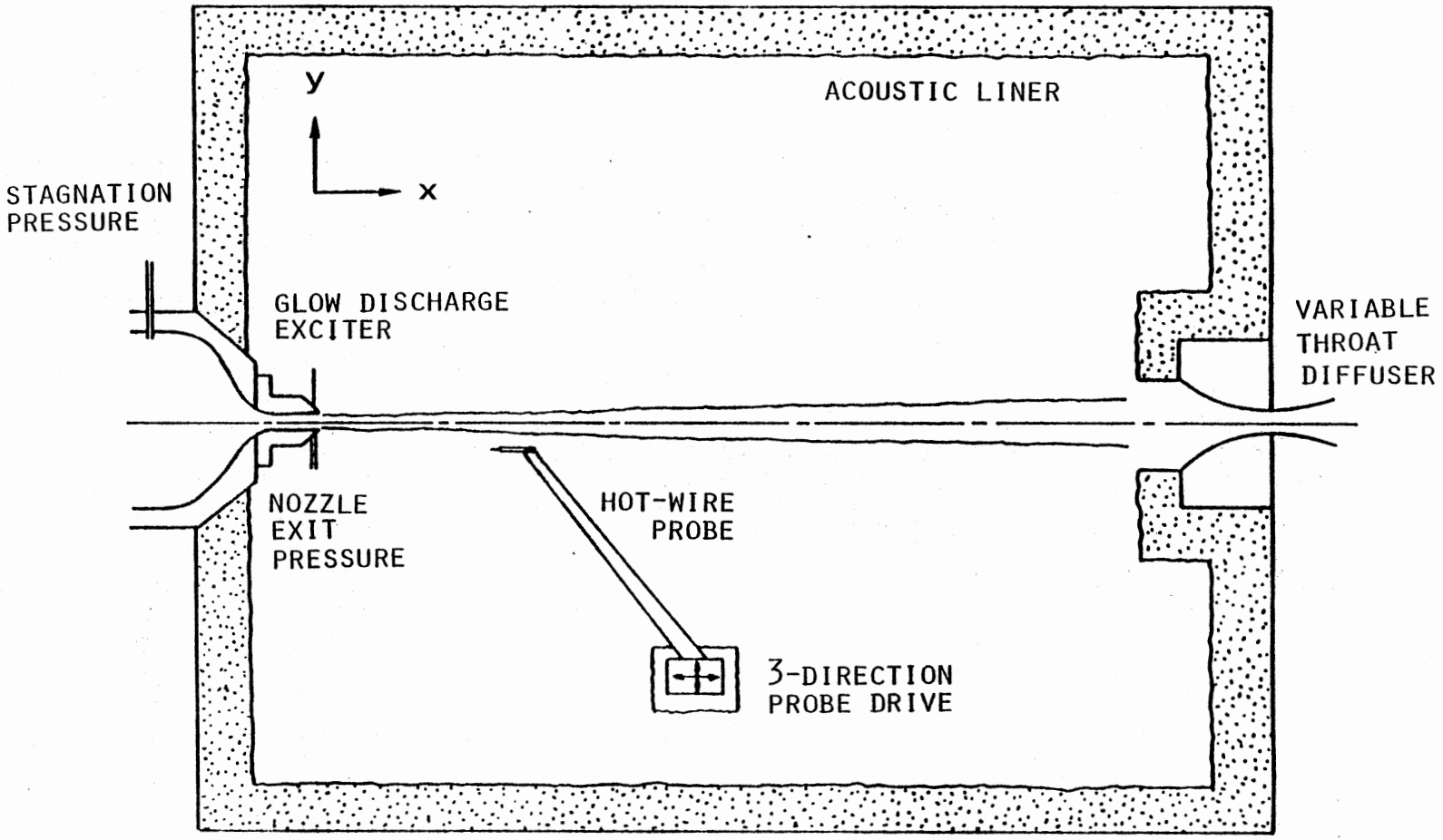

Figure 3. Schematic of Test Chamber

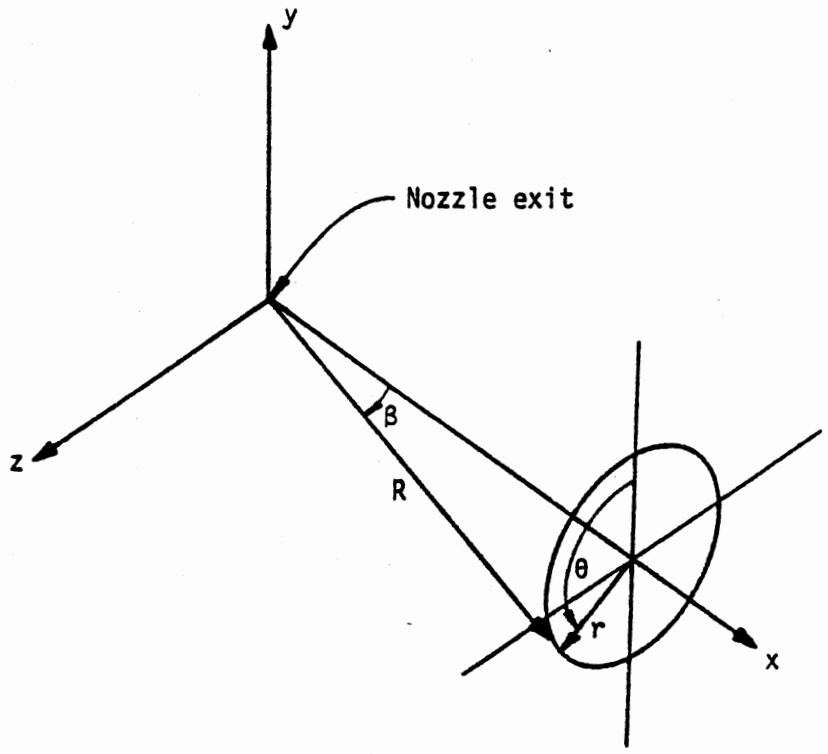

Figure 4. Coordinate System

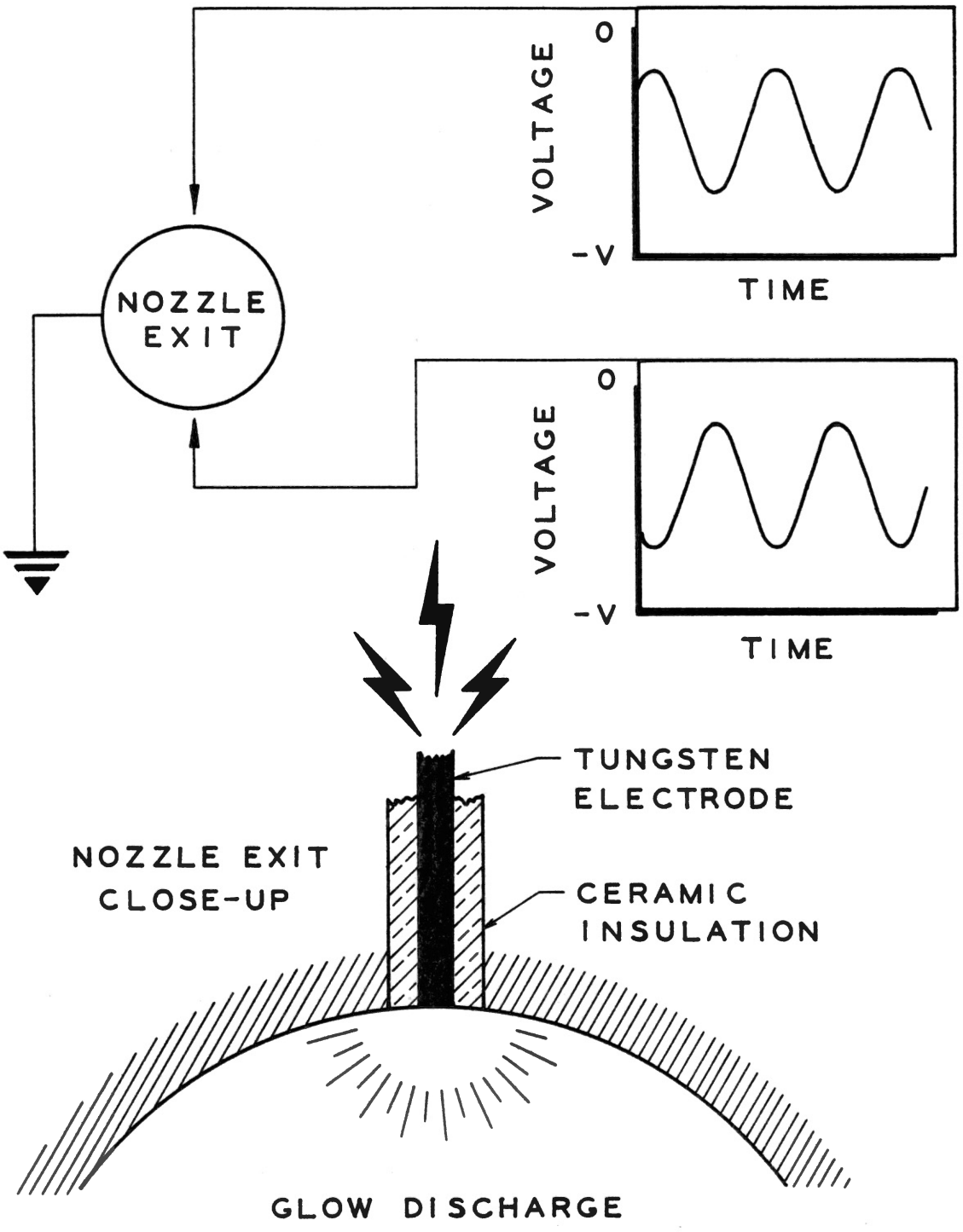

Figure 5. Low Density Glow Discharge Excitation

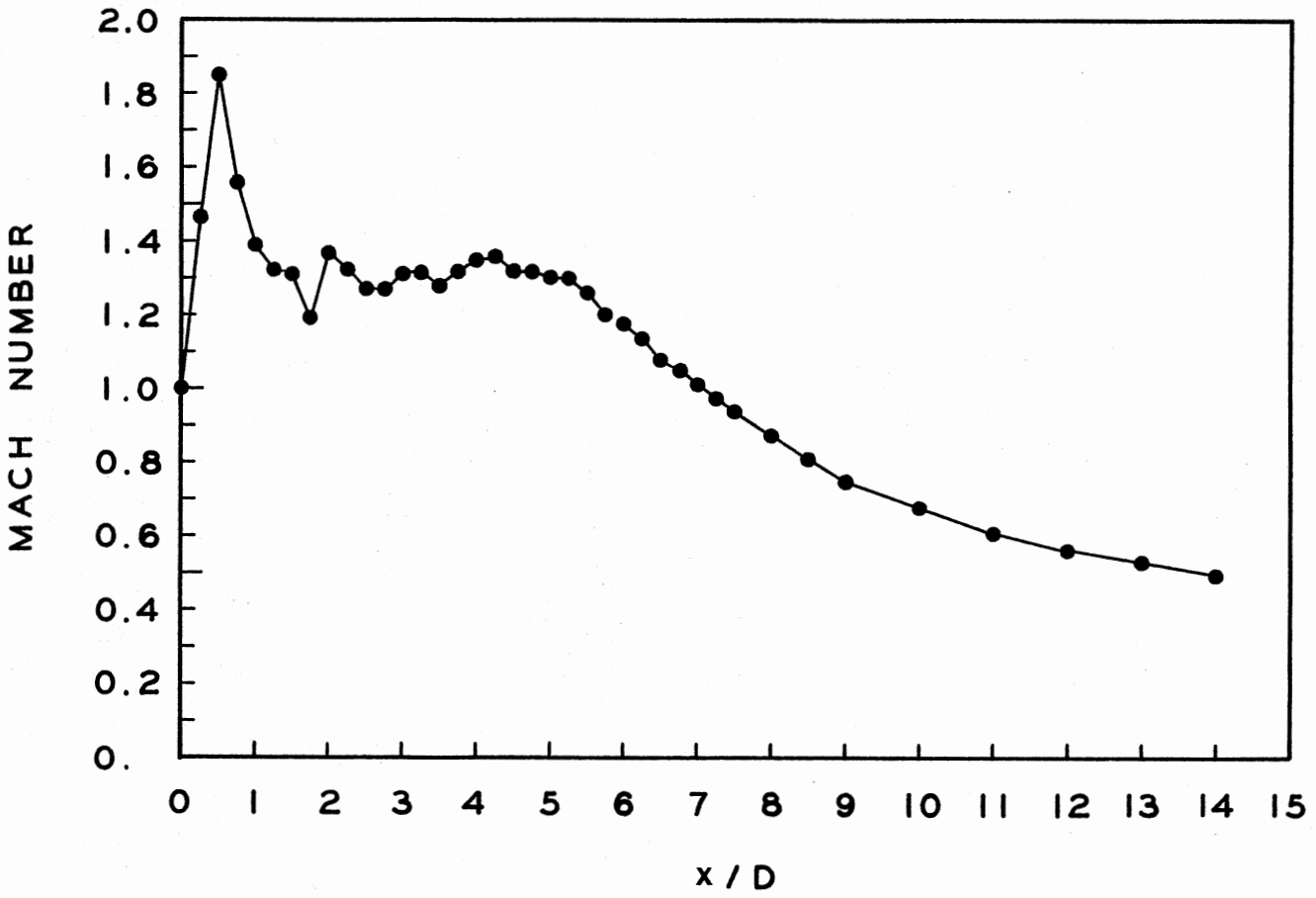

Figure 6. Centerline Mach Number Distributions, M=1.4 Underexpanded Jet

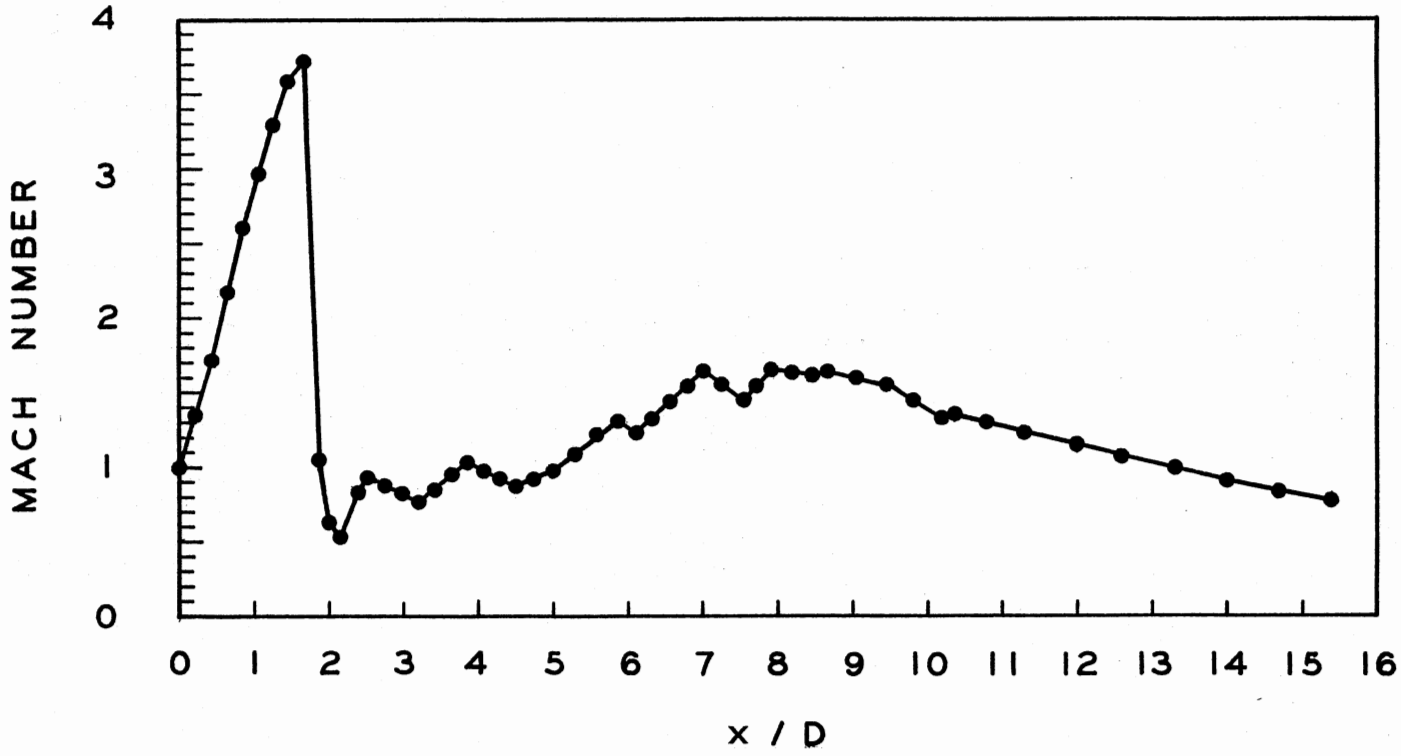

Figure 7. Centerline Mach Number Distributions, M=2.1 Underexpanded Jet

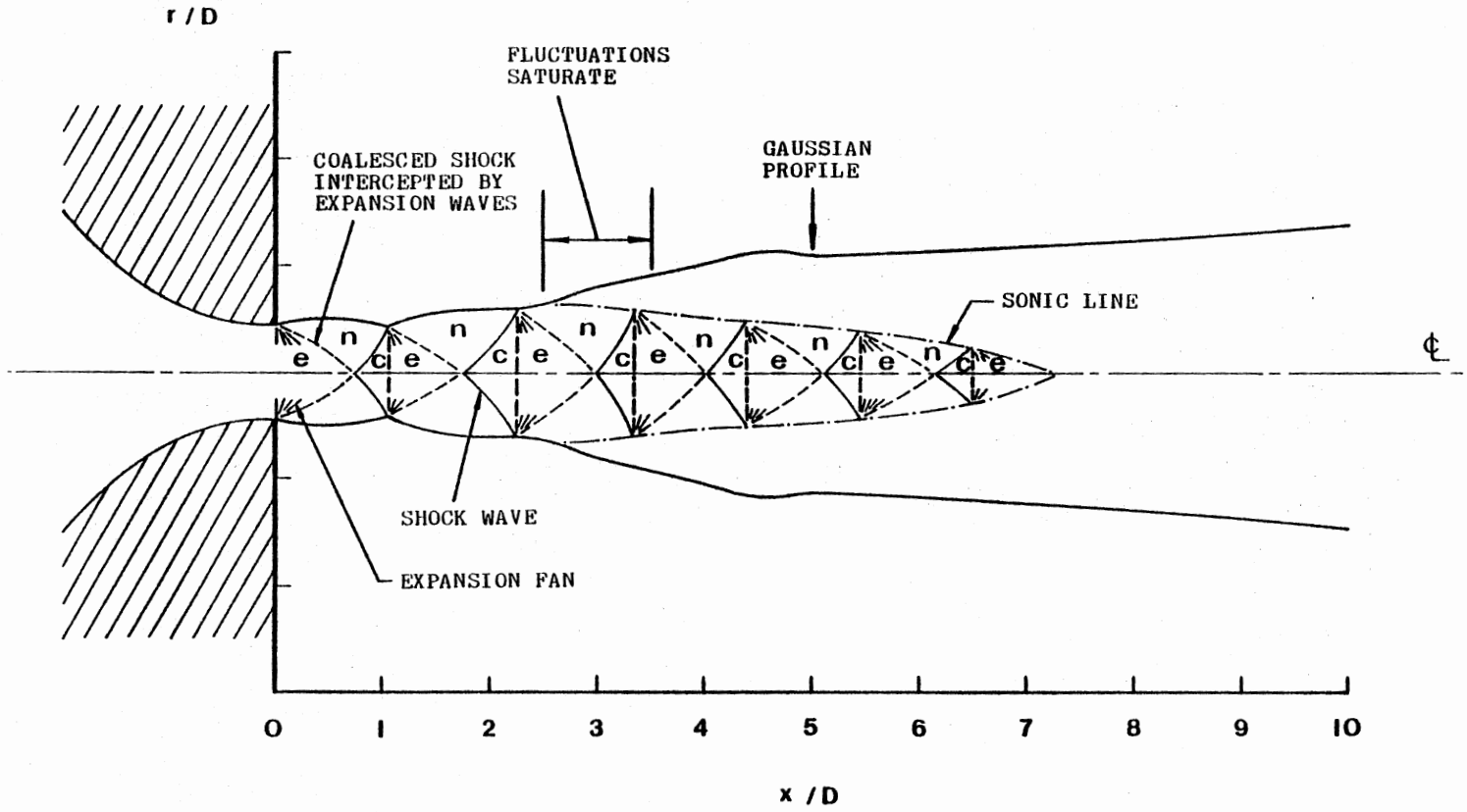

Figure 8. Artistic Impression of the Shock Cell Structure in the M=1.4 Underexpanded Jet

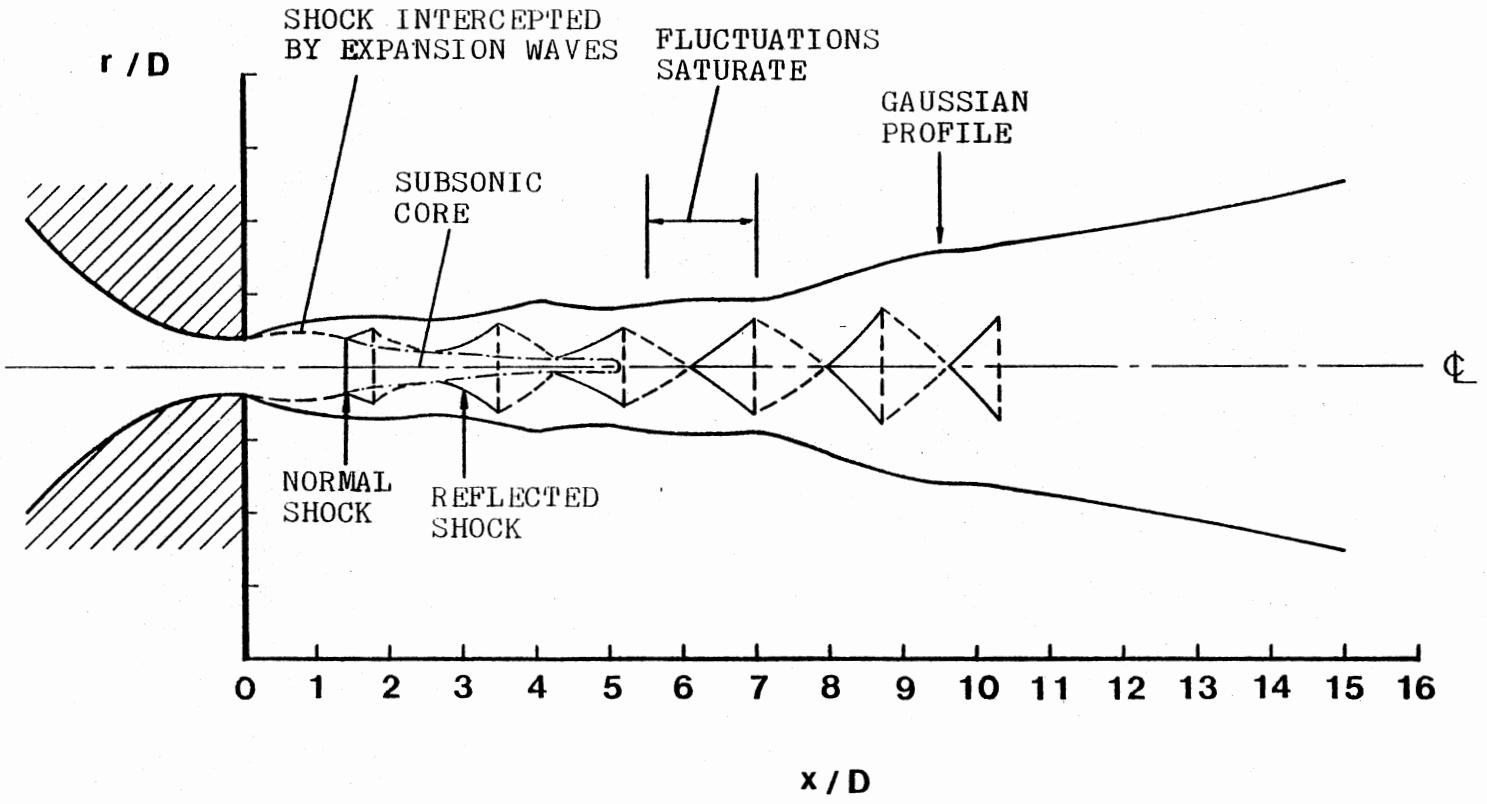

Figure 9. Artistic Impression of the Shock Cell Structure in the M = 2.1 Underexpanded Jet

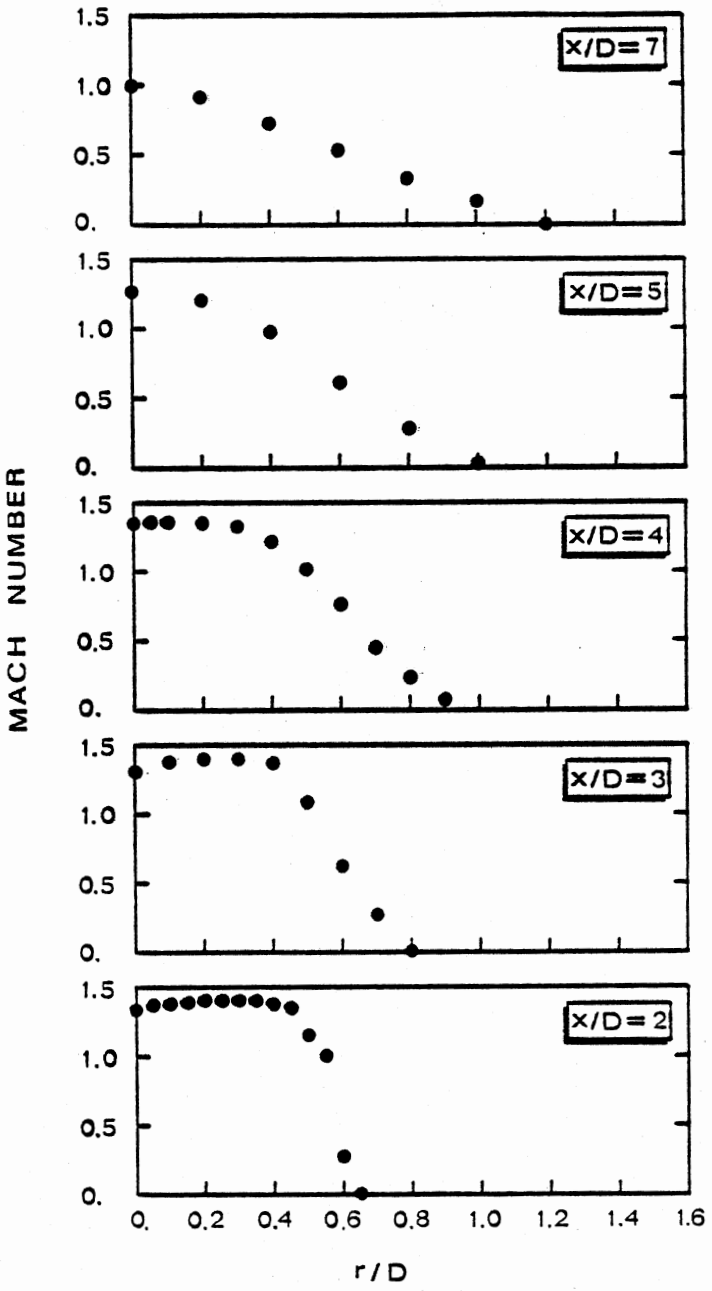

Figure 10. Mean Mach Number Profiles, M=1.4 Underexpanded Jet

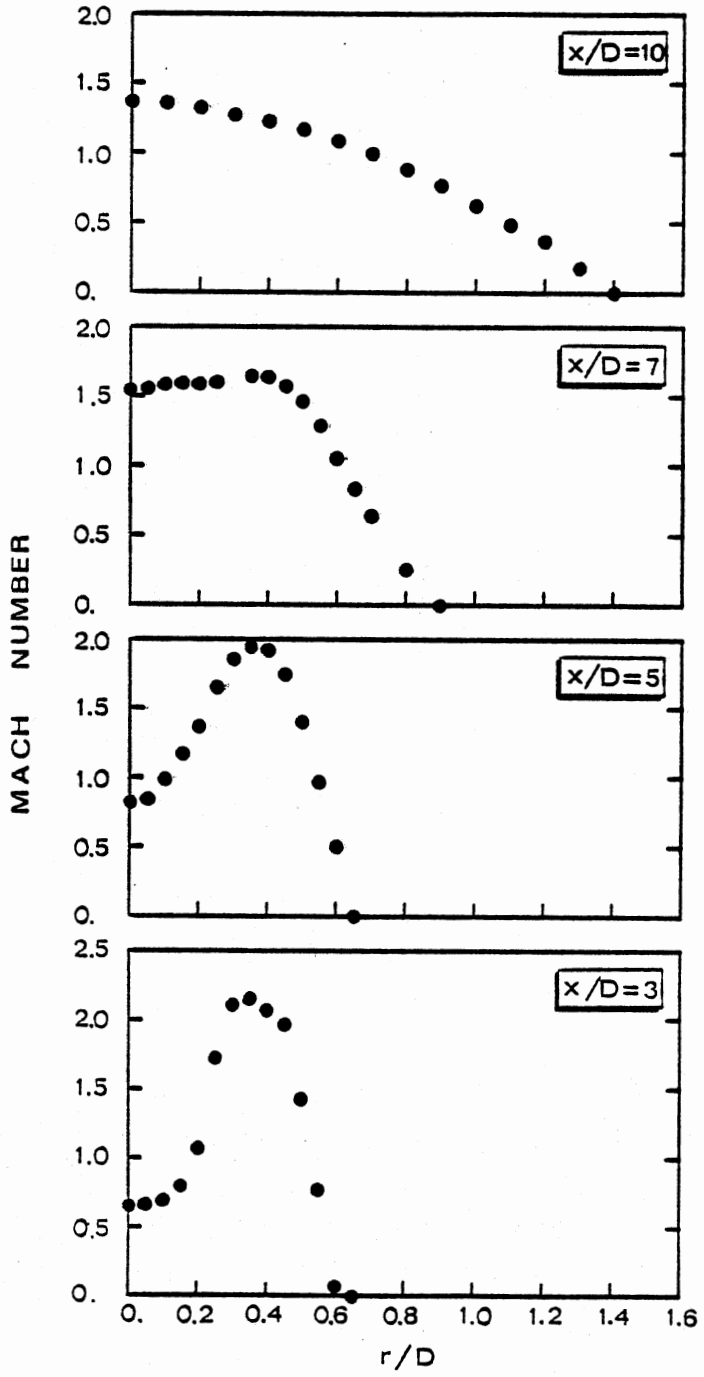

Figure 11. Mean Mach Number Profiles, M=2.1 Underexpanded Jet

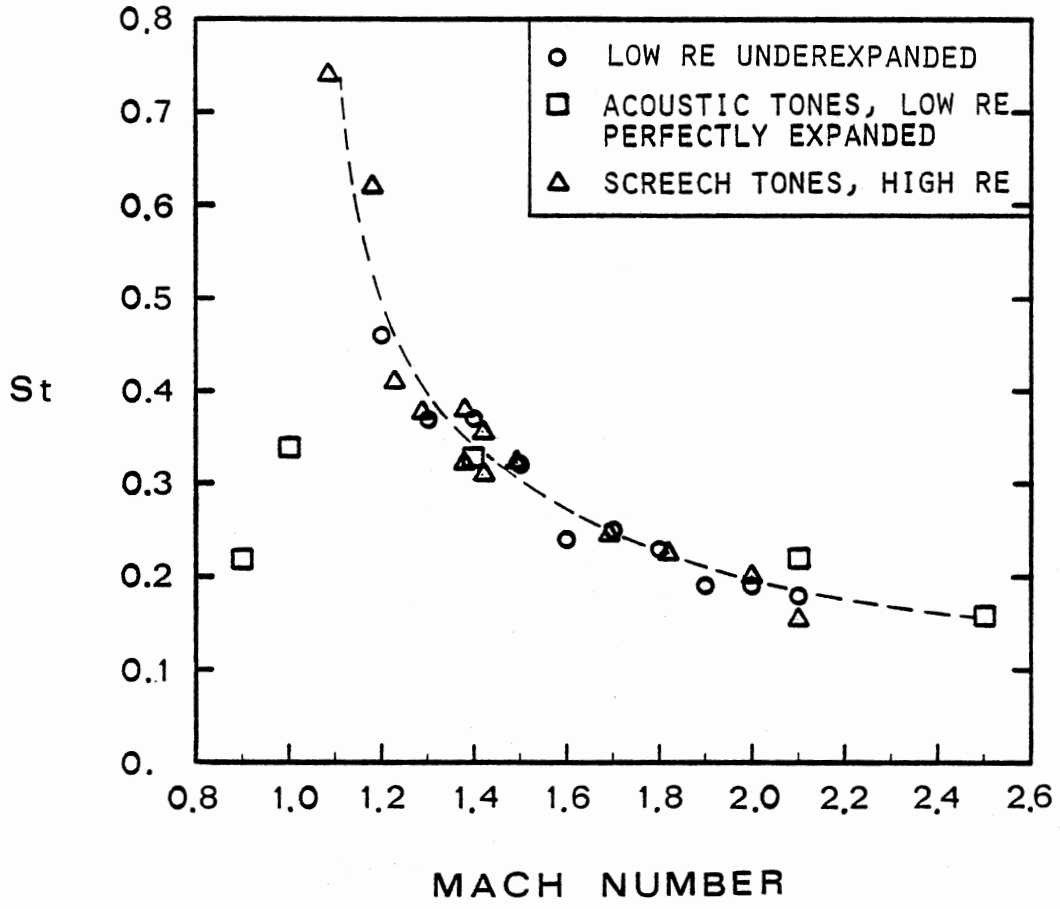

Figure 12. Dominant Instability or Acoustic Frequencies as a Function of Jet Mach Number

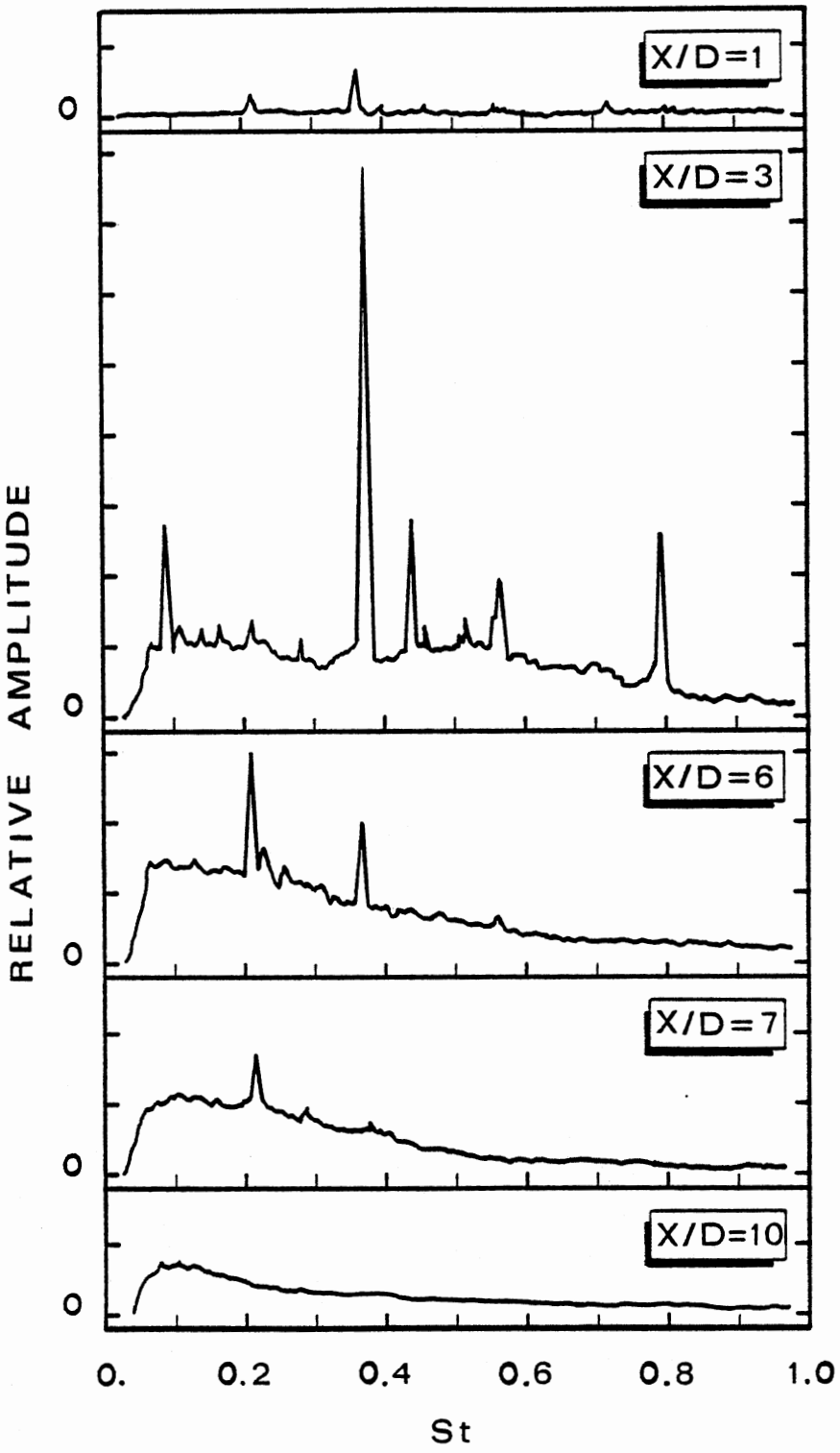

Figure 13. Flow Fluctuation Spectra, M=1.4 Underexpanded Jet

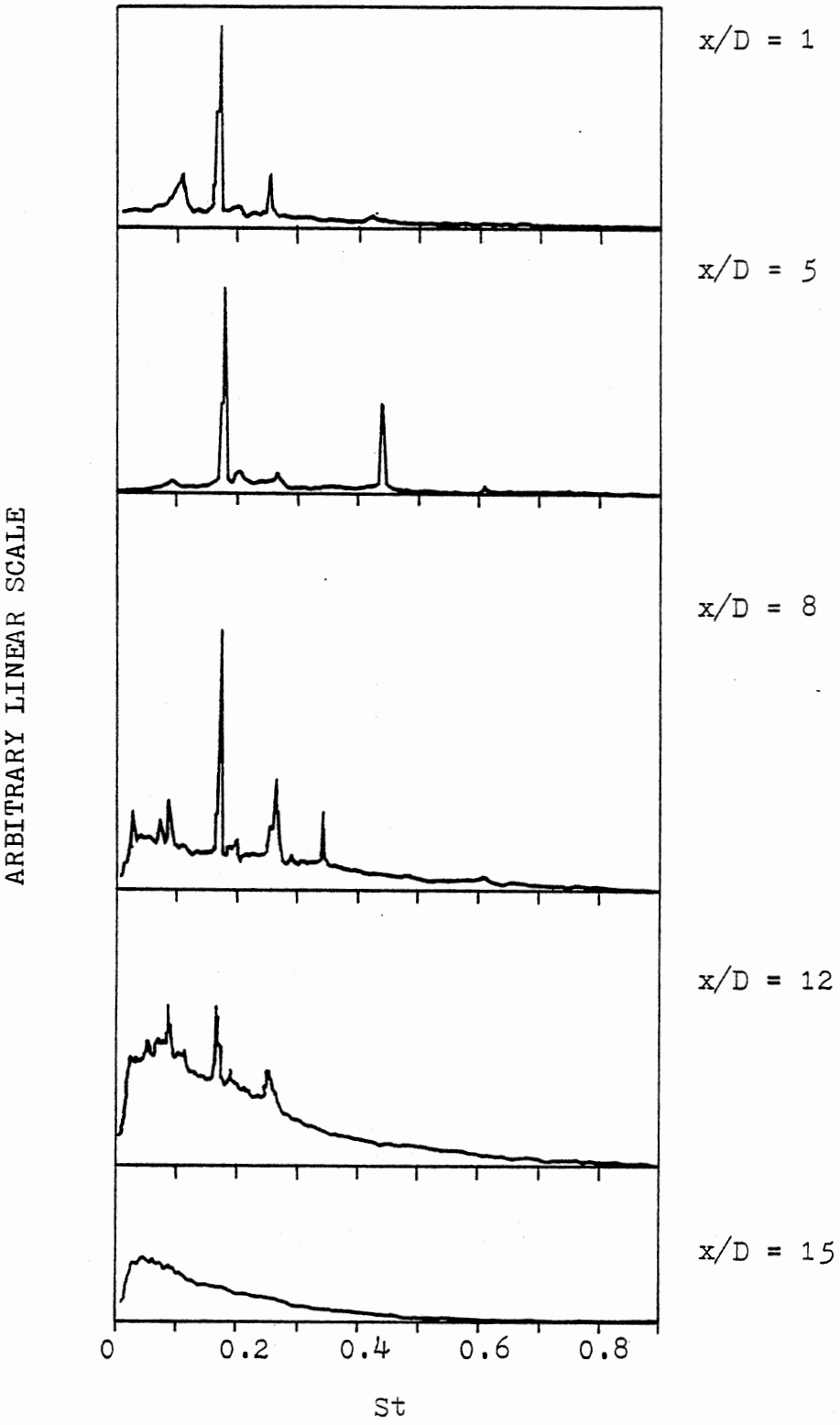

Figure 14. Flow Fluctuation Spectra, M = 2.1 Underexpanded Jet

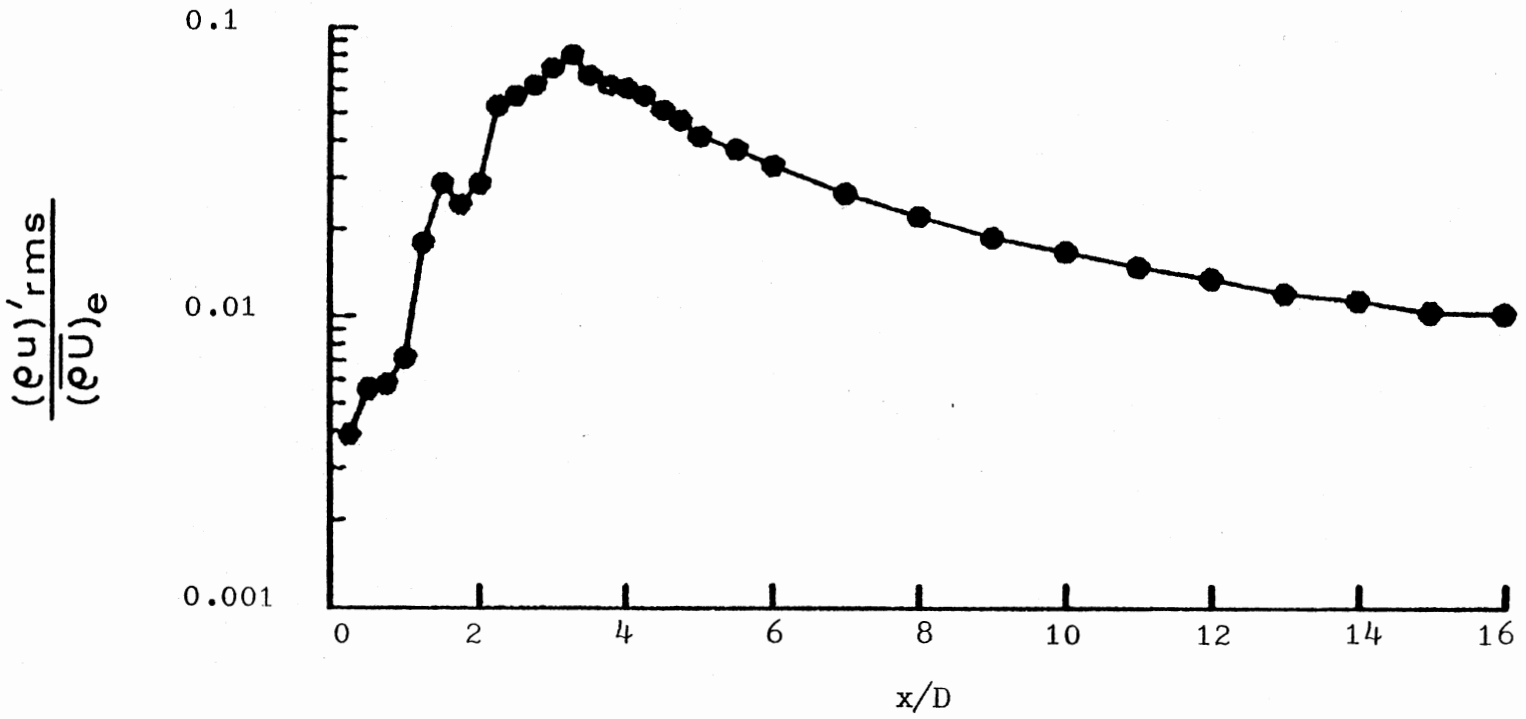

Figure 15. Axial Evolution of Overall Mass-Velocity Fluctuations, M=1.4 Underexpanded Jet

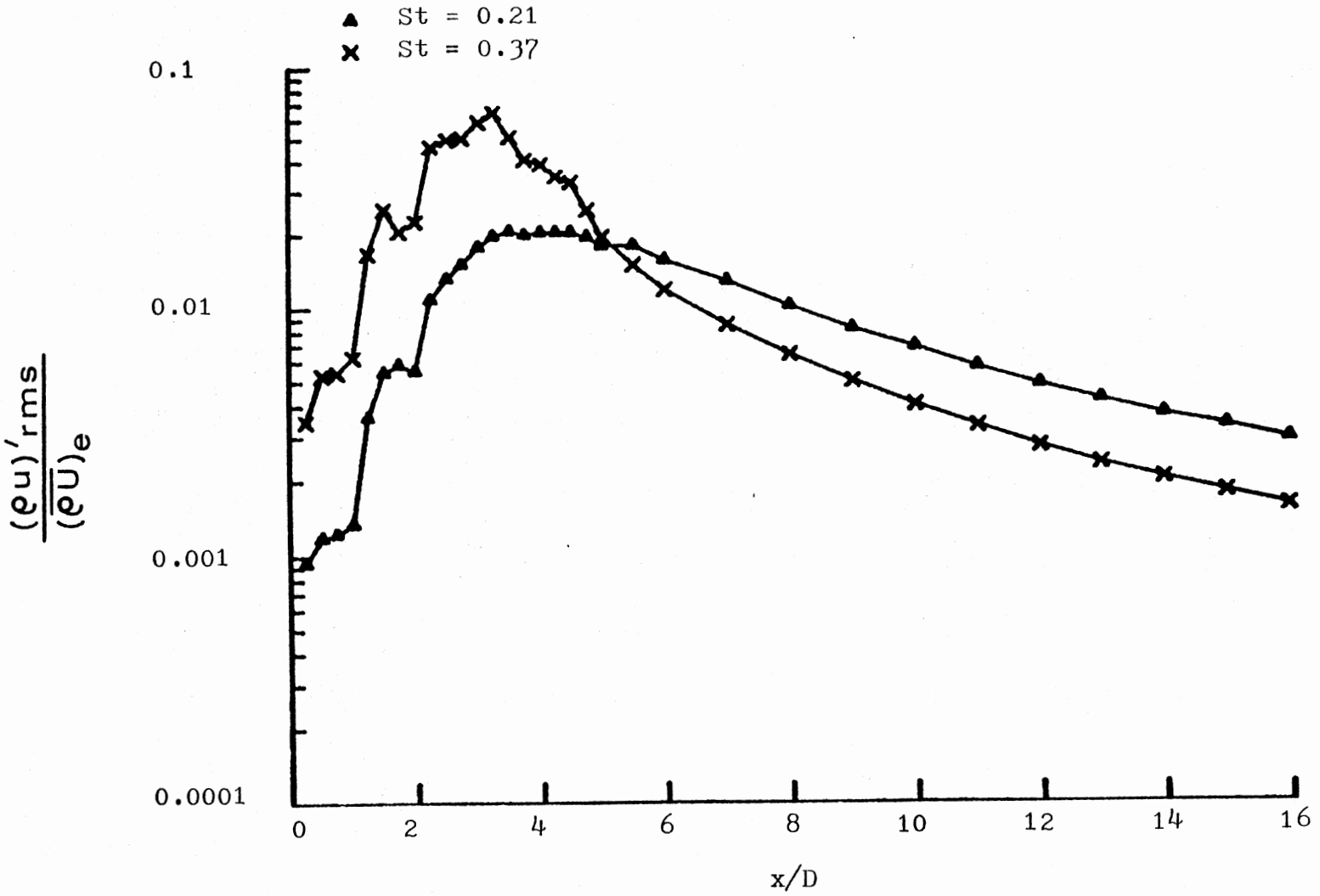

Figure 16. Axial Evolution of Band-Passed Mass-Velocity Fluctuations, M=1.4 Underexpanded Jet

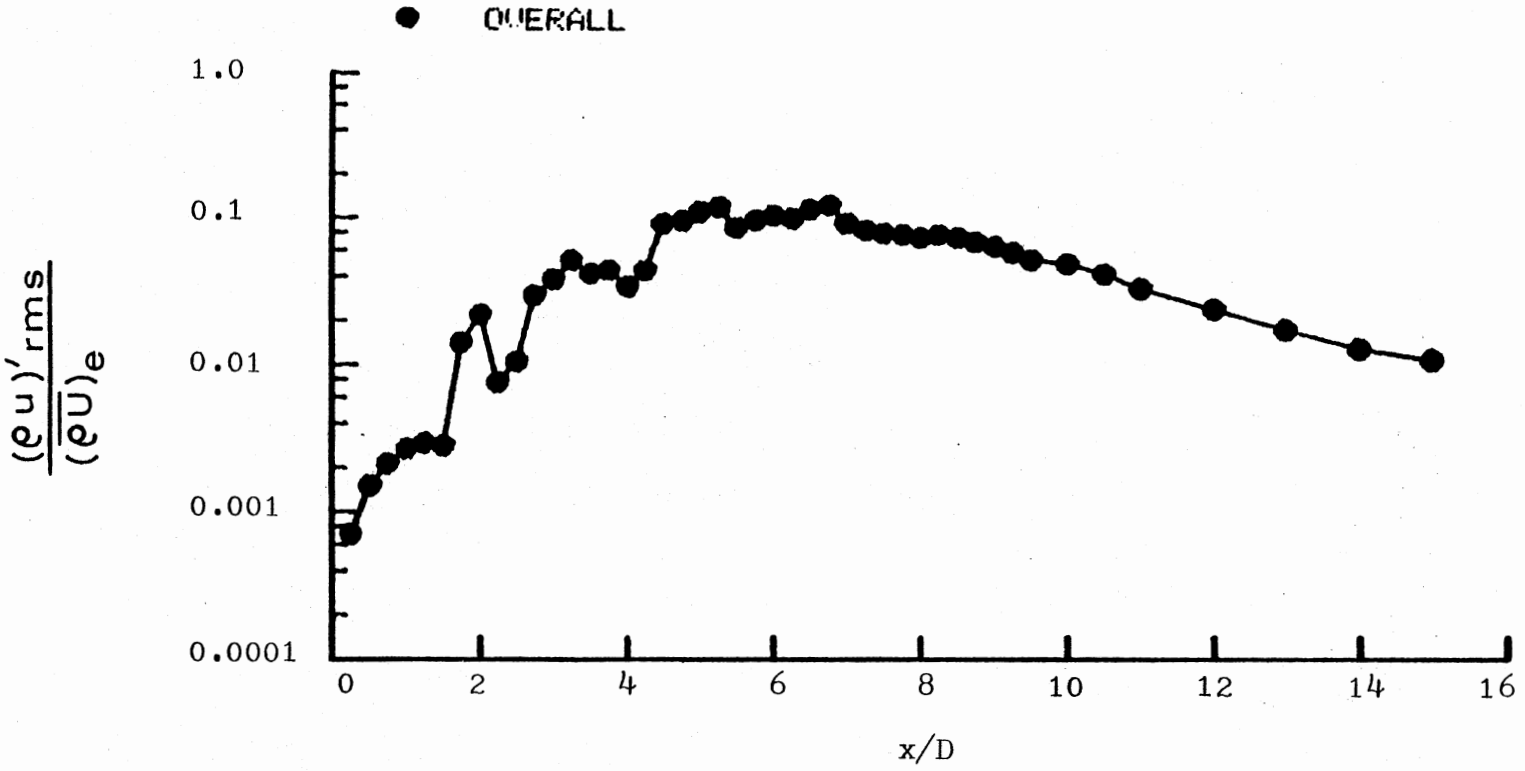

Figure 17. Axial Evolution of Overall Mass-Velocity Fluctuations, M = 2.1 Underexpanded Jet

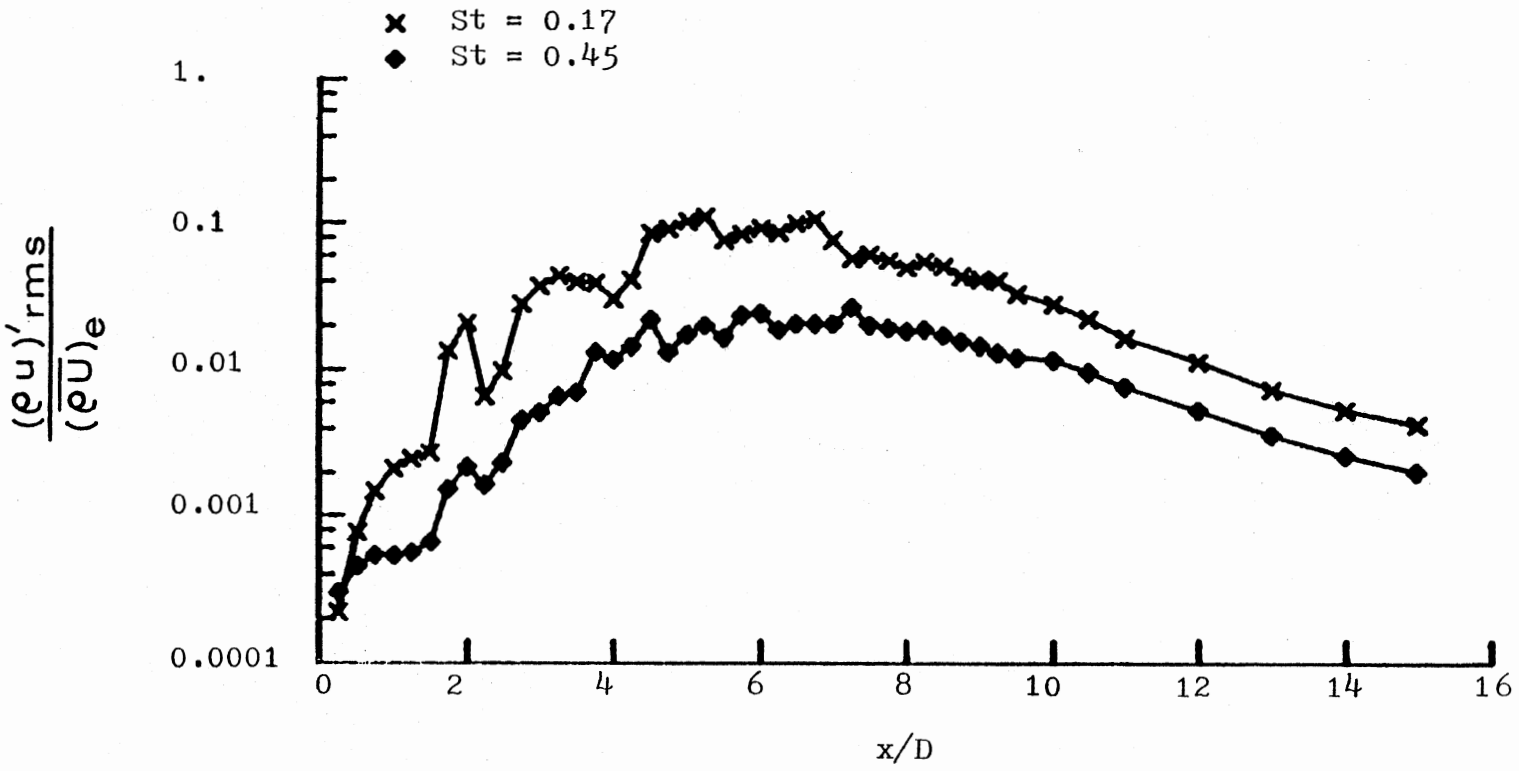

Figure 18. Axial Evolution of Band-Passed Mass-Velocity Fluctuations, M=2.1 Underexpanded Jet

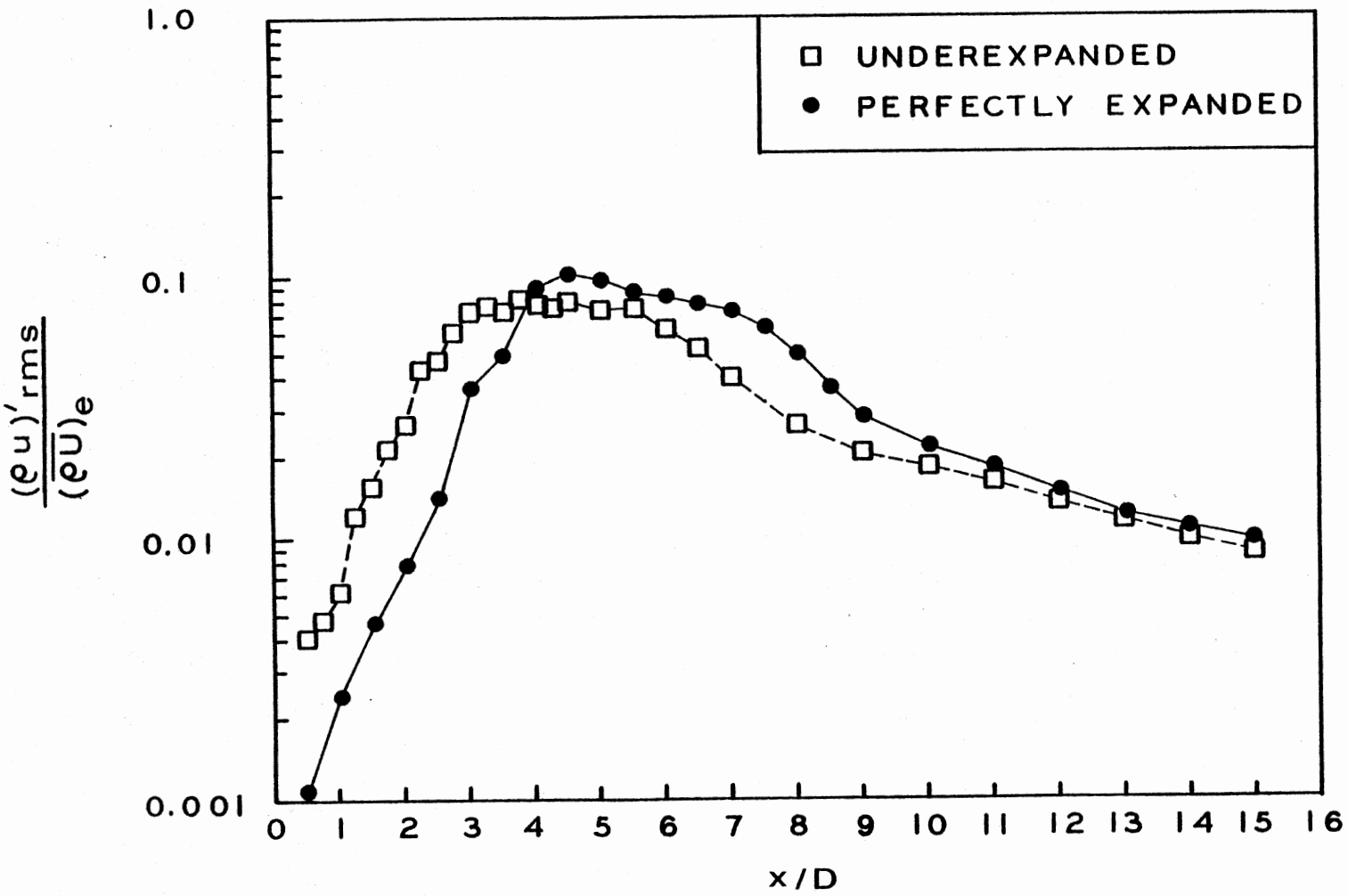

Figure 19. Axial Evolution of Overall Mass-Velocity Fluctuations, M = 1.4 Underexpanded Jet Compared with Perfectly Expanded Jet

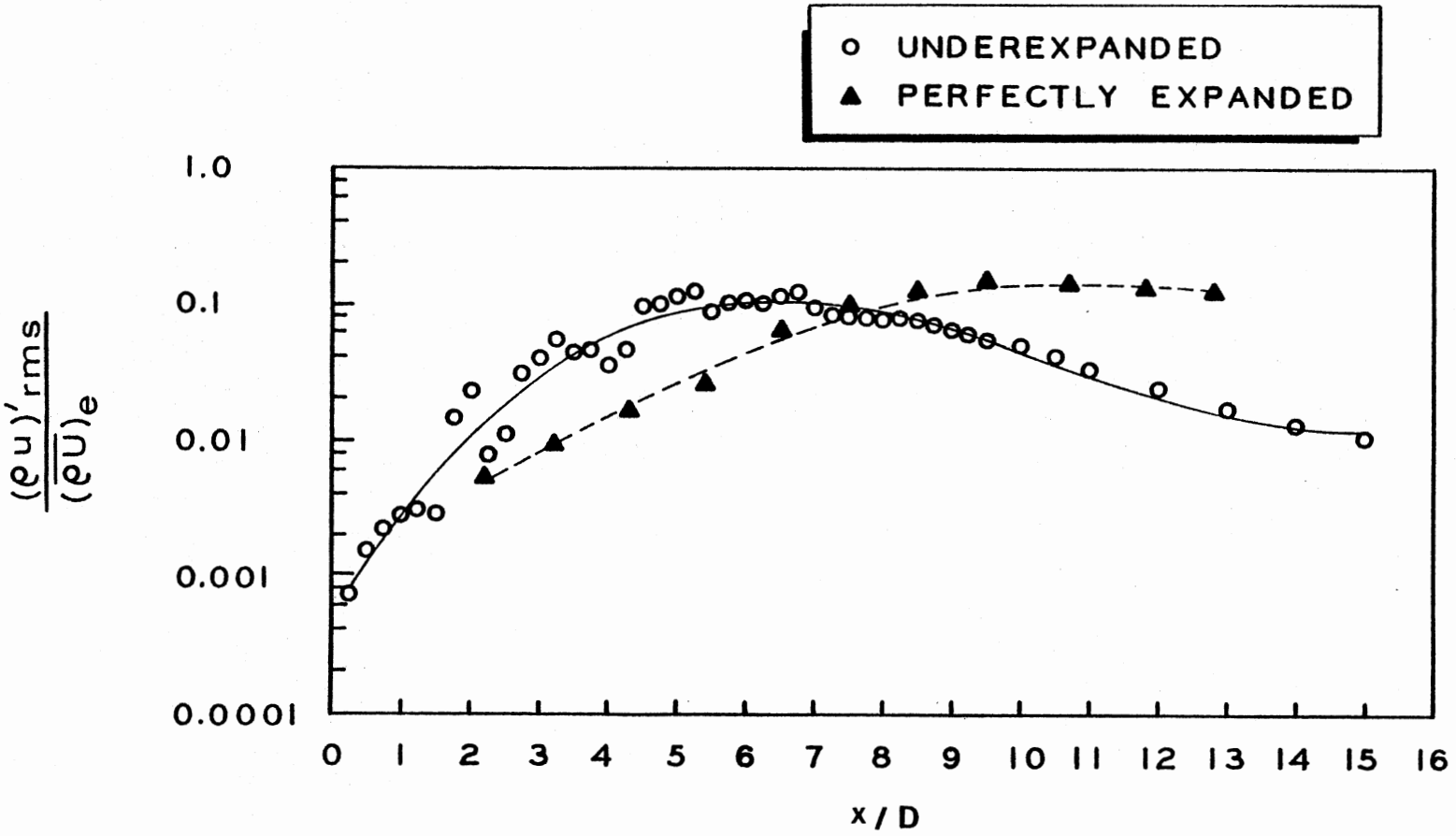

Figure 20. Axial Evolution of Overall Mass-Velocity Fluctuations, M = 2.1 Underexpanded Jet Compared with Perfectly Expanded Jet

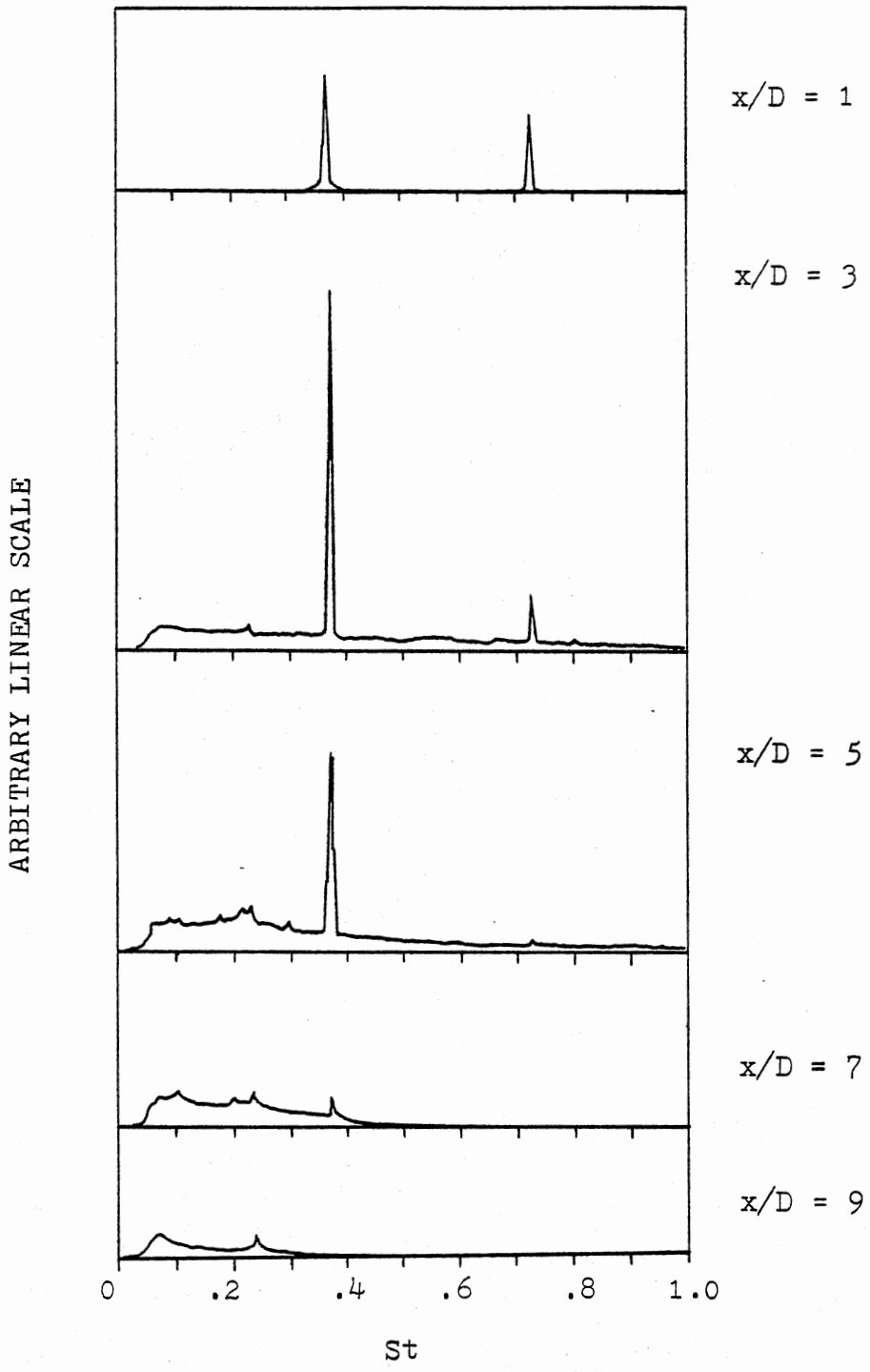

Figure 21. Flow Fluctuation Spectra, M = 1.4 Underexpanded Jet Excited at St=0.37

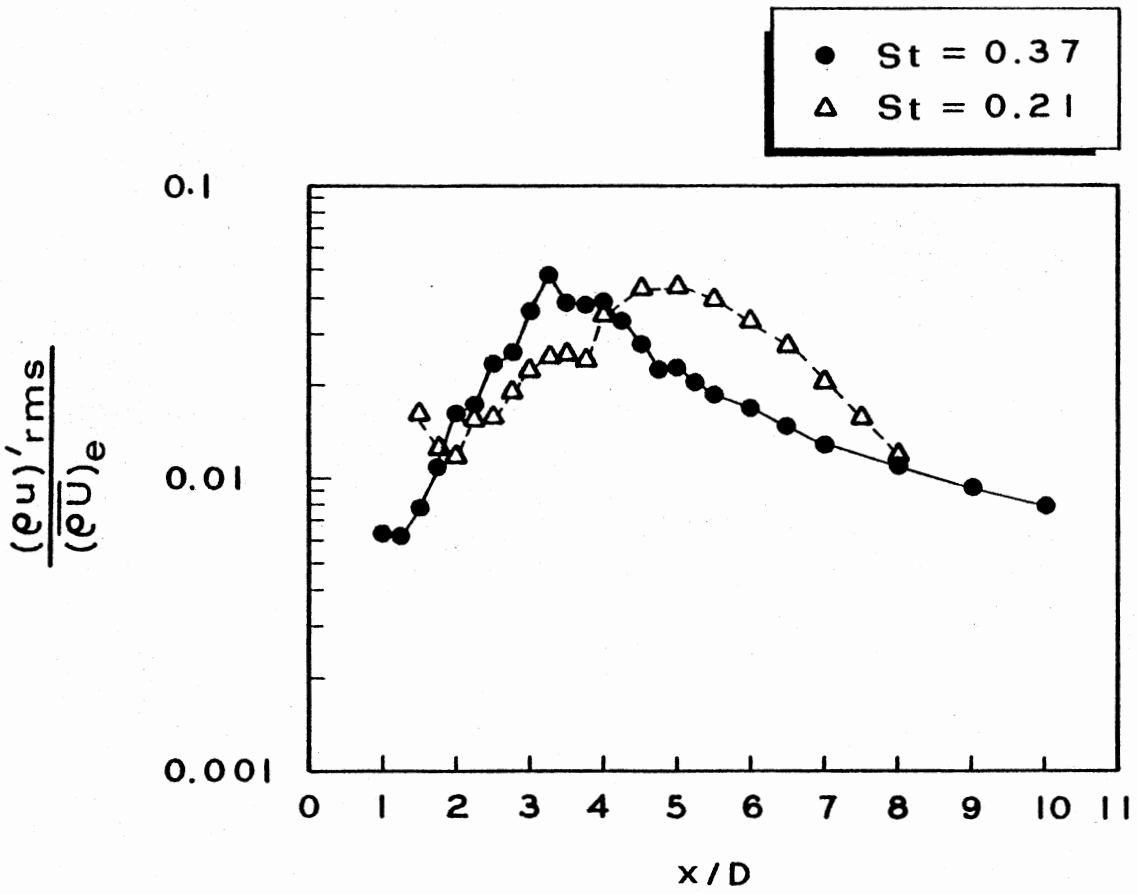

Figure 22. Axial Evolution of Band-Passed Mass-Velocity Fluctuations, Excited M = 1.4 Underexpanded Jet

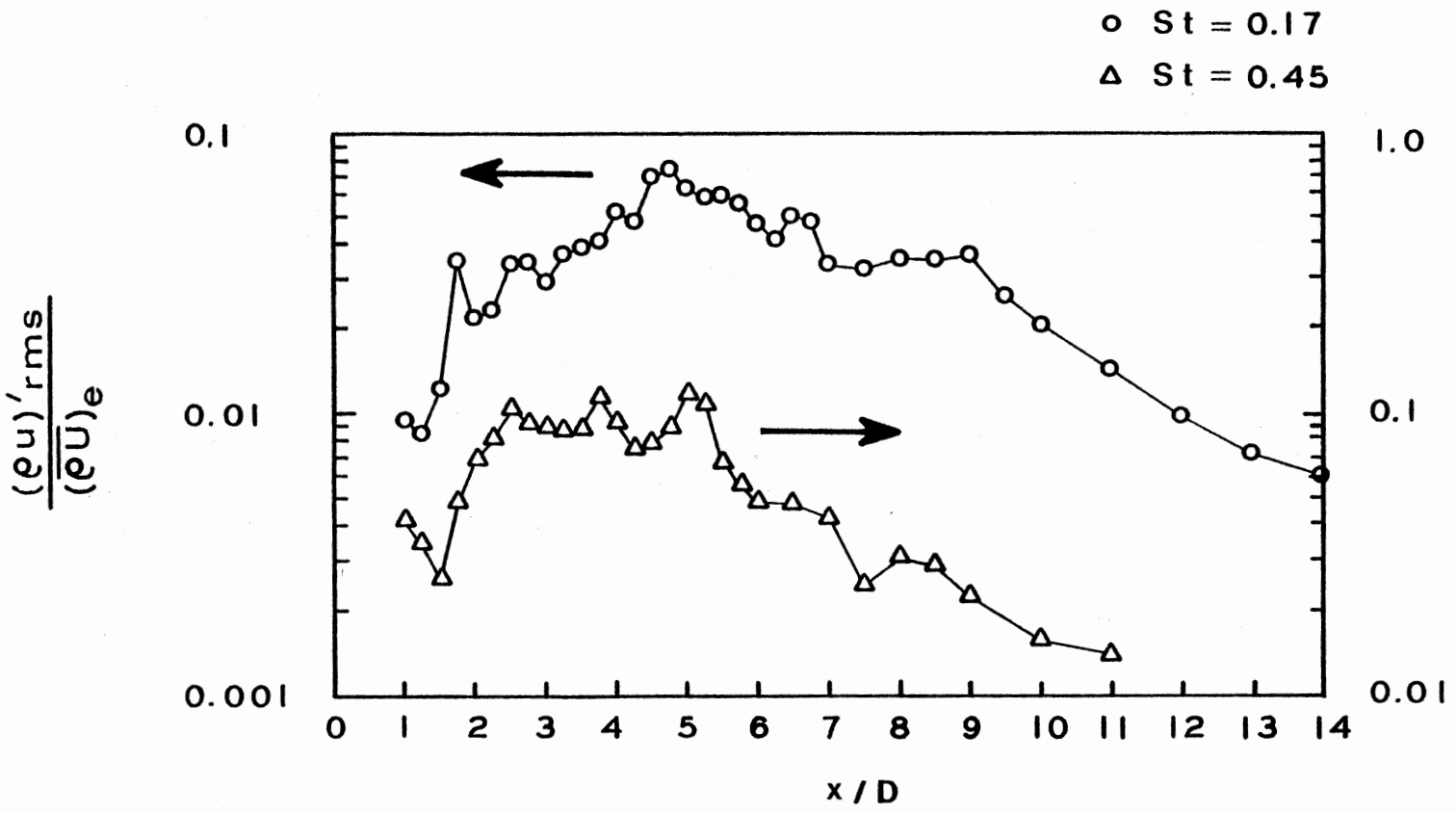

Figure 23. Axial Evolution of Band-Passed Mass-Velocity Fluctuations, Excited M=2.1 Underexpanded Jet

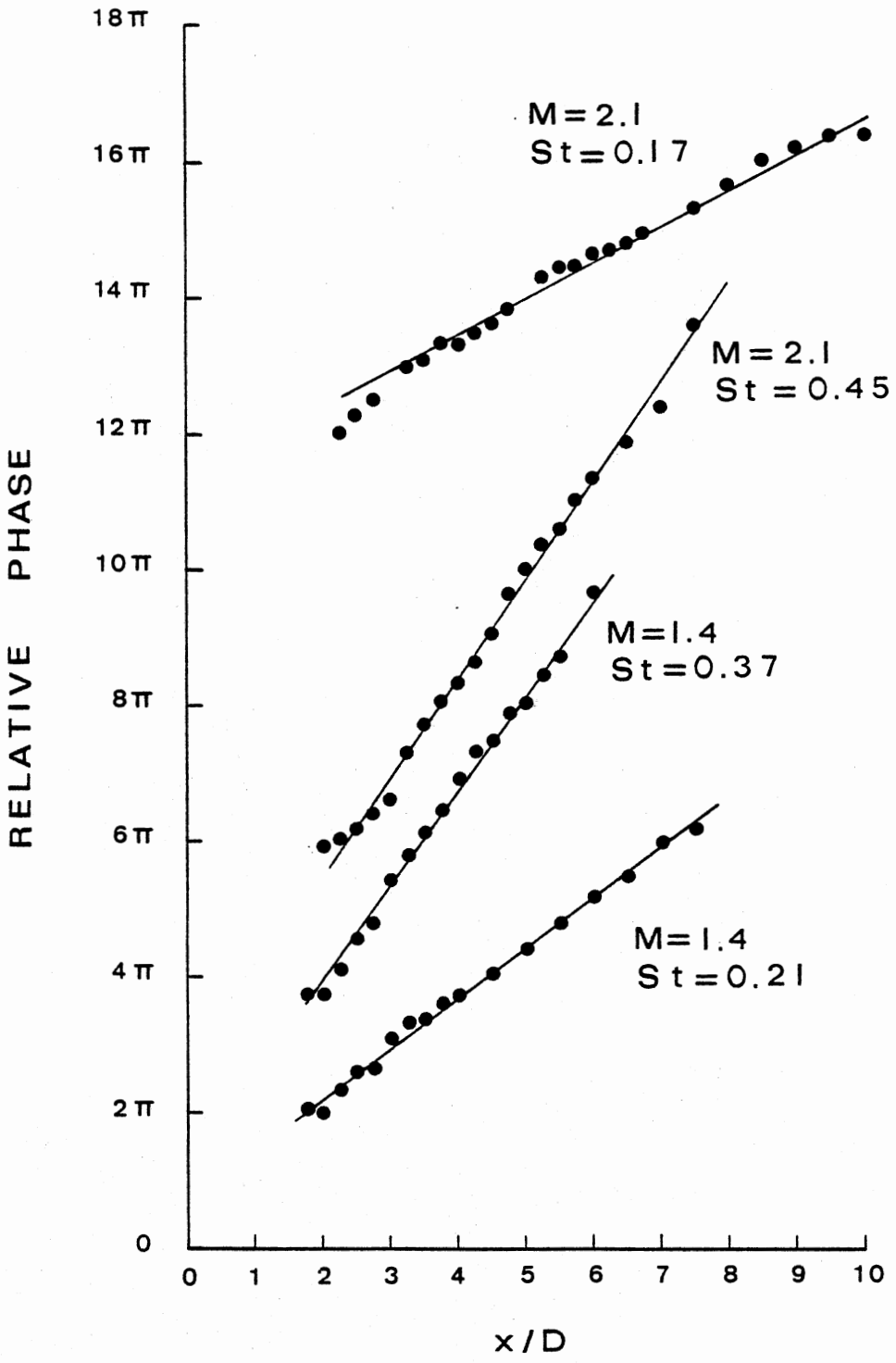

Figure 24. Axial Phase Distributions of Major Instability Components

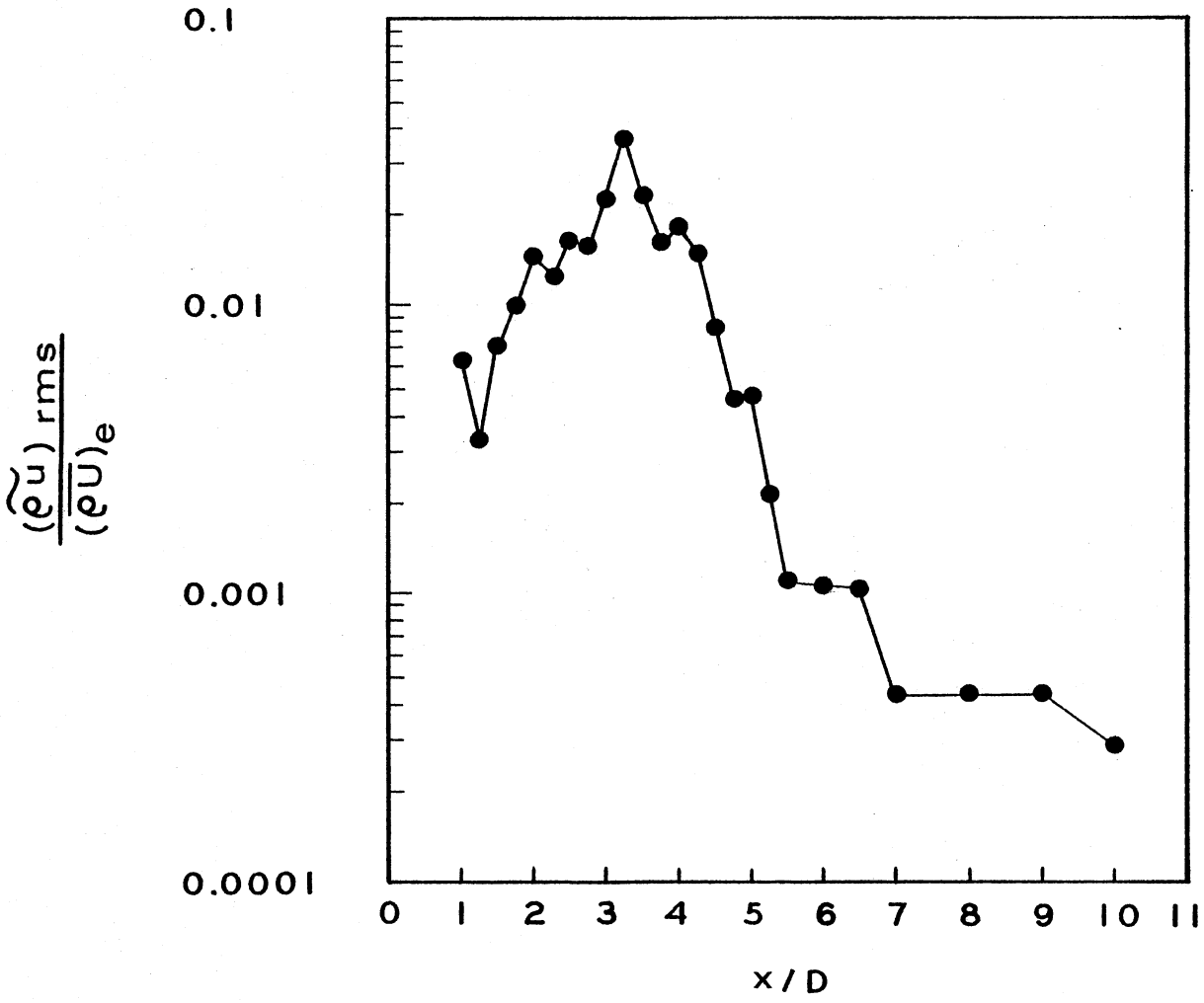

Figure 25. Axial Evolution of Coherent Mass-Velocity Fluctuations, St=0.37, M=1.4 Underexpanded Jet

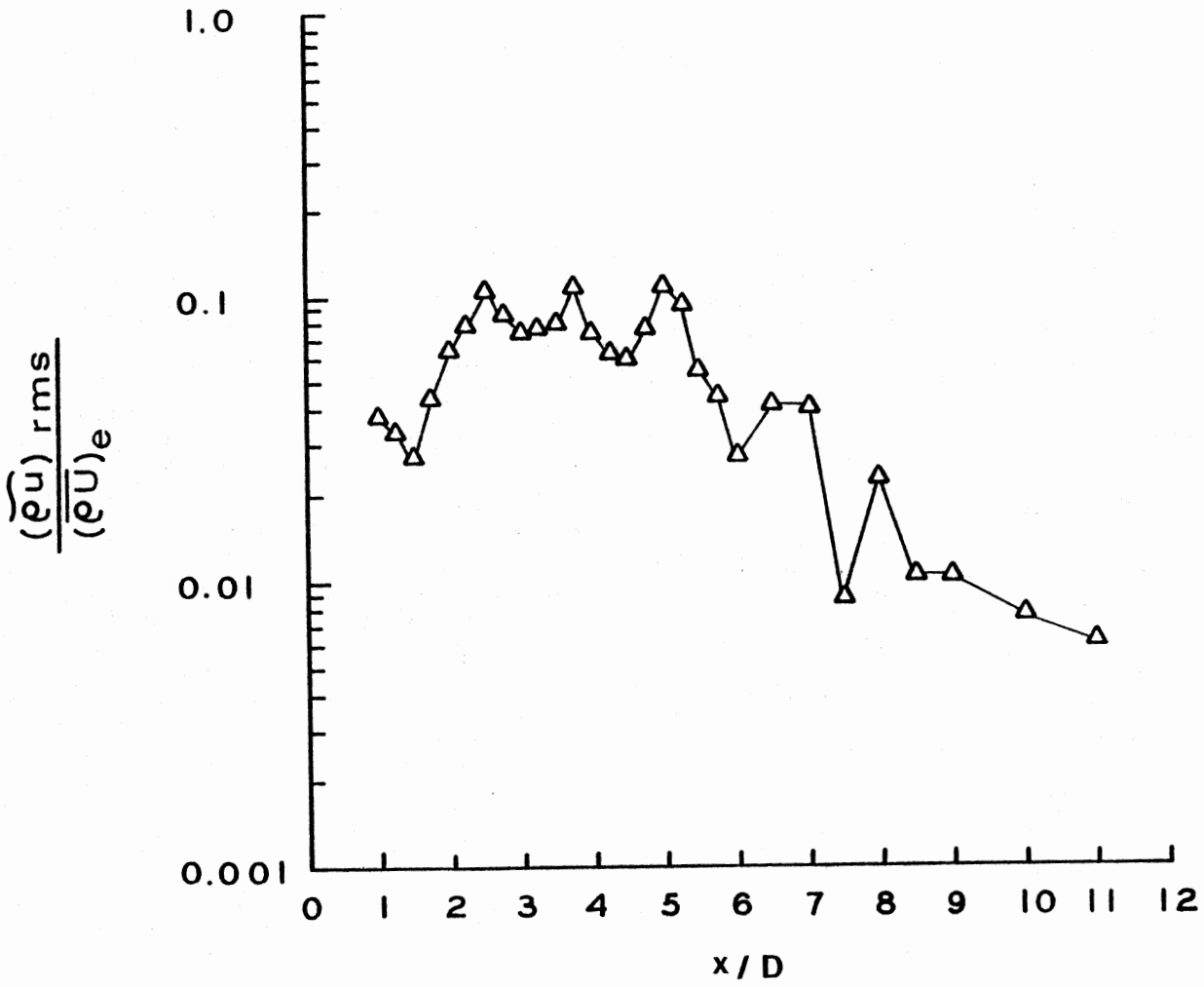

Figure 26. Axial Evolution of Coherent Mass-Velocity Fluctuations, St=0.45, M=2.1 Underexpanded Jet

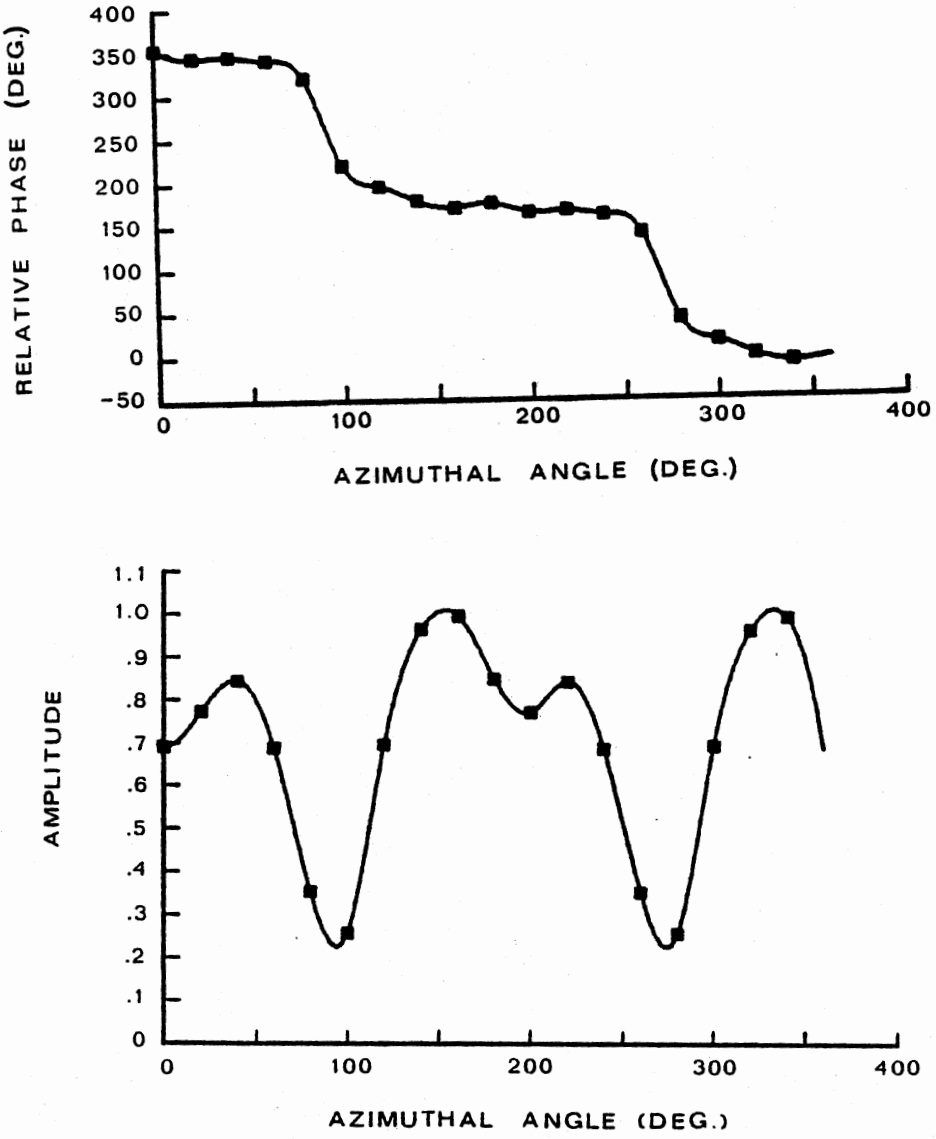

Figure 27. Experimentally Measured Azimuthal Behavior of St=0.37 Coherent Fluctuations, M=1.4 Underexpanded Jet

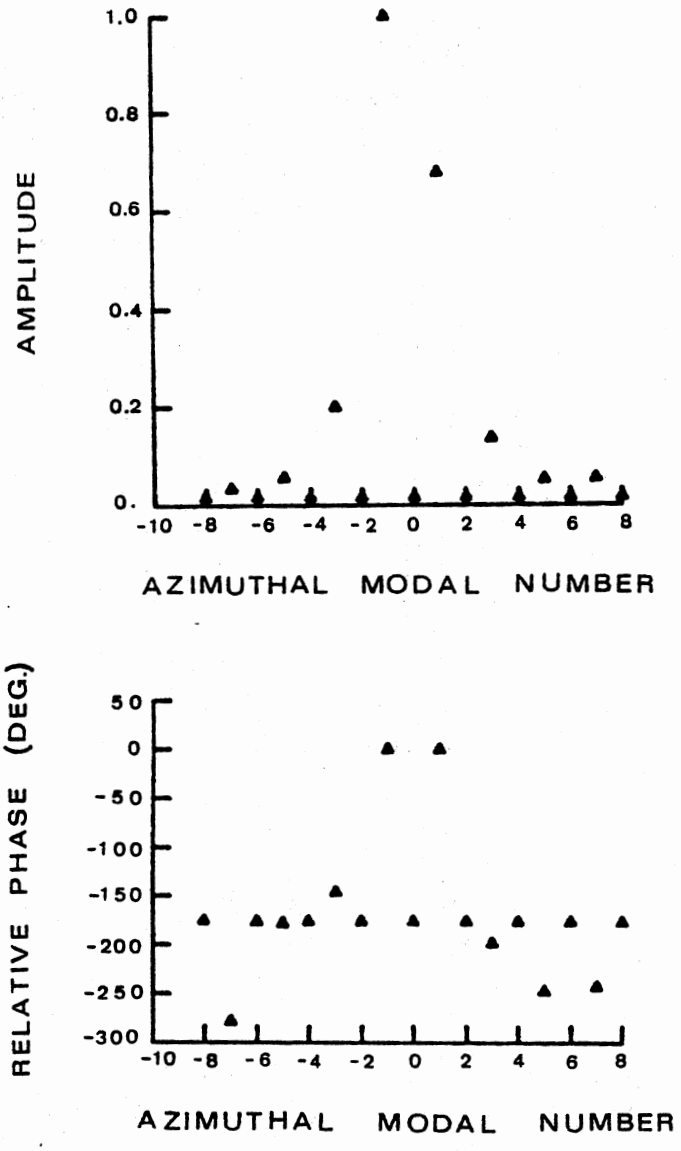

Figure 28. Azimuthal Modal Spectrum of the St=0.37 Coherent Fluctuations, Obtained by Fourier Analyzing the Data Shown in Figure 27

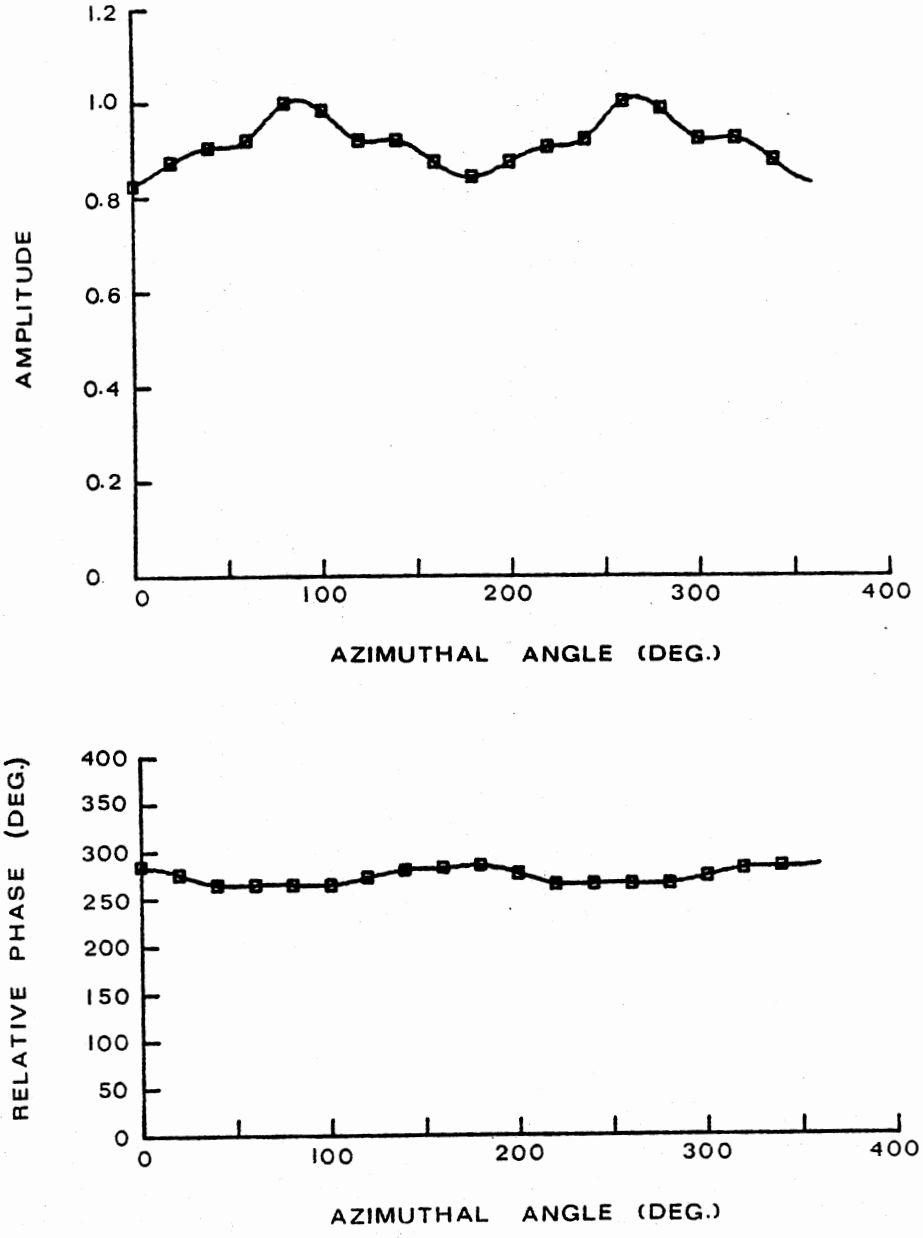

Figure 29. Experimentally Measured Azimuthal Behavior of St=0.21 Coherent Fluctuations, M=1.4 Underexpanded Jet

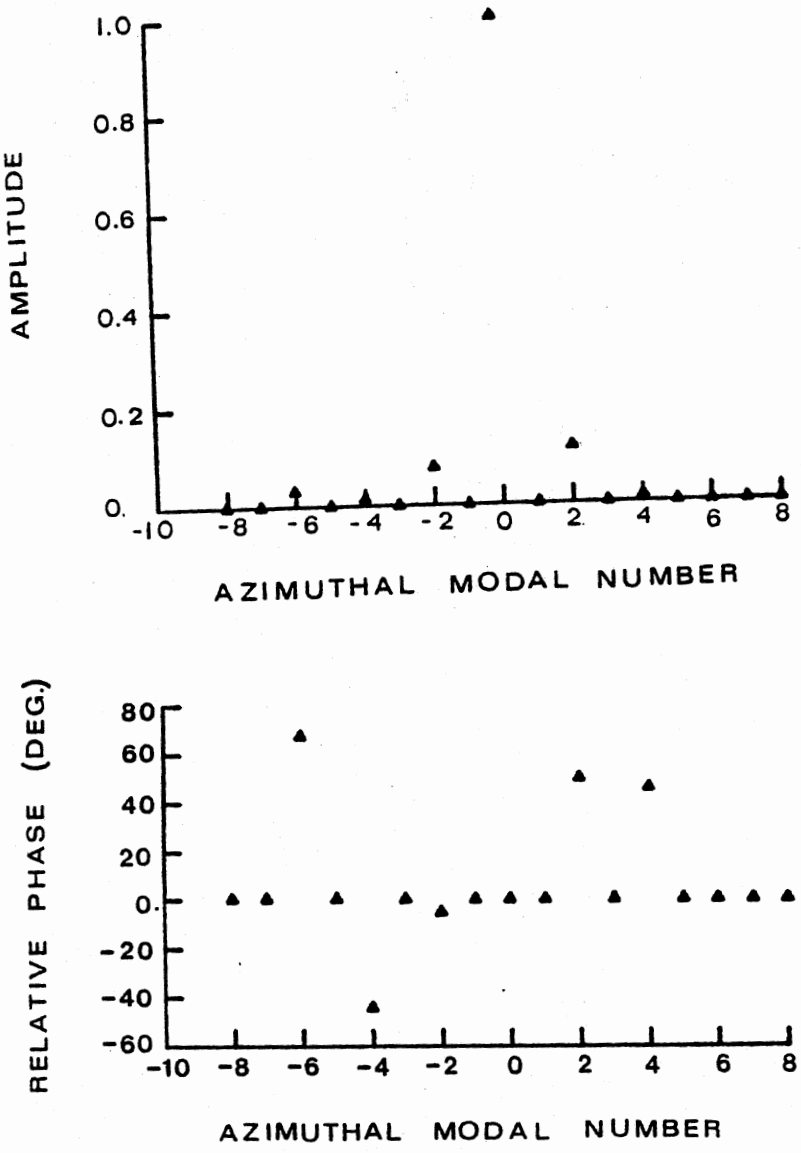

Figure 30. Azimuthal Modal Spectrum of the St=0.21 Coherent Fluctuations, Obtained by Fourier Analyzing the Data Shown in Figure 29

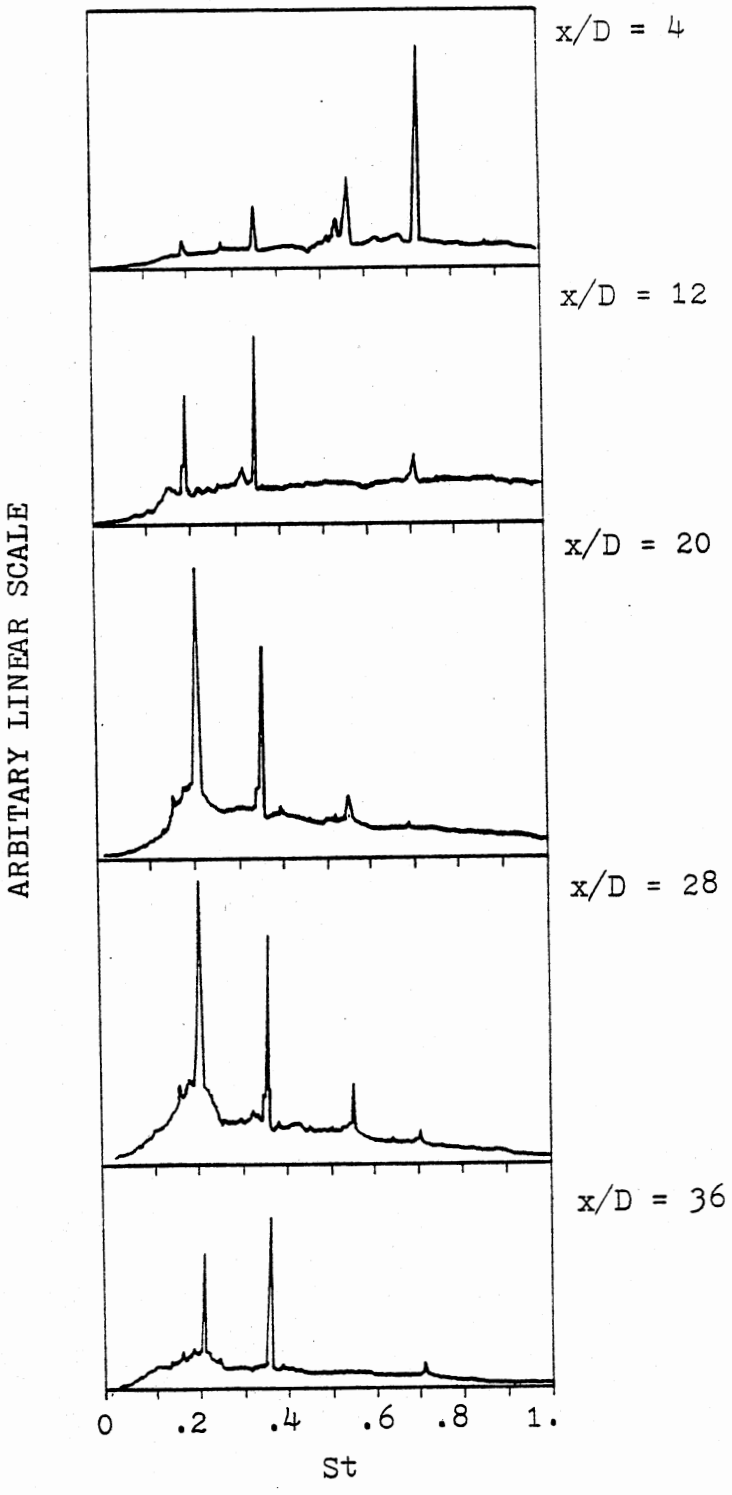

Figure 31. Acoustic Spectra, M=1.4 Underexpanded Jet, y/D= -10

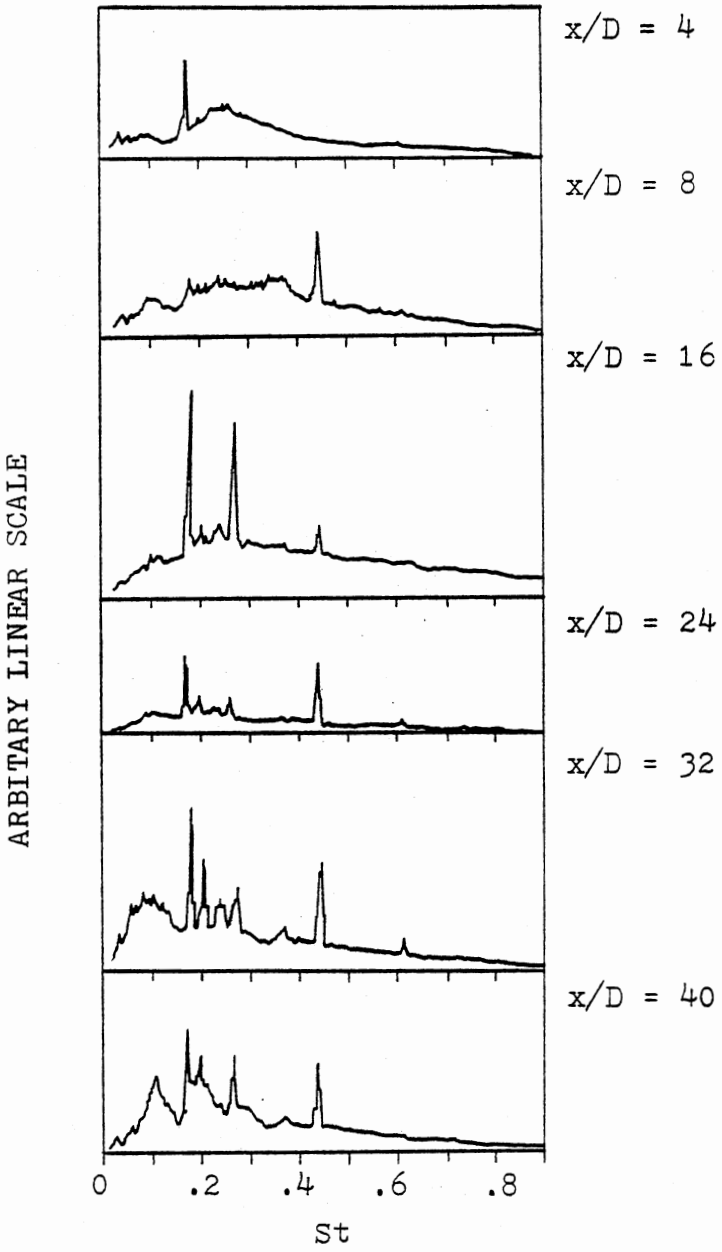

Figure 32. Acoustic Spectra, M=2.1 Underexpanded Jet, y/D= -10

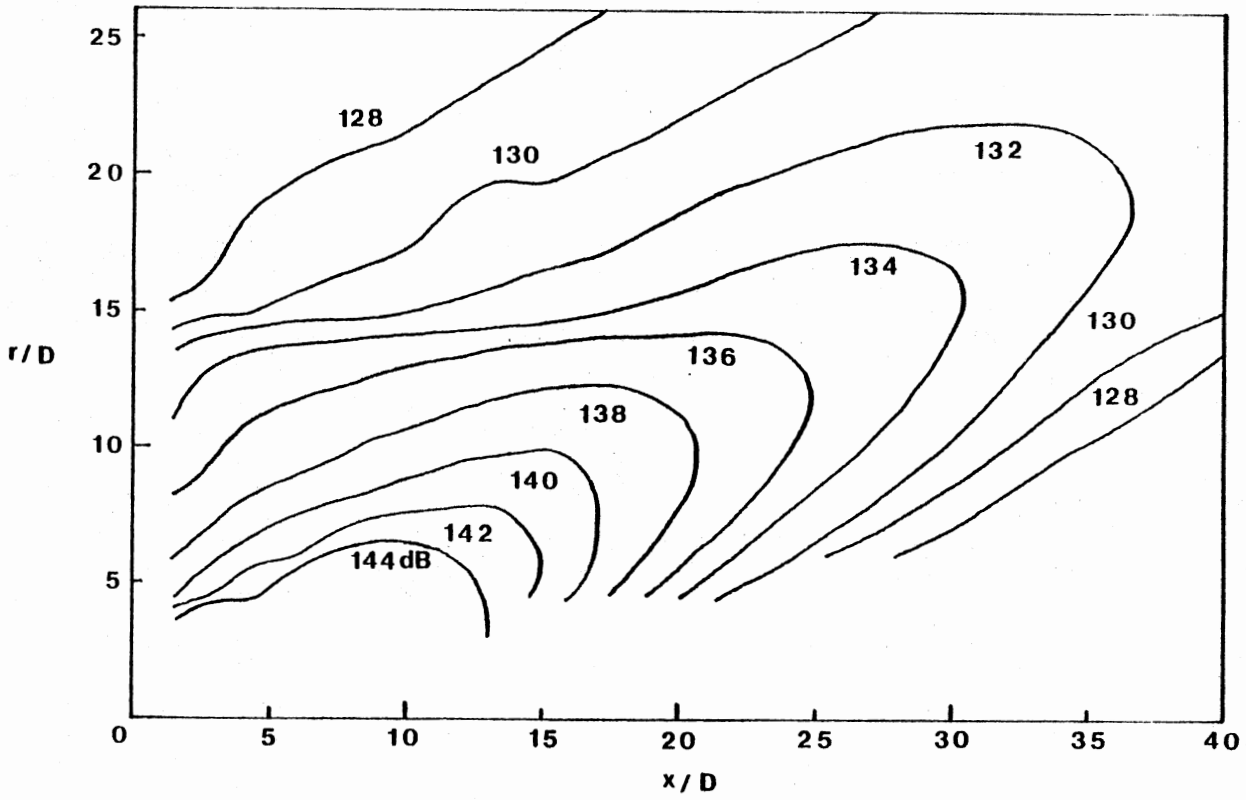

Figure 33. Overall Sound Pressure Level Contours, M = 1.4 Underexpanded Jet

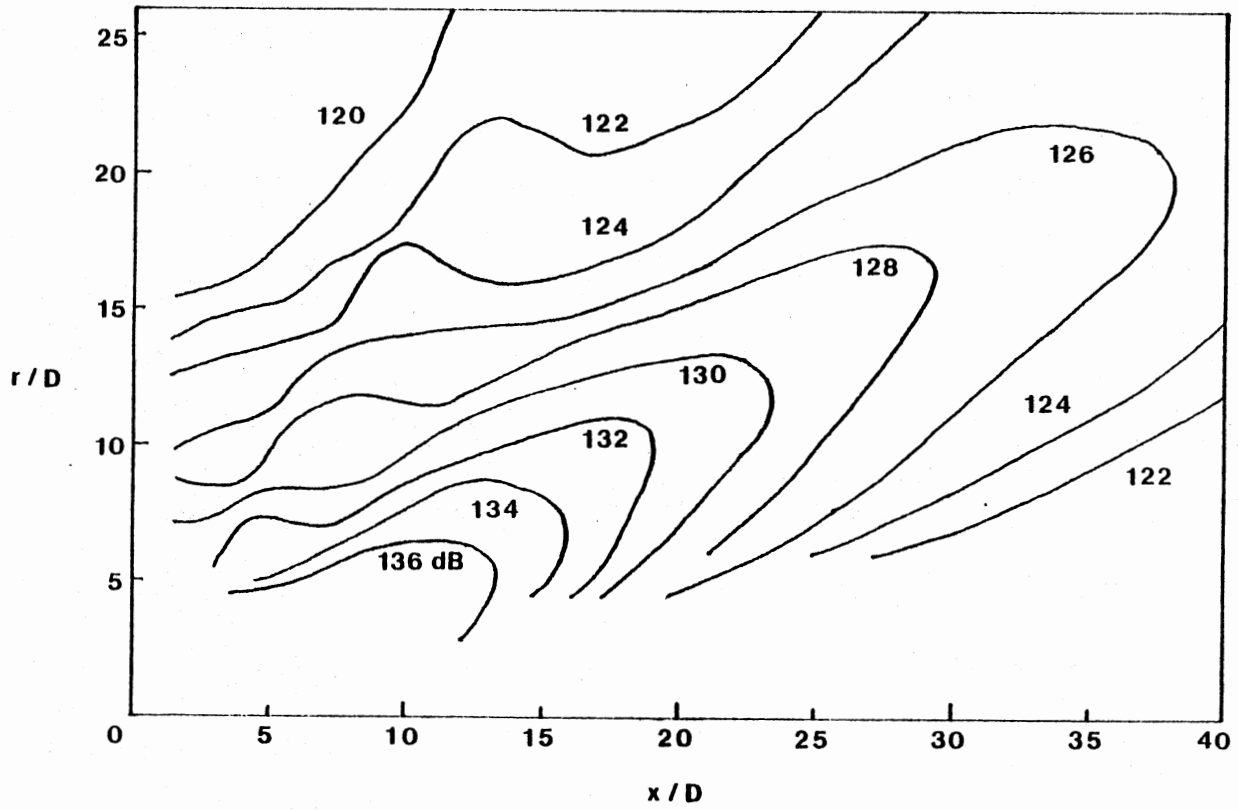

Figure 34. St=0.37 Band-Passed Sound Pressure Level Contours, M=1.4 Underexpanded Jet

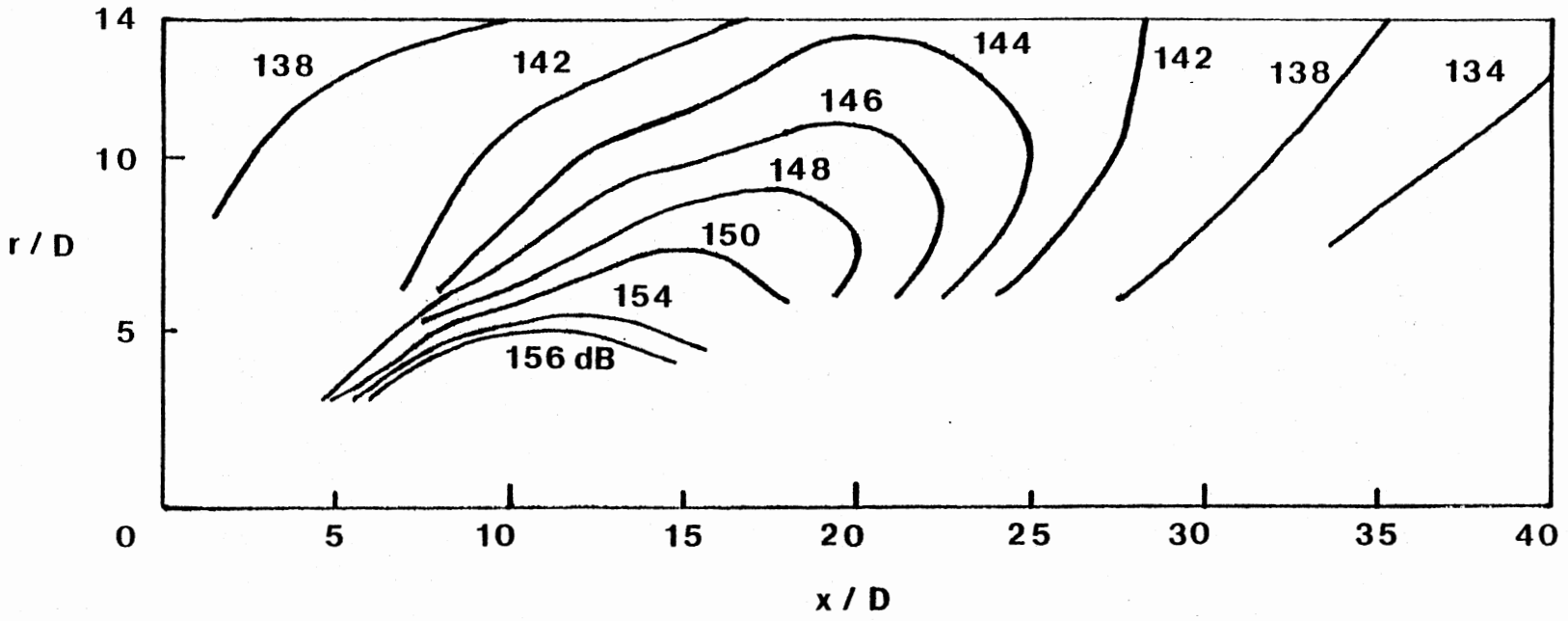

Figure 35. Overall Sound Pressure Level Contours, M=2.1 Underexpanded Jet

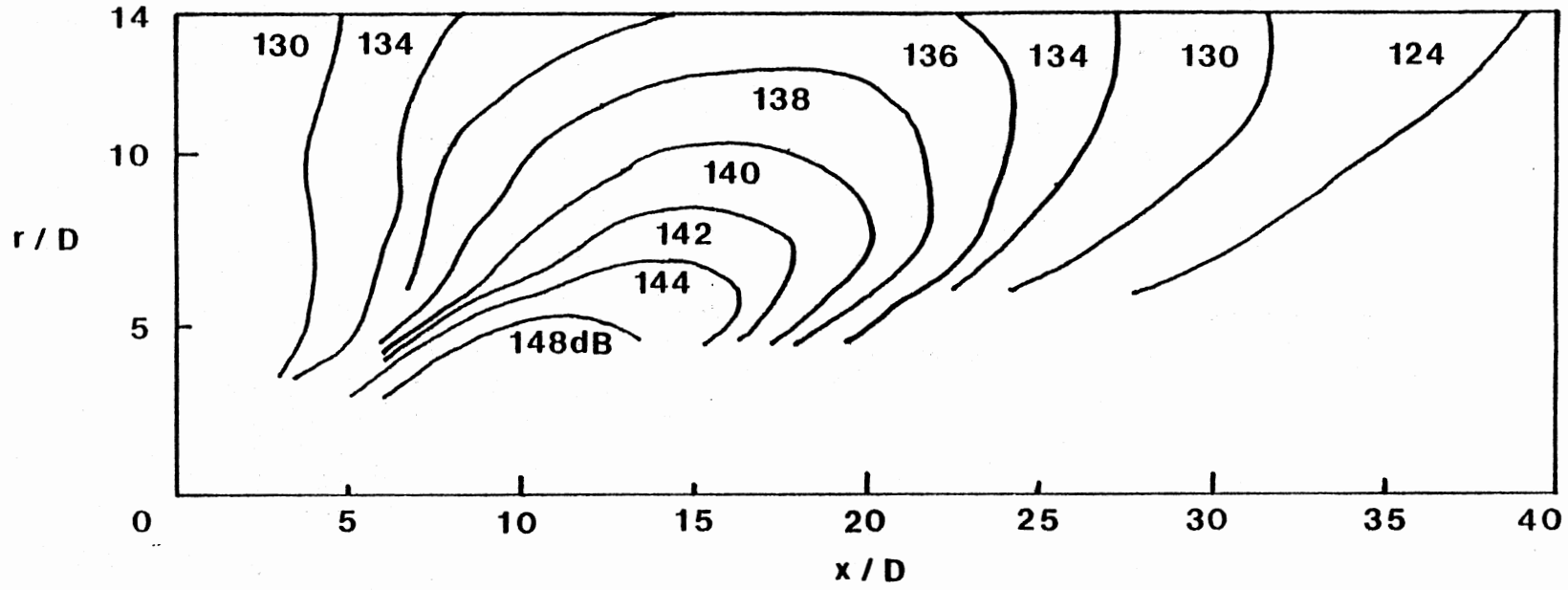

Figure 36. St=0.45 Band-Passed Sound Pressure Level Contours, M=2.1 Underexpanded Jet

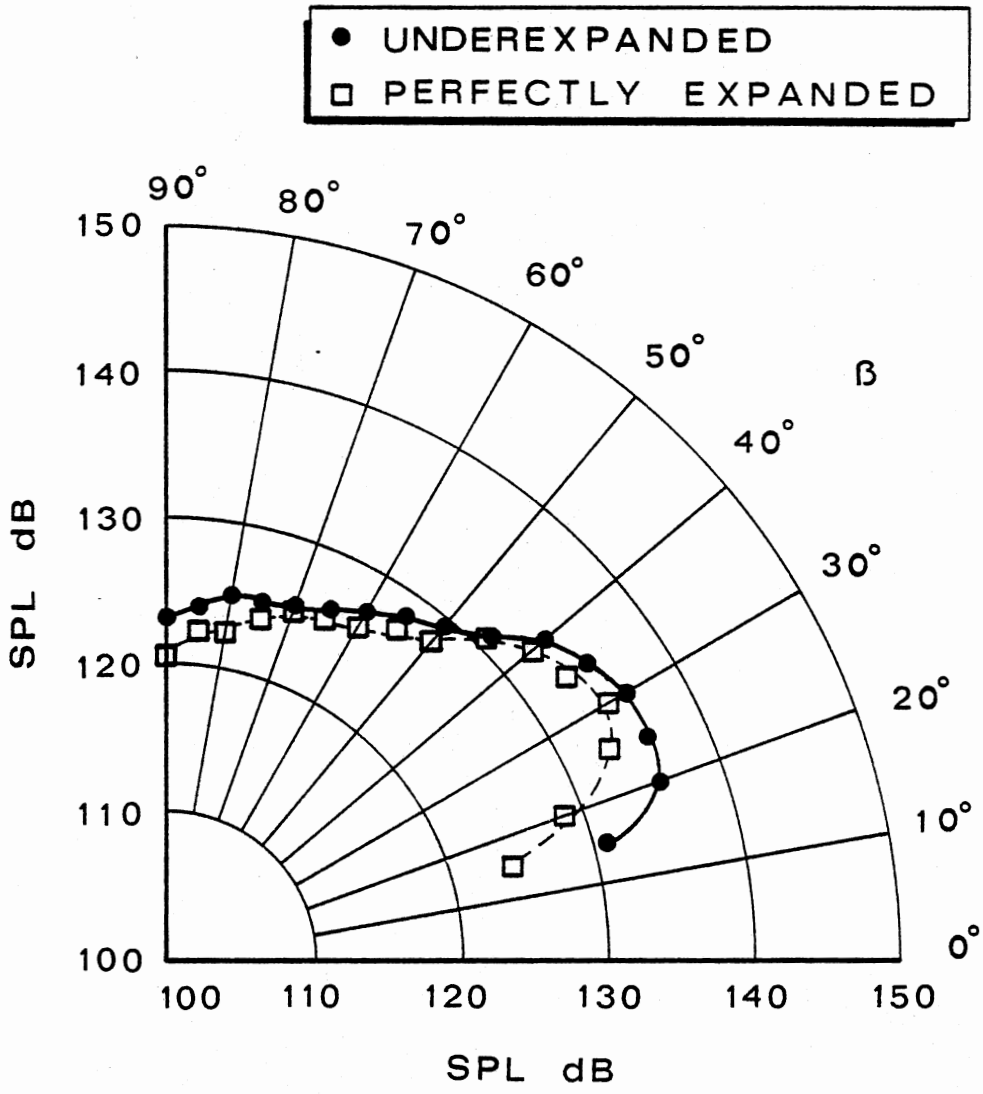

Figure 37. Overall Sound Pressure Level Directivity Distributions, R/D=30, M=1.4, Underexpanded Jet Compared with Perfectly Expanded Jet

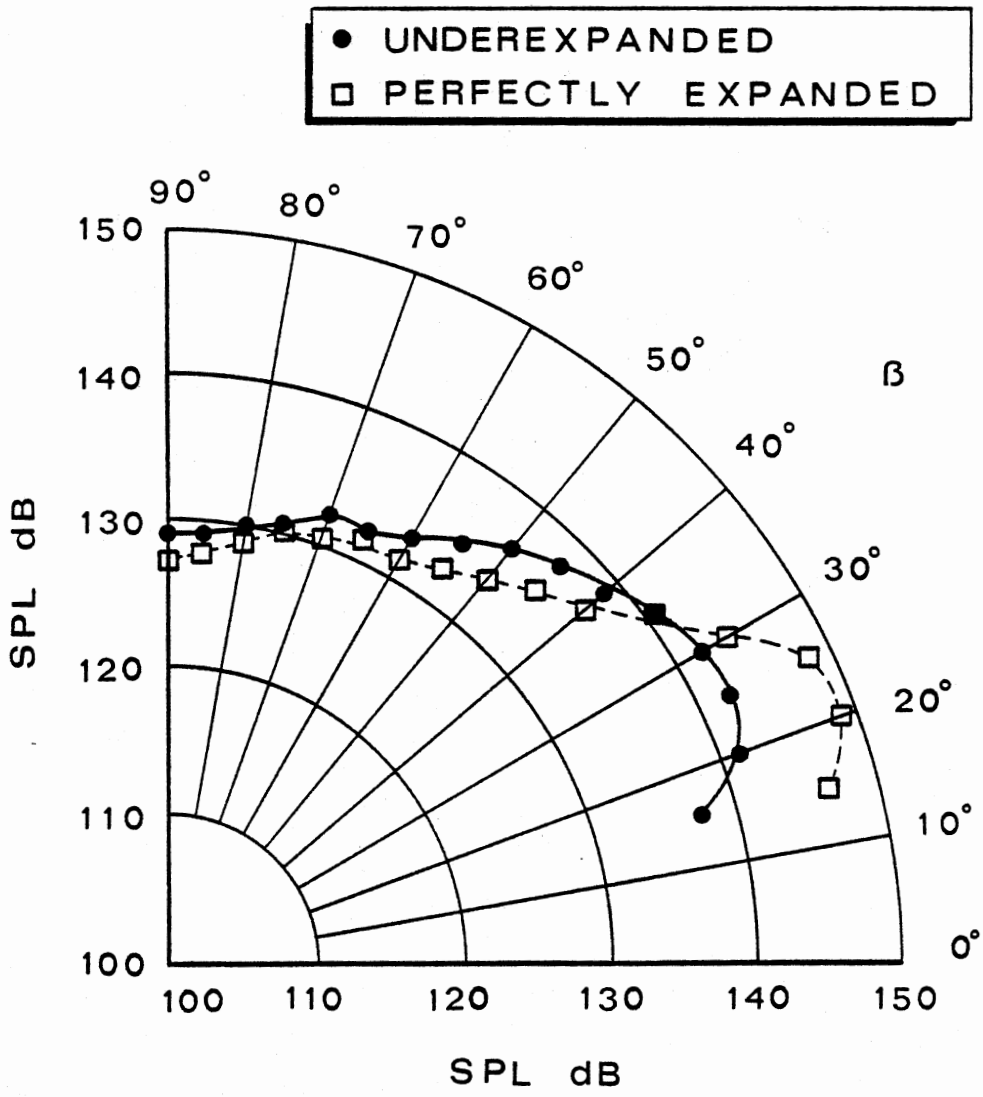

Figure 38. Overall Sound Pressure Level Directivity Distributions, R/D=30, M=2.1, Underexpanded Jet Compared with Perfectly Expanded Jet

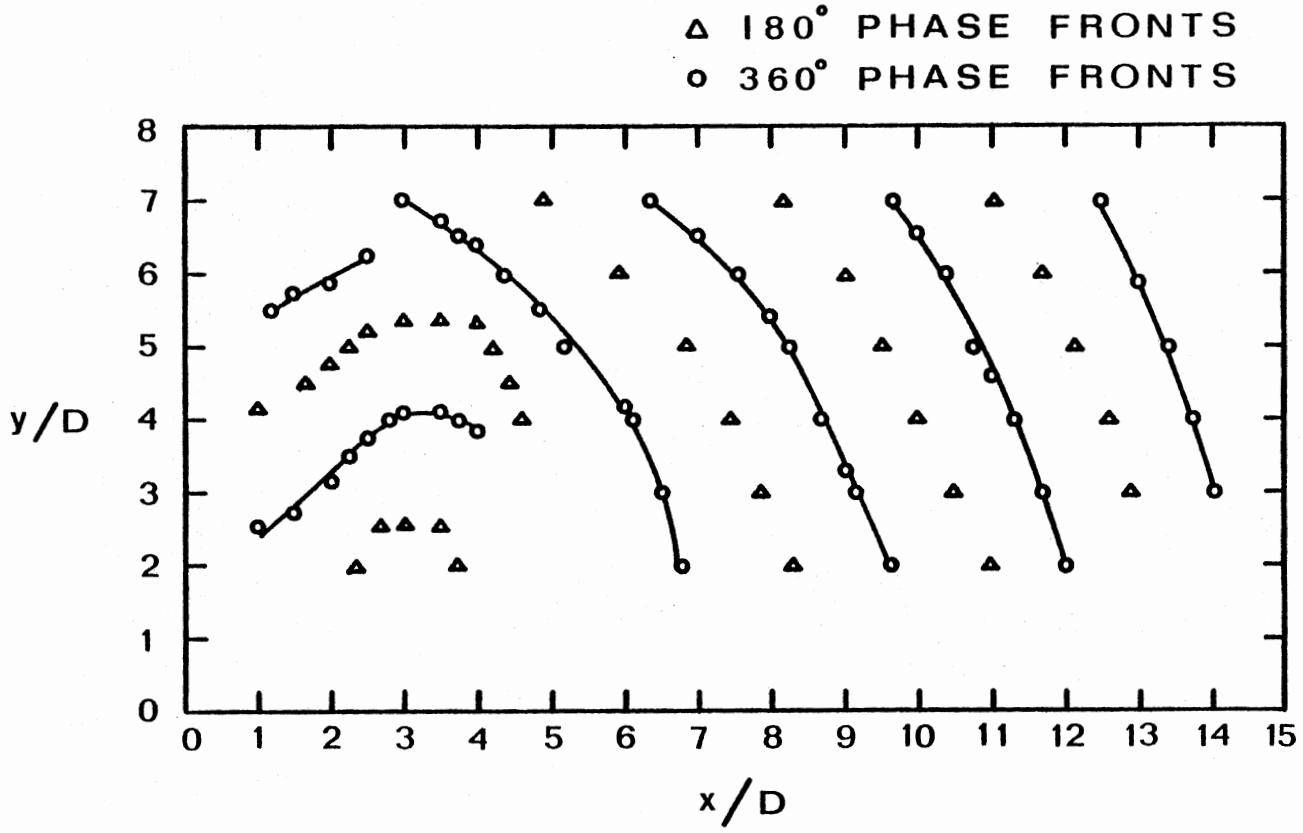

Figure 39. St=0.37 Acoustic Phase Front Distributions, M=1.4 Underexpanded Jet

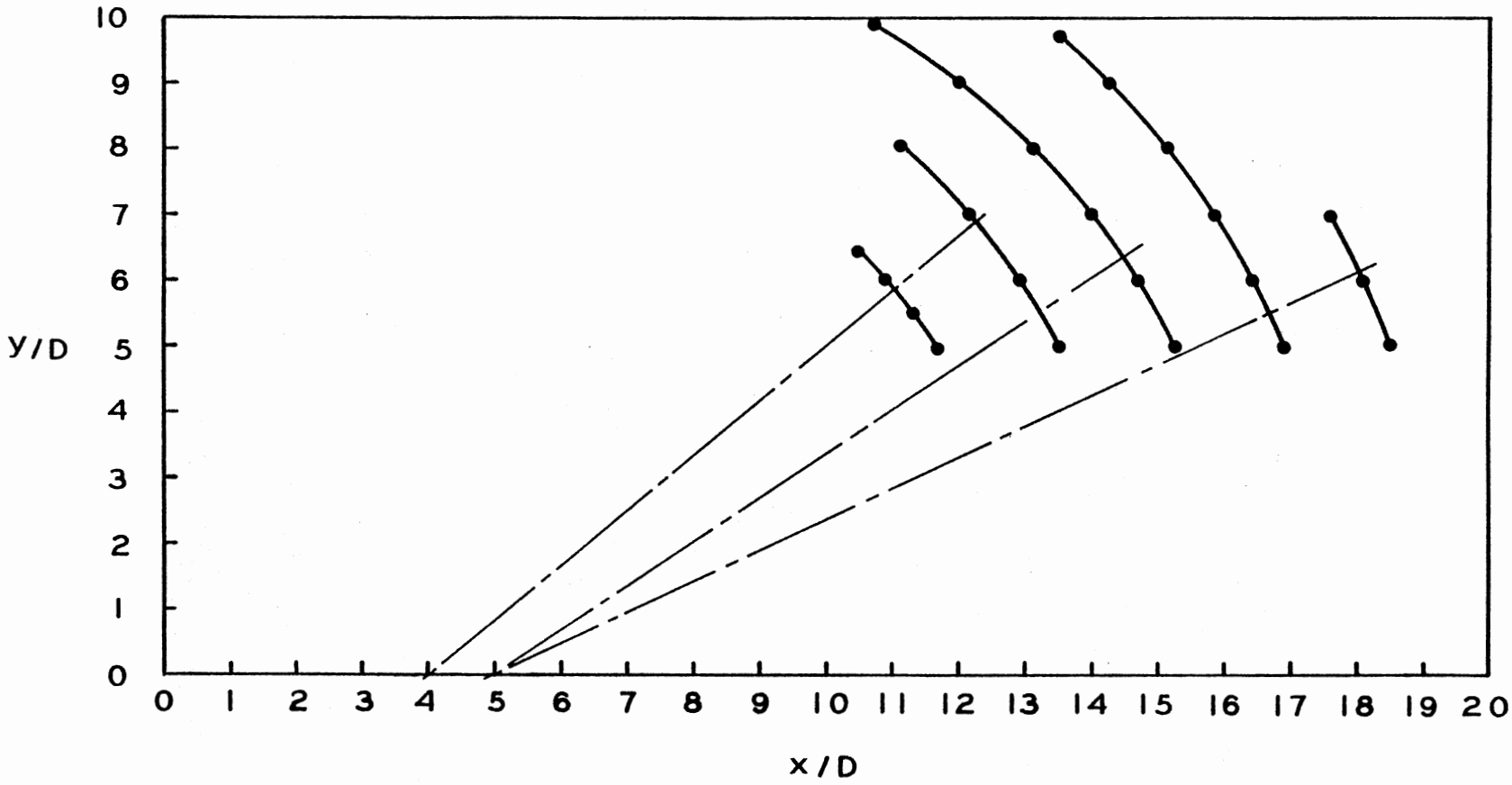

Figure 40. St=0.45 Acoustic Phase Front Distributions, M=2.1 Underexpanded Jet

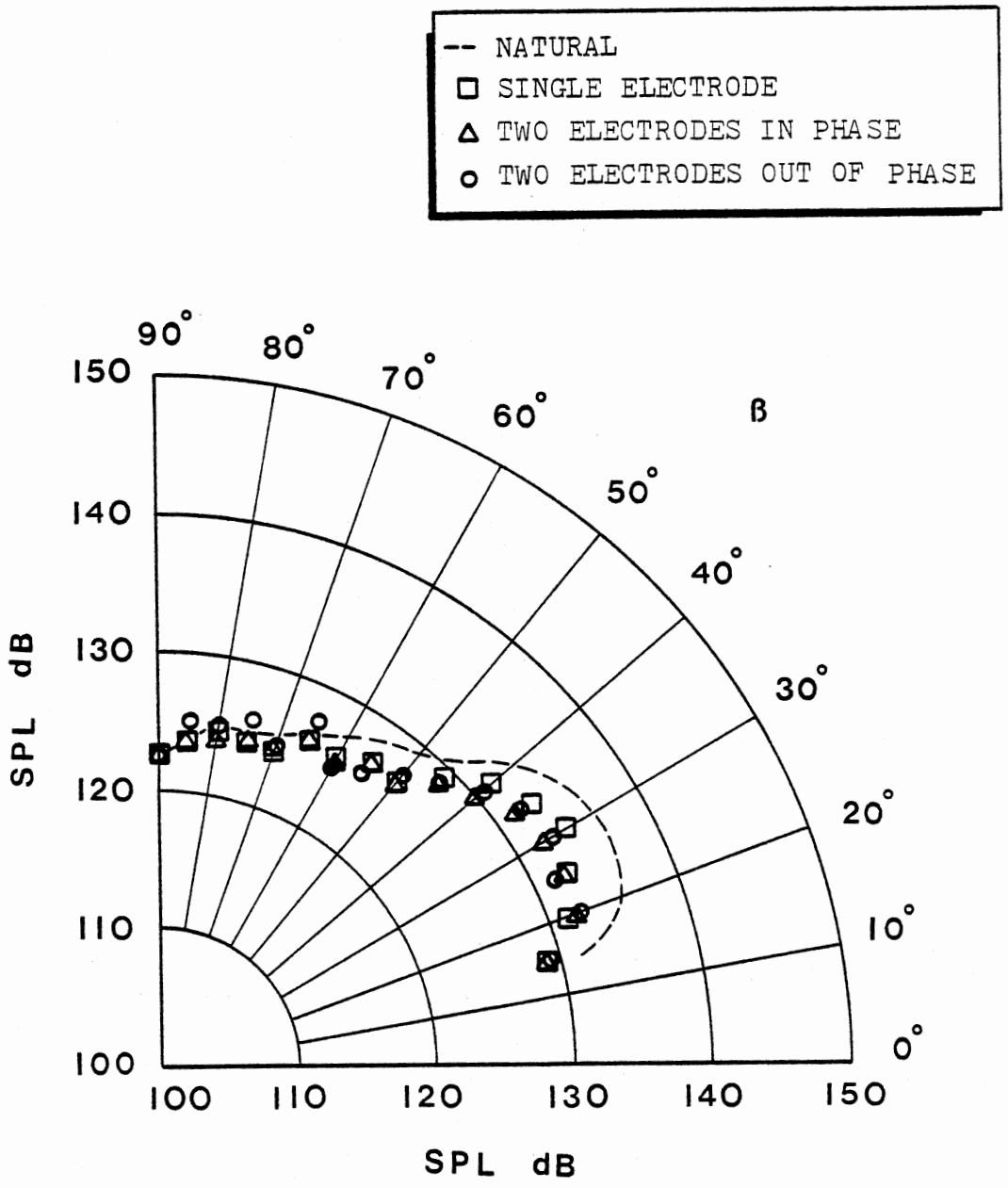

Figure 41. Effect of Excitation on Overall Sound Pressure Level Distributions, M=1.4 Underexpanded Jet, R/D=30

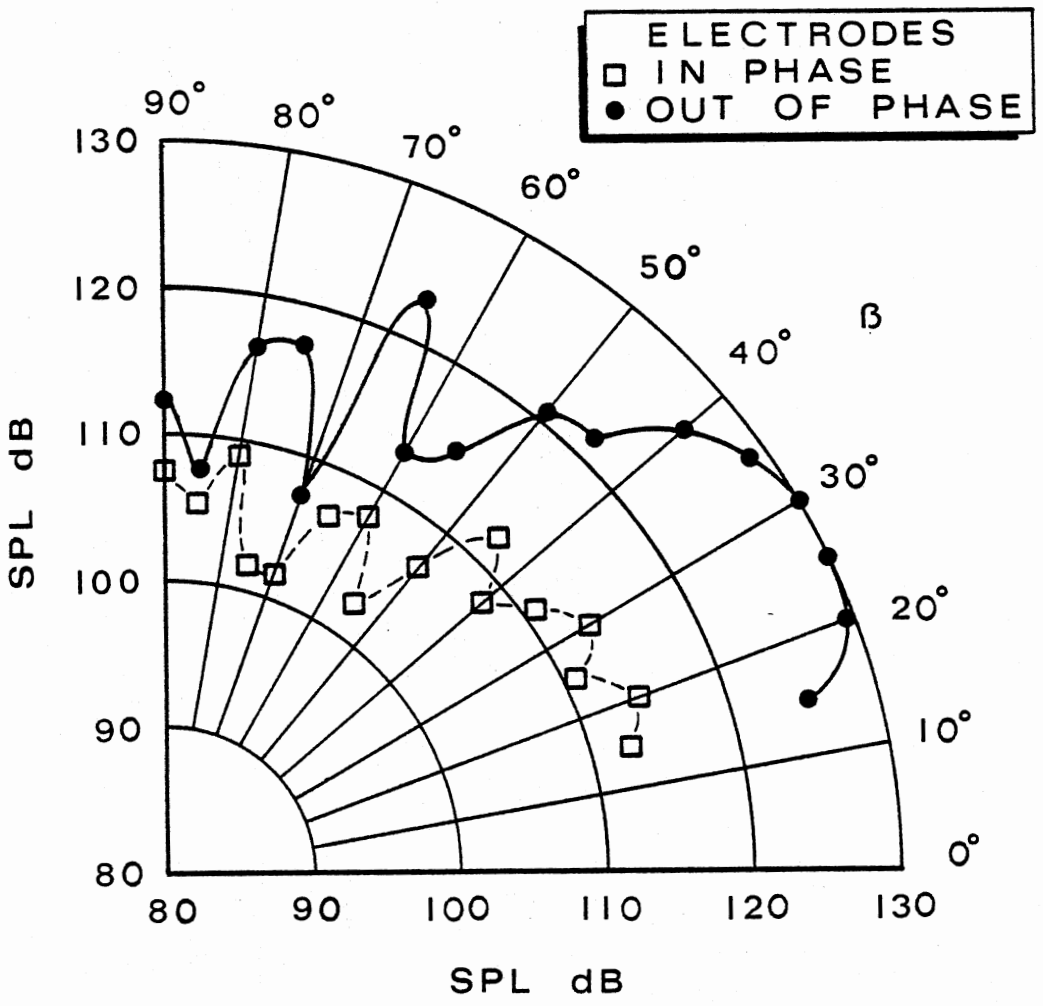

Figure 42. St=0.37 Coherent Sound Pressure Level Directivity Distributions, M=1.4 Underexpanded Jet, R/D=30

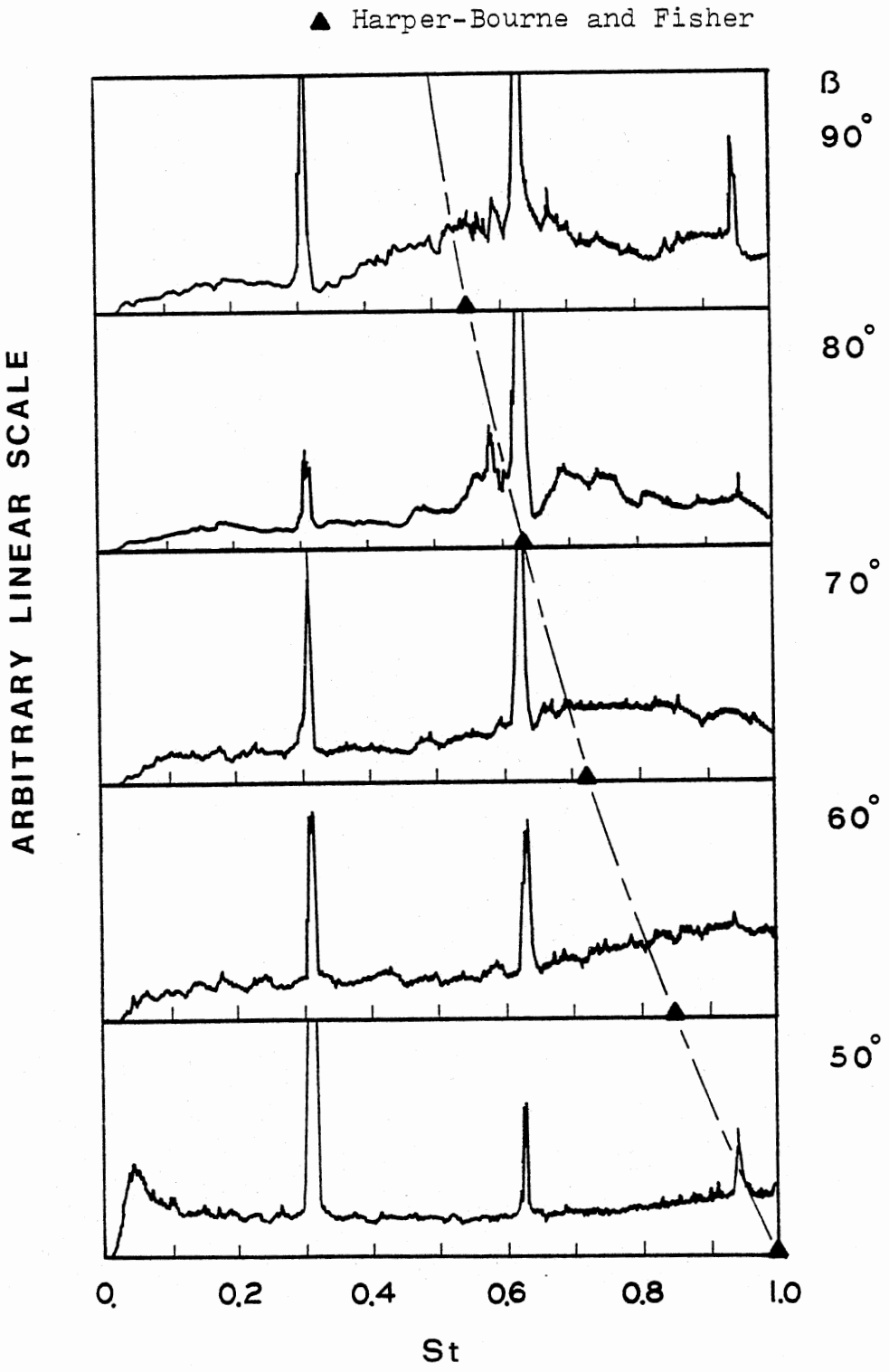

Figure 43. Acoustic Spectral Evolution, R/D=30, Re=68000, M=1.6 Underexpanded Jet

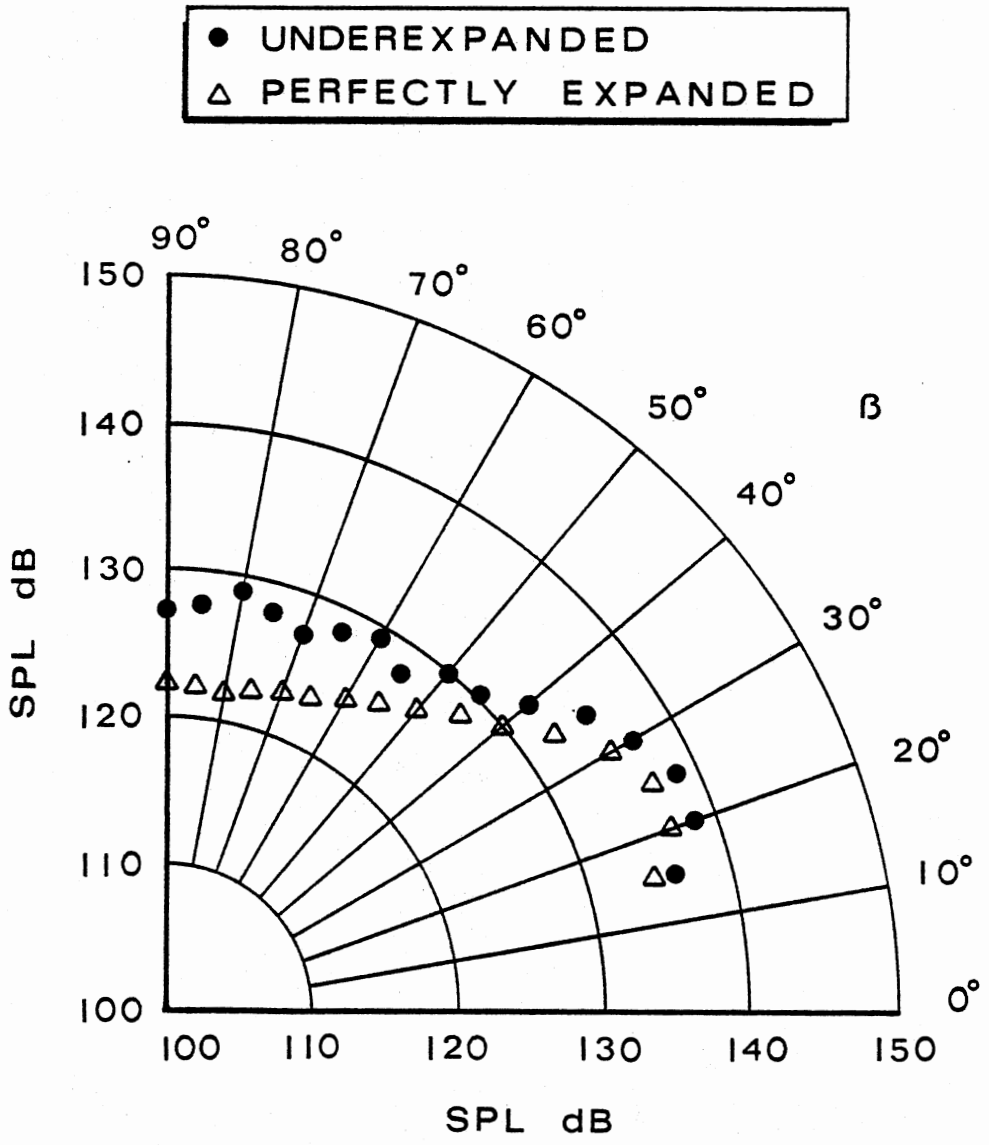

Figure 44. Overall Sound Pressure Level Directivity Distributions, R/D=30, M=1.6, Underexpanded Jet Compared with Perfectly Expanded Jet

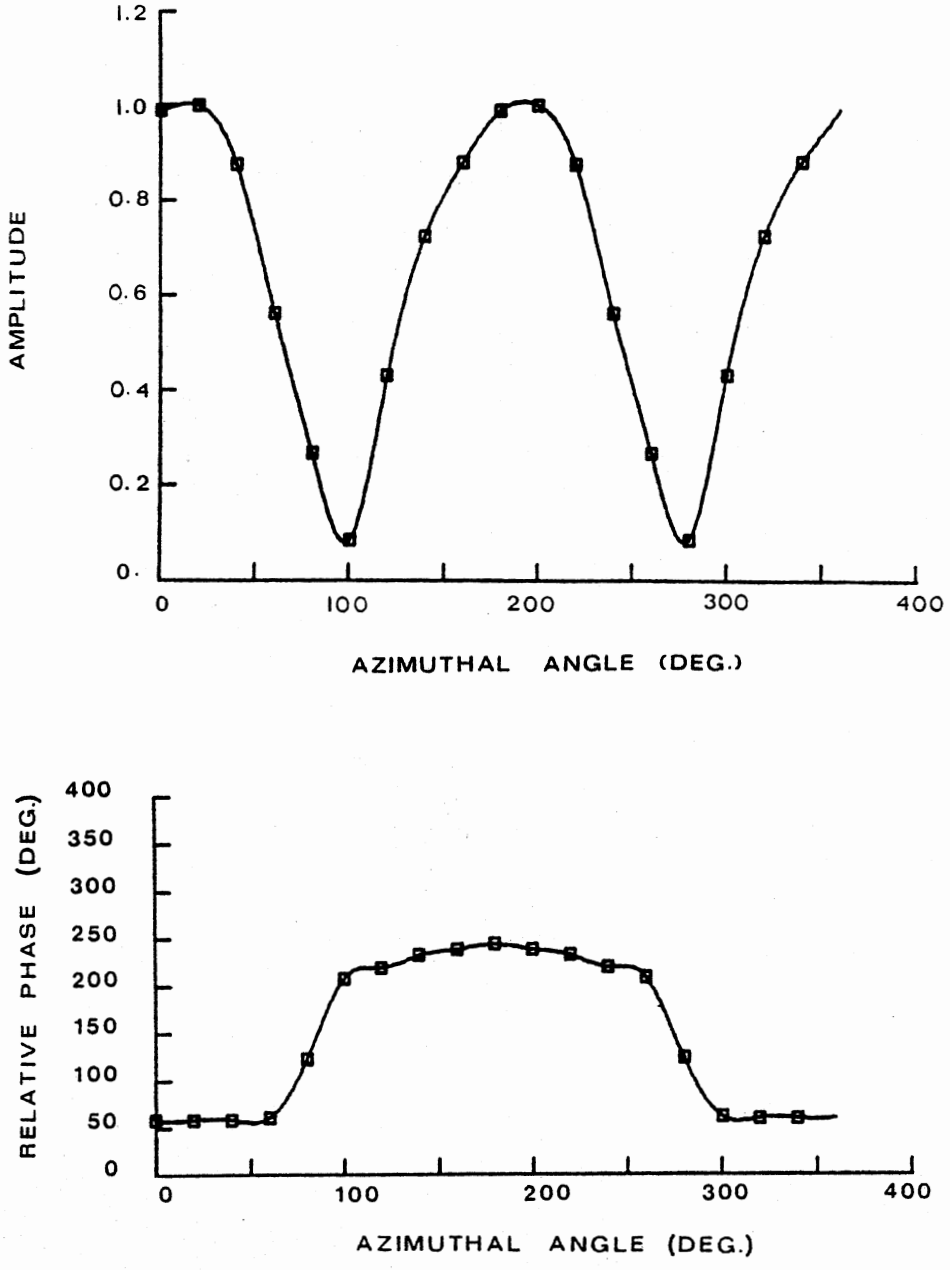

Figure 45. Experimentally Measured Azimuthal Behavior of St=0.3 Coherent Fluctuations, M=1.6, Re=68000 Underexpanded Jet

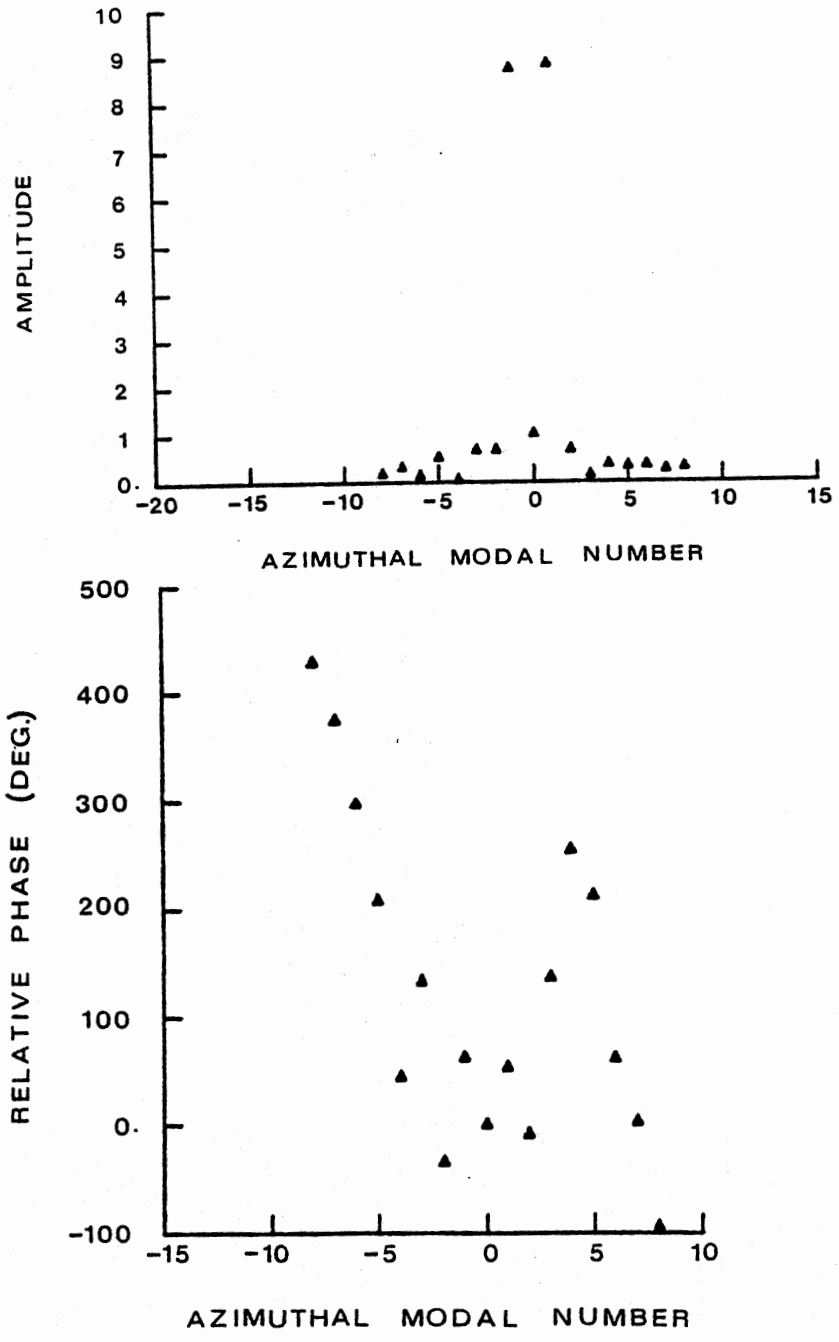

Figure 46. Azimuthal Modal Spectrum of the St=0.3 Coherent Fluctuations, Obtained by Fourier Analyzing the Data Shown in Figure 45

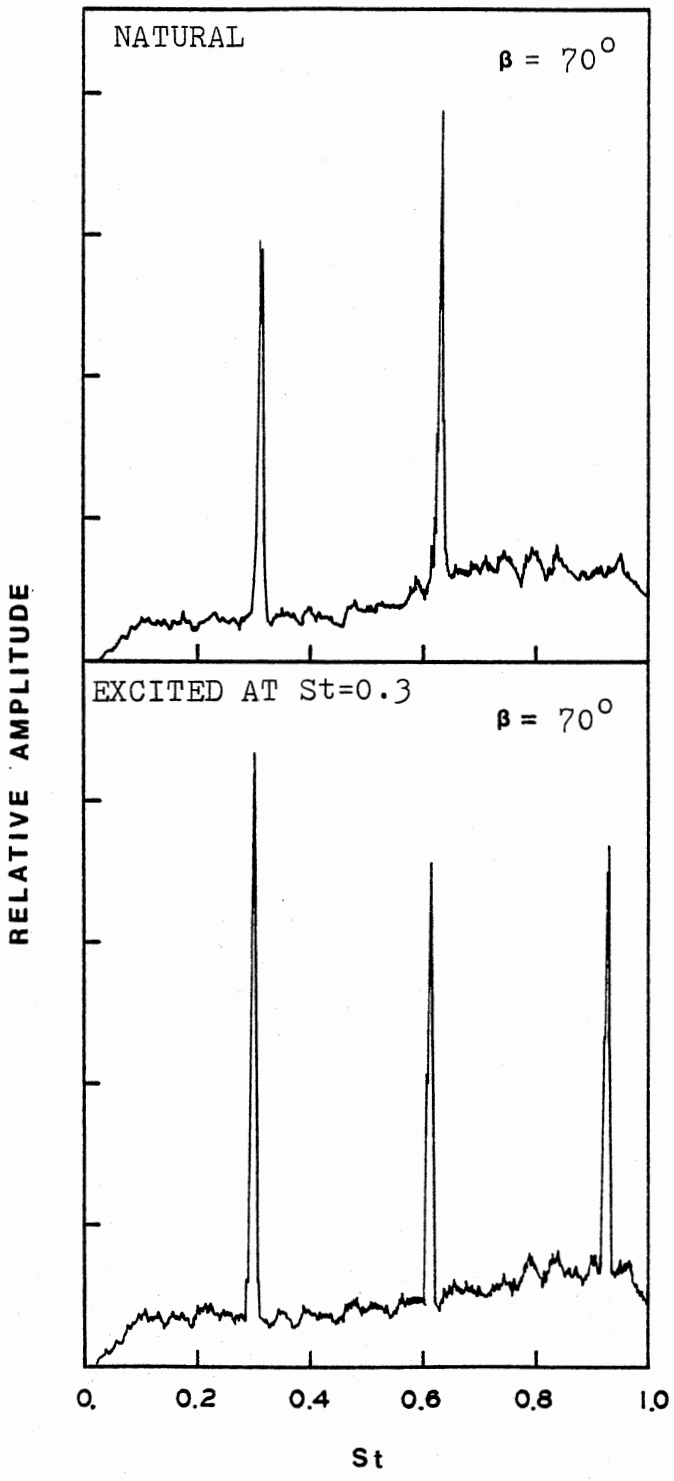

Figure 47. Acoustic Spectra, Natural Compared with Excited, R/D=30, Re=68000, M=1.6 Underexpanded Jet

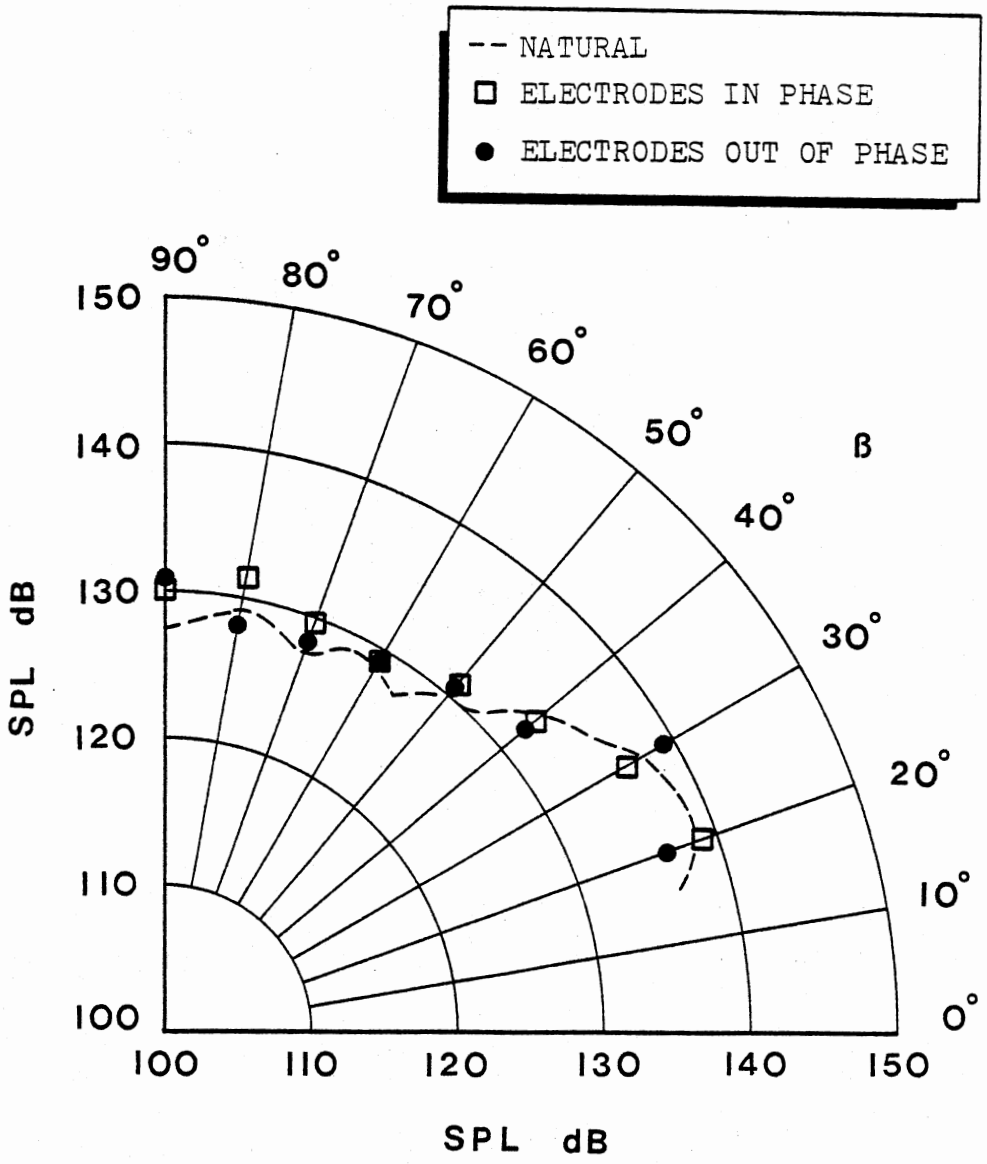

Figure 48. Overall Sound Pressure Level Directivity Distributions, R/D=30, Re=68000, M=1.6 Underexpanded Jet Excited at St=0.3

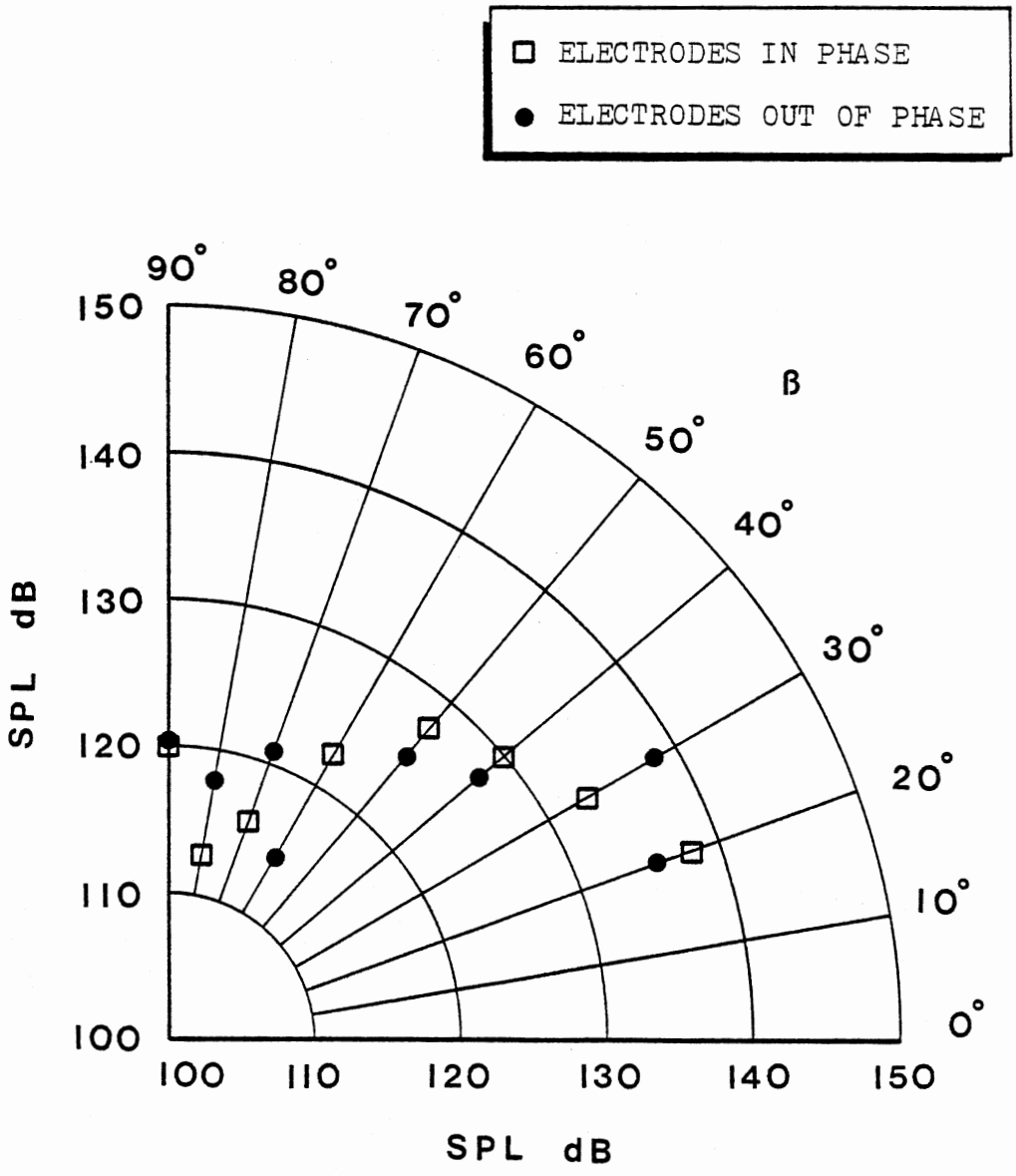

Figure 49. St=0.3 Coherent Sound Pressure Level Directivity Distributions, R/d=30, Re=68000, M=1.6 Underexpanded Jet

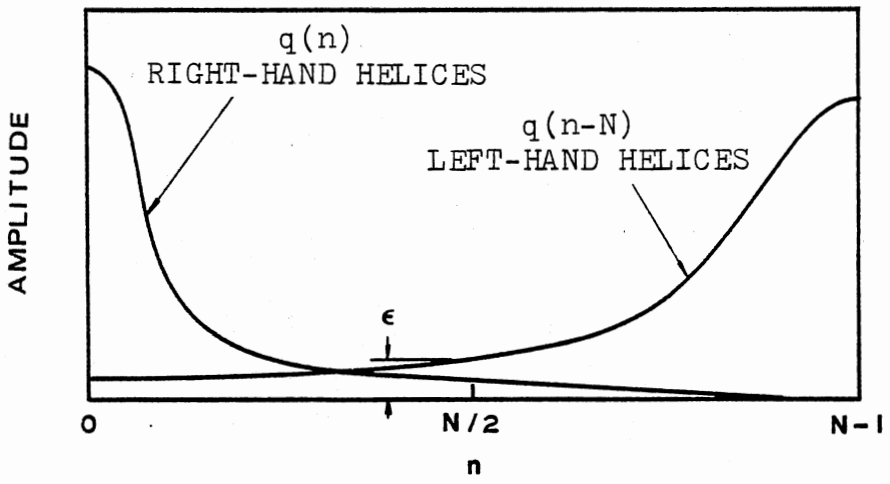

a.) Graphical Interpretation of Eq. A.9 Showing the Possible Area of Overlapping Gives an Error of ϵ near N/2 if Eq. A.10 is Applied

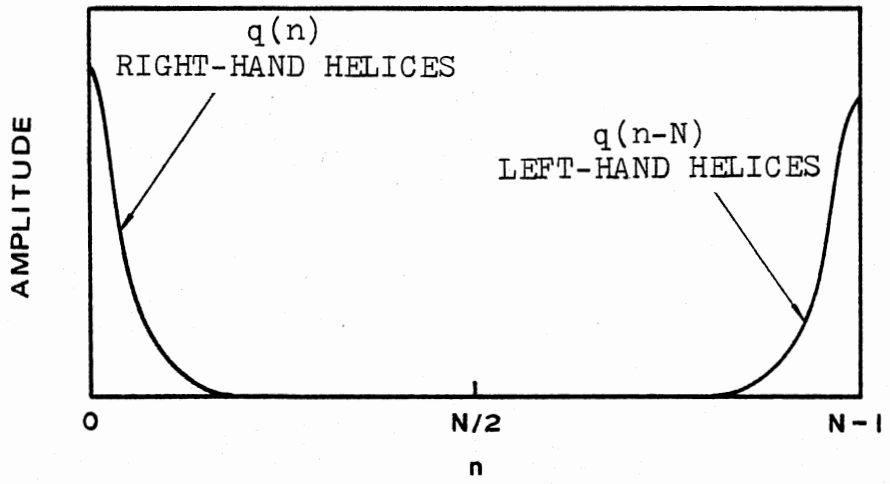

b.) Graphical Interpretation of Eq. A.10 with the Assumption of N Approaching Infinity, so that $\lim_{N\to\infty} \epsilon = 0$

Figure 50. Physical Pictures of the Final Derivation of the Azimuthal Modal Analysis

APPENDIX C

TABLES

TABLE I

EXPERIMENTAL CONDITIONS

Fully Expanded Mach Number	M	1.4	2.1	1.6
Fully Expanded Jet Velocity	U	408 m/s	526 m/s	449 m/s
Nozzle Contour	---	Convergent	Convergent	Convergent
Nozzle Exit Diameter	d	7.92 mm	6.99 mm	7.92 mm
Jet Effective Diameter	D	8.36 mm	9.47 mm	8.74 mm
Reynolds Number	Re	8000	7900	68000
Characteristic Frequency	U/D	48.8 kHz	55.6 kHz	51.4 kHz
Stagnation Pressure	P_o	0.0626 atm	0.069 atm	0.528 atm
Test Chamber Pressure	P_{ch}	0.0197 atm	0.00754 atm	0.124 atm
Stagnation Temperature	T_o	297° K	297° K	297° K

TABLE II

INSTABILITY PROPERTIES OF Re=8000, M=1.4 AND 2.1 UNDEREXPANDED SUPERSONIC JETS

Mach Number	Shock Cell Length	Strouhal Number	Growth Rate	Axial Wave Number	Phase Velocity	Phase Mach Number	Axial Wave Length	Azimuthal Modal Number
M	L/D	St	$-k_i D$	$k_r D$	c/U	c/a_o	λ/D	n
1.4	1.09	0.04-1.2	1.3	-	-	-	-	-
		0.21	1.1	2.34	0.56	0.66	2.68	0
		0.37	1.3	3.83*	0.62*	0.74*	1.64*	± 1
		0.37	1.3	4.36	0.55	0.66	1.44	± 1
2.1	1.55	0.04-1.2	0.99	-	-	-	-	-
		0.09	0.88					
		0.17	1.1	1.65	0.66	1.01	3.8	± 1
		0.27	0.93					
		0.36	0.95					
		0.45	0.88	4.59	0.6	0.91	1.37	

* Obtained by Hot-Wire/Microphone Cross-Correlation

VITA

Tieh-Feng Hu

Candidate for the Degree of

Doctor of Philosophy

Thesis: FLOW AND ACOUSTIC PROPERTIES OF LOW REYNOLDS NUMBER UNDEREXPANDED SUPERSONIC JETS

Major Field: Mechanical Engineering

Biographical:

Personal Data: Born in Taipei, Taiwan, Republic of China, July 31, 1952, the son of Mr. and Mrs. Tsu-Chung Hu.

Education: Graduated from Ta-An Middle School, Taipei, Taiwan, Republic of China, in June, 1967; received diploma from Taipei Institute of Technology, Taipei, Taiwan, Republic of China, in June, 1973; received Master of Science degree in Mechanical Engineering from Oklahoma State University, Stillwater, Oklahoma, United States of America, in December 1977; completed requirements for the Doctor of Philosophy degree at Oklahoma State University in December, 1981.

Professional Societies: American Institute of Aeronautics and Astronautics.